

Vertically aligned ZnO nanowires on p-GaN for UV-Visible Light Emitting Diode (LED) applications

Project Completion Report

F.No 41-963/2012 (SR) dated 26/07/2012
01.07.2012 - 31.12.2015

Submitted to



ज्ञान-विज्ञान विमुक्तये

**University Grant Commission
Bahadur Shah Zafar Marg
New Delhi - 110 002**

By

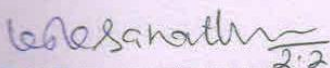


**Dr. K. Jeganathan
Professor
Centre for Nanoscience and Nanotechnology
School of Physics
Bharathidasan University
Tiruchirappalli - 620 024.**

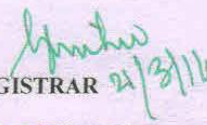
UNIVERSITY GRANTS COMMISSION
BAHADUR SHAH ZAFAR MARG
NEW DELHI - 110 002

PROFORMA FOR SUBMISSION OF INFORMATION AT THE TIME OF SENDING THE
FINAL REPORT OF THE WORK DONE ON THE PROJECT

1. Title of the Project:
"Vertically aligned ZnO nanowires on p-GaN for UV-Visible light emitting diode (LED) applications"
2. NAME AND ADDRESS OF THE PRINCIPAL INVESTIGATOR: Prof. K. Jeganathan, Coordinator, Centre for Nanoscience and Nanotechnology, School of Physics, Bharathidasan University
3. NAME AND ADDRESS OF THE INSTITUTION: Bharathidasan University, Palkalai Perur, Tiruchirappalli - 620 024
4. UGC APPROVAL LETTER NO. AND DATE:
F. No 41-963/2012 (SR) dated 26.07.2012 & F. No 41-963/2012 (SR) dated 24.06.2015
5. DATE OF IMPLEMENTATION : 01.07.2012
6. TENURE OF THE PROJECT : 31.12.2015
7. TOTAL GRANT ALLOCATED : Rs. 12,46,687/-
8. TOTAL GRANT RECEIVED : Rs. 11,83,548/-
9. FINAL EXPENDITURE : Rs. 11,83,542/-
10. OBJECTIVES OF THE PROJECT
Kindly refer annexure - I
11. WHETHER OBJECTIVES WERE ACHIEVED: Yes
12. ACHIEVEMENTS FROM THE PROJECT:
Kindly refer annexure -II
13. SUMMARY OF THE FINDINGS
Kindly refer annexure - III
14. CONTRIBUTION TO THE SOCIETY
Kindly refer annexure - IV
15. WHETHER ANY PH.D. ENROLLED/PRODUCED OUT OF THE PROJECT:
Yes, Mr. P. Dharmaraj enrolled for his Ph.D
16. NO. OF PUBLICATIONS OUT OF THE PROJECT: Four (List attached)


2.2.16
PRINCIPAL INVESTIGATOR

Dr. K. JEGANATHAN
PI of the UGC Project
Center for Nanoscience and Nanotechnology
School of Physics, Bharathidasan University
Tiruchirappalli - 620 024.


REGISTRAR 24/3/16

REGISTRAR
BHARATHIDASAN UNIVERSITY
TIRUCHIRAPPALLI 620 024

UNIVERSITY GRANTS COMMISSION
BAHADUR SHAH ZAFAR MARG
NEW DELHI - 110 002

STATEMENT OF EXPENDITURE IN RESPECT OF MAJOR RESEARCH PROJECT

1. Name of Principal Investigator : Prof K. Jeganathan
2. Deptt. of Principal Investigator : Physics
University/College : Bharathidasan University
3. UGC approval Letter No. and Date : F. No 41-963/2012 (SR) dated 26/07/2012
4. Title of the Research Project :Vertically aligned ZnO nanowires on p-GaN for
UV- Visible light emitting diode (LED) applications
5. Effective date of starting the project : 01.07.2012

6 a. Period of Expenditure: From 01.07.2012 to 31.12.2015

b. Details of Expenditure

S. No	Items	Amount Approved Rs.	Amount received Rs.			Expenditure incurred Rs.		Balance available	
			1 st Instalment	2 nd Instalment	Total	01.07.2012 to 31.12.2013	01.01.2014 to 31.12.2015		
1	Books & Journal	50,000	50,000	---	50,000	42,828	7,166	49,994	6
2	Equipments	5,00,000	5,00,000	---	5,00,000	5,00,000	---	5,00,000	---
3	Manpower	4,76,387	2,64,000	1,64,748	4,28,748	2,04,129	2,24,619	4,28,748	---
4	Contingency	50,000	25,000	20,000	45,000	25,000	20,000	45,000	---
5	Travel/fieldwork	30,000	15,000	12,000	27,000	14,930	12,070	27,000	---
6	Chemicals/Classsawa re/Consumables	75,000	37,500	30,000	67,500	37,500	30,000	67,500	---
7	Hiring Services	Nil	Nil	Nil	Nil	Nil	Nil	Nil	---
8	Overhead	65,300	65,300	---	65,300	65,300	---	65,300	---
	Total	12,46,687	9,56,800	2,26,748	11,83,548	8,89,687	2,93,855	11,83,542	6

c. Staff

Date of Appointment: 08.10.2012

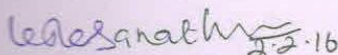
S. No	Items	From	To	Amount approved	Amount received	Expenditure Incurred
1	Honorarium to PI (Retired teachers) @18,000/- p.m	Nil	Nil	Nil	Nil	Nil
2	Project Fellow: Non-GATE/Non-NET – Rs 14,000/- p.m for initial two years and Rs. 16,000 for third year	08.10.2012	30.06.2015	4,76,387	4,28,748	4,28,748 (fellowship claimed from 08.10.2012 to 02.04.2015 only)

1. It is certified that the appointment(s) have been made in accordance with the terms and conditions laid down by the Commission.

2. If as a result of check or audit objection some irregularly is noticed at later date, action will be taken to refund, adjust or regularize the objected amounts.

3. Payment @ revised rates shall be made with arrears on the availability of additional funds.

It is certified that the grant of Rs. 11,83,548/- (Rupees Eleven lakhs eighty three thousand five hundred and forty eight only) received from the University Grants Commission under the scheme of support for Major Research Project entitled "Vertically aligned ZnO nanowires on p-GaN for UV-Visible light emitting diode (LED) applications" vide UGC letter No. F.41-963/2012 (SR) dated 26.07.2012 & UGC letter No. F.41-963/2012 (SR) dated 24.06.2015, a sum of Rs. 11,83,542/- (Rupees Eleven lakhs eighty three thousand five hundred and forty two only) has been utilized for the purpose for which it was sanctioned and in accordance with the terms and conditions laid down by the University Grants Commission. The unspent amount of Rs. 6/- (Rupees Six only) under the head of books and periodicals will be refunded to UGC through RTGS.


PRINCIPAL INVESTIGATOR

Dr. K. JEGANATHAN
PI of the UGC Project
Center for Nanoscience and Nanotechnology
School of Physics, Bharathidasan University


FINANCE OFFICER

FINANCE OFFICER,
BHARATHIDASAN UNIVERSITY,
TIRUCHIRAPPALLI


REGISTRAR

REGISTRAR
BHARATHIDASAN UNIVERSITY
TIRUCHIRAPPALLI 620 024

UNIVERSITY GRANTS COMMISSION

BAHADUR SHAH ZAFAR MARG

NEW DELHI - 110 002

Utilization certificate

Certified that the grant of Rs. 11,83,548/- (Rupees Eleven lakhs eighty three thousand five hundred and forty eight only) received from the University Grants Commission under the scheme of support for Major Research Project entitled "Vertically aligned ZnO nanowires on p-GaN for UV-Visible light emitting diode (LED) applications" vide UGC letter No. F.41-963/2012 (SR) dated 26.07.2012 & UGC letter No. F.41-963/2012 (SR) dated 24.06.2015, a sum of Rs. 11,83,542/- (Rupees Eleven lakhs eighty three thousand five hundred and forty two only) has been utilized for the purpose for which it was sanctioned and in accordance with the terms and conditions laid down by the University Grants Commission. The unspent amount of Rs. 6/- (Rupees Six only) under the head of books and periodicals will be refunded to UGC through RTGS.

K. Jeganathan
2.2.16
PRINCIPAL INVESTIGATOR

Dr. K. JEGANATHAN
PI of the Ugc Project
Center for Nanoscience and Nanotechnology
School of Physics, Bharathidasan University
Tiruchirappalli - 620 024.

[Signature]
FINANCE OFFICER

FINANCE OFFICER,
BHARATHIDASAN UNIVERSITY,
TIRUCHIRAPPALLI.

[Signature]
21/2
REGISTRAR

REGISTRAR
BHARATHIDASAN UNIVE
TIRUCHIRAPPALLI 620

Annexure - I

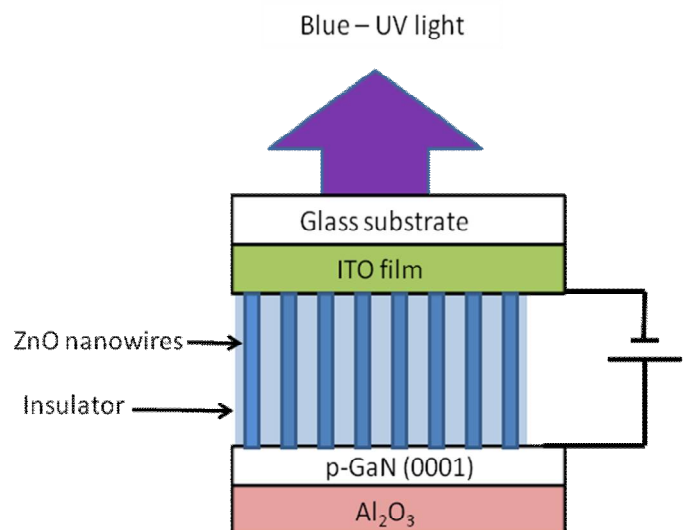
Objectives

1. Fabrication and optimization of growth conditions for vertical standing homogeneous ZnO nanowires on p-type GaN epitaxial layer grown on Al₂O₃ (0001) substrates.
2. Fabrication of NW LEDs structure using p and n – electrode by filling air gaps using insulator like spin on glass / polystyrene.
3. I-V-L characteristics of NW LEDs including extraction efficiency, colour rendering and chromaticity.

Annexure - II

Achievements

ZnO nanowire arrays have been grown on various substrates such as p-type Si (111), p-type GaN (0001) epitaxial film grown on Al₂O₃ substrates and ITO coated glass substrates by radio frequency (RF) magnetron sputtering. The homogeneity of the vertical standing ZnO nanowires have been improved by varying the growth parameters such as Ar/O₂ pressure, RF powder and substrate temperature. The optical, structural and electrical properties of the NWs have also been investigated in detail. The overview of hybrid NW LED device structure accomplished is shown below. N-type ZnO NWs were grown on p-GaN epitaxial template and the heterojunction LED was formed by placing ITO/glass electrode on top of the ZnO nanowire arrays. As shown in the figure, the tips of the nanowires in direct contact with the electrode form a p-n heterojunction structure of NW LEDs. LED structure have been extensively characterized by means of optical and electrical properties.



1. Fabrication and characterization of one-dimensional zinc oxide nanostructures

Introduction

Zinc Oxide (ZnO) with stable wurtzite crystal structure, wide and direct band gap of 3.37 eV at room temperature as well as large exciton binding energy of 60 meV, have attracted extensive research interest for their electronic and optoelectronic devices, such as light emitting and laser diodes in the ultraviolet spectral region. Because of its unique properties, it has lot of potential applications such as piezoelectricity, spintronics, electronics and biosensors. The advantage of ZnO is low price and easy availability, placing it as a potential candidate for industrial applications. In recent years, the fabrication of one-dimensional (1-D) ZnO nanostructures (such as nanowires, nanorods and nanotubes) have attracted a considerable attention as it is expected to be a building blocks for future nanoscale devices.

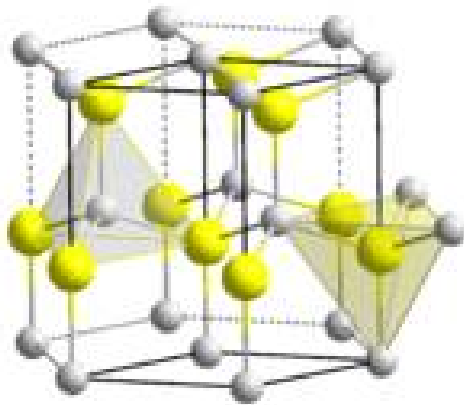


Fig. 1 Wurtzite crystal structure of ZnO

Important parameters related to the physical properties of ZnO are tabulated in Table 1. It should be noted that still there exists uncertainty in some of these values like hole mobility, thermal conductivity etc.

Table 1 Physical properties of Zinc Oxide

Property	Value
Lattice parameters at 300 K	
<i>a</i>	0.32495 nm
<i>c</i>	0.52069 nm
Density	5.606 g/cm ³
Stable phase	Wurtzite
Melting point	1975 °C
Thermal conductivity	1-1.2 (W/(mK))
Linear expansion coefficient (/C)	<i>a</i> : 6.5x10 ⁻⁶ K ⁻¹ <i>c</i> : 3.0x10 ⁻⁶ K ⁻¹
Static dielectric constant	8.656
Refractive index	2.008 - 2.029
Energy band gap	3.37 eV, direct
Exciton binding Energy	60 meV
Electron effective mass	0.23 m ₀
Electron Hall mobility	200 cm ² /Vs
Hole effective mass	0.59 m ₀
Hole Hall Mobility	5-50 cm ² /Vs

Experimental method

Depositions of 1D nanostructures were carried out by radio frequency (RF) magnetron sputtering using a pure 2 inch ZnO target on the commercially available n-type silicon (111) substrates. 2 inch ZnO target was prepared by the simple solid state reaction technique. Prior to deposition, the substrates were cleaned by the standard procedure. Initially, the sputtering chamber was evacuated to the base pressure of 5 x 10⁻⁶ mbar. The oxide target was pre-sputtered about 10 minutes in pure argon ambient at the pressure of 0.01mbar in order to remove the surface impurities present on the target. The distance between the target and substrate was kept constant at 50 mm and RF power. The substrate temperature, deposition time and deposition pressure are varied in order to understand the evaluation of the 1-D nanostructures. According to the deposition conditions, the deposition rate and the thickness of the deposited materials will vary and

are monitored by the digital thickness monitor (Model DTM - 101). The substrate was heated by the ceramic heater through PID (EMKO ESM-4430) controller. The temperature on the surface of the substrate was measured by the standard thermocouple.

The surface morphology and composition of the 1-D nanostructures were examined by a field emission scanning electron microscope (FESEM, Carl Zeiss-Sigma) equipped with an energy dispersive X-ray spectrometer (EDX, Oxford instruments-INCAx). The crystal structure of the nanostructures were characterized by a Rigaku X-ray diffractometer with Cu-K α radiation at $\lambda = 1.5406 \text{ \AA}$. The diffraction patterns were recorded using θ -2 θ geometry between 10° and 80° with step size of 0.05° for the structural identification. Micro-Raman scattering of nanostructures were recorded in the back scattering geometry using LabRam HR800 Raman spectrometer at an excitation wavelength of 632.8 nm with a spot size of $\sim 1\mu\text{m}$. The temperature dependent photoluminescence (PL) measurements were recorded using a HORIBA JOBIN YVON monochromator (0.55 m) over the temperature range of 10-330 K by the closed cycle helium cryostat. He-Cd laser (325 nm) with a power of 30 mW was used as an excitation source and the dispersed luminescence signal from the sample was collected by a charge coupled device through an appropriate optical arrangement.

Results and discussion

The FESEM images shown in Fig. 2 depict the top and 45° tilted views of ZnO nanowires grown under different growth durations of 15, 30, 60 and 120 min respectively. The FESEM images clearly show that the nanowires are vertically aligned on the substrates having hexagonal cross section. However, the density, length and diameter distributions of the ZnO nanowires exhibit a strong dependence of growth duration. Fig. 3 represents the variations of average diameter, density and length of the nanowires for different growth durations. The average diameter of the nanowires increases gradually up to the growth duration of 60 min, after that the diameter leads to decrease by the increase of the growth duration to 120 min which is attributed to the tapering of the nanowires. The reason for tapering is clearly described below. Further, the average length of the nanowires found to increase linearly from 150 to 1394 nm with the increase of the growth duration from 15 to 120 min.

The density of the nanowires increases up to 30 min growth duration ($0.57 \times 10^{10} \text{ cm}^{-2}$) as due to the formation of new nuclei on the substrate. Nevertheless, the density

decreases to $0.36 \times 10^{10} \text{ cm}^{-2}$ with the increase of the growth duration to 60 min and this trend can be attributed to the coalescence of nanowires at the boundaries. In contrast, the density of nanowires found to monotonously increase to $1.44 \times 10^{10} \text{ cm}^{-2}$ with the increase of growth duration to 120 min. This

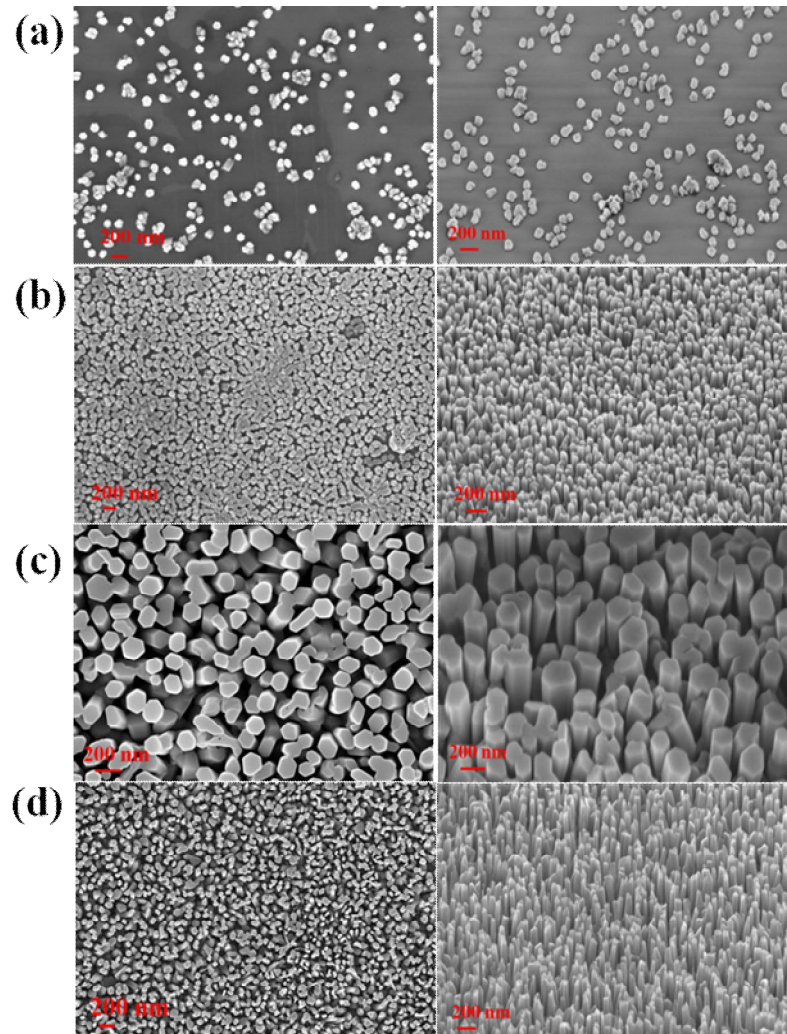


Fig. 2 FESEM top and 45° tilted views of ZnO nanowires grown at different growth durations (a) 15 min, (b) 30 min, (c) 60 min and (d) 120 min.

unexpected behavior can be explained by the multiple tapering on the edges of nanowires which obviously result the high density nanowires in extended growth duration of 120 min. Furthermore, the structural and optical properties of the well oriented and vertically aligned nanowires are very important for the fabrication of efficient optoelectronic devices. Consequently, a detailed investigation has been extended to the nanowires grown under pure Ar atmosphere for 120 min at 550 °C.

A tilt view (45°) of the vertically aligned ZnO nanowires grown on n-type silicon (111) substrate using rf magnetron sputtering technique is shown in Fig. 4 (a). One can easily observe that the nanowires have tapered tips and are well aligned vertically with an average diameter of 80 nm and length of about $\sim 1.4 \mu\text{m}$. Generally, the growth of the nanowires is promoted by the direct impingement of adatoms on the tip of the nanowires in addition to the migration of adatoms through the side walls of the nanowires. In the case of adatoms migration through the side walls of the nanowires, the growth is enhanced only if the migration length of the adatoms is greater than the length of the nanowires, otherwise it will be desorbed from the surface of the nanowires and hence direct impingement of adatoms are only responsible for the subsequent growth of nanowires.

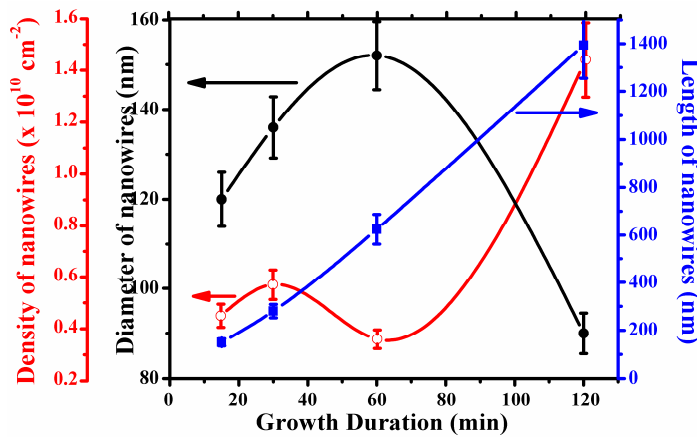


Fig. 3 Diameter, Length and Density distributions of ZnO nanowires as a function of different growth durations.

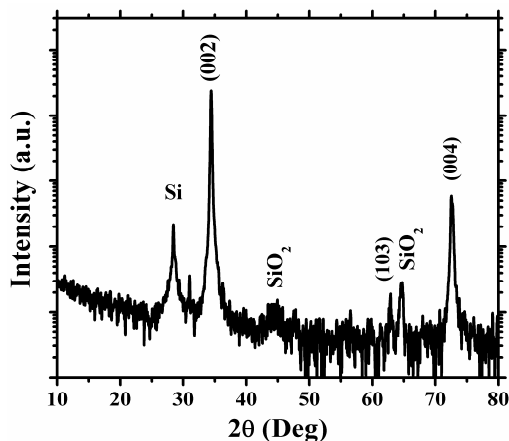


Fig. 5 XRD pattern of vertically aligned ZnO nanowires (The silicon and silicon dioxide peaks arise from the substrate).

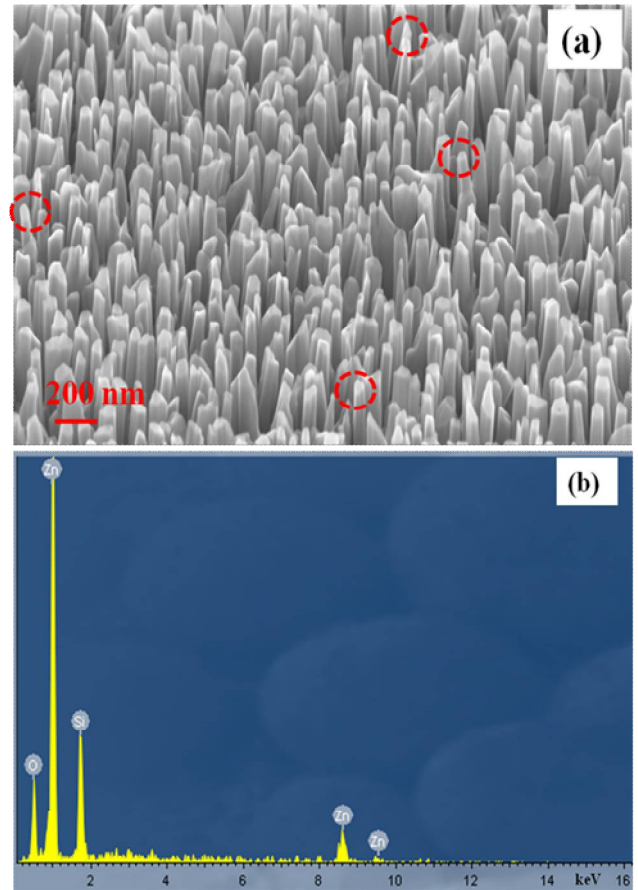


Fig. 4 (a) 45° tilted view of the vertically aligned ZnO nanowires grown on the silicon (111) substrate for the growth duration of 120 min. (b) EDX spectrum of the array of ZnO nanowires.

Therefore, the migration length of the adatoms is an important parameter and depends on the many growth parameters such as substrate temperature, sputtering pressure, target - substrate distance and furthermore the position of nanowires on the substrate surface. If the energy of the adatoms is small, consequently the migration length becomes small. Hence, it could not reach the growth front of the nanowires. Therefore, the number of adatoms on the tip of the nanowires will be reduced which may induce the tapering in the nanowires. In our case, the tip of the nanowires is not tapered up to the growth duration of 60 min and its length is about 625 nm. Further increasing the growth duration to 120 min, the length of the nanowires is approximately doubled (~1394 nm). On the other hand, the ZnO nanowires have tapered tips as shown in Fig. 4 (a). It could be ascribed that the migration length of the adatoms is expected to be ~ 1 μm as the tapering occur at above this length for the given growth conditions. Due to the smaller migration length of adatoms, the tapering is observed in the nanowires grown for 120 min. EDX spectrum of the vertically aligned ZnO nanowires is recorded using the electron beam of 10 kV accelerating voltage as shown in Fig. 4 (b). The vertically aligned ZnO nanowires consist of purely zinc and oxygen. The presence of silicon in the EDX spectrum is associated to the substrate, which is attributed to the interaction of electron with the silicon substrate through the air gap between the vertical standing nanowires. With the detection of limit of EDX, there are no impurities found in the array of nanowires.

Fig. 5 depicts the X-ray diffraction pattern of undoped ZnO nanowires grown on silicon (111) substrate for 120 min by rf magnetron sputtering technique. The dominant and weak peaks at 34.43° and 72.63° correspond to (002) and (004) reflections of ZnO respectively, which confirm the hexagonal wurtzite structure of the nanowires with the preferential orientation along c-axis. The narrow full width at half maximum (FWHM, 618 arc. sec) of the dominant (002) peak reveals the high crystalline nature of the nanowires. The observed peak at 28.55° corresponds to the (111) reflection of silicon (JCPDS - 78-2500) which is attributed from the substrate. Further, the additional peaks at 44.54° and 64.56° correspond to the silicon dioxide (JCPDS - 89-3606). The appearance of the silicon dioxide peak confirms the existence of silicon dioxide layer on the surface of the substrate, which may be formed during the earlier stage of growth at elevated temperature by the process of oxidation from the reactive oxygen radicals. In addition to this, a very small peak at 62.87° belongs to the (103) reflection of ZnO. The observation of this weak peak indicates the quasi-alignment of nanowires. The calculated in-plane

and out-plane lattice parameters ($a = 3.251 \text{ \AA}$ and $c = 5.204 \text{ \AA}$) are in good agreement with the standard bulk values which demonstrates that the nanowires are completely relaxed with high crystalline quality despite large mismatch between ZnO and silicon substrate.

Fig. 6 (a) shows a typical micro-Raman spectrum of the vertically aligned ZnO nanowires grown on the silicon substrate. The sharp and dominant peaks at 99.4 cm^{-1} and 437.1 cm^{-1} correspond to the non-polar E_2 phonon modes. The dominant peak at 99.4 cm^{-1} is attributed to the lattice vibrations of zinc atoms and assigned as E_2^{low} phonon mode. The peak at 437.1 cm^{-1} corresponds to E_2^{high} phonon mode and attributed to the lattice vibrations of oxygen atoms, which is very sensitive to crystalline nature and defects of the nanostructures. The appearance of E_2^{high} phonon mode confirms the wurtzite structure of the ZnO nanowires. The peak positions of the E_2 phonon modes are in good agreement with the standard bulk values of ZnO. The narrow FWHM (1.4 and 9.1 cm^{-1}) of the non-polar phonon modes (E_2^{low} and E_2^{high}) substantiates the high optical and crystalline qualities of the nanowires which corroborates with the XRD results. The peak at 276 cm^{-1} is assigned as $B_1(\text{low})$ and the appearance of this peak evidences the breakdown of translation symmetry in the nanostructures. The observed peak at 582 cm^{-1} could not be attributed to the $E_1(\text{LO})$ phonon mode, because it is one of the forbidden modes of vibration in the back scattering geometry. Hence, it may be attributed to either $B_1(\text{high})$ or $A_1(\text{LO})$. It is well known that $B_1(\text{low})$ and $B_1(\text{high})$ modes are silent. However, the earlier reports show that the silent modes are observable in the case of nanostructures due to the breakdown of the translational symmetry. These modes should be comparable in intensities and the line width of $B_1(\text{low})$ mode must be very small as compared to $B_1(\text{high})$ mode. But, in our case, the intensities of the silent mode are not comparable. Consequently, the peak at 582 cm^{-1} could not be attributed to $B_1(\text{high})$ mode. Therefore, the observed peak is assigned to be $A_1(\text{LO})$ and it is generally observed at the wave number of 574 cm^{-1} . It is blue shifted from its original position owing to the increase of free carrier concentration. A strong correlation have already been established between position of the $A_1(\text{LO})$ mode and free carrier concentrations. The $A_1(\text{LO})$ phonon mode shifts to the higher wave numbers with broadening of peak owing to the coupling between phonons and plasmons, can be associated to the increase of free carrier concentration in ZnO nanowires. The peaks at $233, 302, 520, 620$ and 670 cm^{-1} are attributed from the silicon substrate. The micro-Raman spectrum of the bare silicon

substrate is shown in Fig. 6 (b) for the comparison and the enlarged view shown in the inset of Fig. 6 (b) clearly depicts the weak peaks.

Fig. 7 (a) shows the temperature dependent PL spectra of the undoped ZnO nanowires measured in the temperature range of 10–330 K. The observed emission peak at 3.343 eV is typical donor to bound exciton (D^0X) emission. By increasing the temperature from the low temperature (10 K) to room temperature, D^0X peak shifts monotonically towards the low energy side. A 166 meV red shift of the band edge emission over this temperature range is caused by the thermal expansion of the lattice and electron-phonon interactions. The intensity of the peak decreases with increasing the temperature as a result of the refreezing of phonons and stimulation of non-radiative recombination processes. It is reported that the longitudinal optical (LO) phonon energy of bulk ZnO is ~ 72 meV. The observed emission peaks at 3.26 and 3.18 eV are

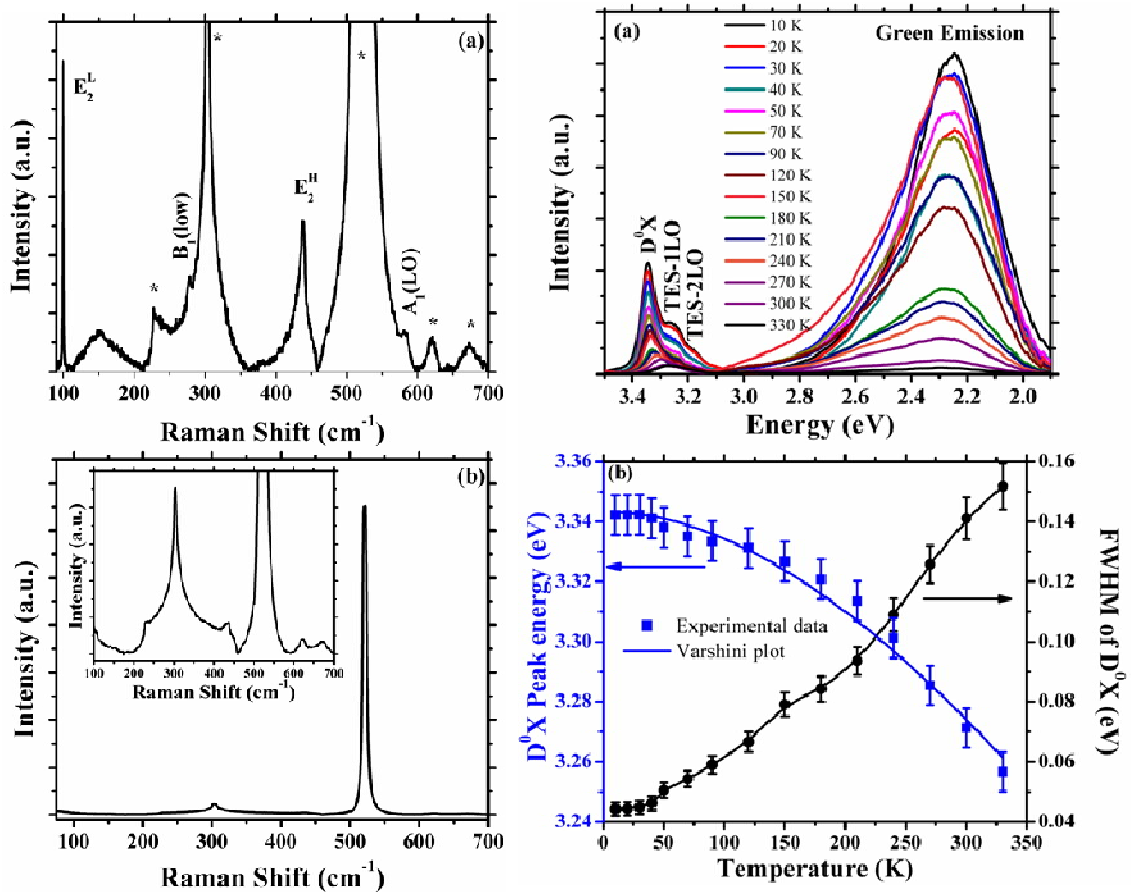


Fig. 6 (a) Micro-Raman spectrum of vertically aligned ZnO nanowires recorded in back scattering geometry with an excitation wavelength of 632.8 nm. (b) Micro-Raman spectrum of the bare silicon substrate. The inset shows the enlarged view of the Raman spectrum of silicon.

Fig. 7 (a) Temperature dependent PL spectra of ZnO nanowires grown on silicon (111) substrate. (b) Variations of D^0X peak energy (eV) and FWHM (eV) as a function of temperature (K).

associated to the first and second LO phonon replicas of two electron satellite lines. The dominant and broad emission at 2.28 eV is associated to the singly ionized oxygen vacancies and this green luminescence is attributed to the electron transition from the shallow donor level (V_o) to a shallow acceptor level (V_{zn}). As the ZnO nanowires were grown under pure Ar atmosphere, the oxygen vacancy is expected and further the growth temperature of 550 °C is more responsible for reducing the oxygen radicals available for the crystallization at the growth front. The green emission intensity drastically increases and overshoots the D^0X emission as the decrease of temperature. Fig. 7 (b) shows the variation of D^0X peak energy of the ZnO nanowires as a function of temperature. Varshni's empirical equation can be fitted with the experimental data to find the temperature dependence of D^0X peak and can be written as

$$E(T) = E(0) - \left(\frac{\alpha T^2}{T + \beta} \right)$$

where $E(T)$ and $E(0)$ are the band gap at an absolute temperature T and 0 K respectively. α and β are the Varshni thermal coefficients. From the fitted curve, the Varshni parameters $E(0)$, α and β were found to be 3.3434 eV, 1.01×10^{-3} eV/K and 1006 K respectively. The obtained values are comparable to the earlier reported values. The PL line width of D^0X emission increases with the temperature as shown in Fig. 7 (b). Earlier reports show that there is a strong correlation between the broadening of band edge emission and carrier concentration. At 10 K, if the broadening of band edge emission is solely attributed by the thermal broadening, then its value should be ~ 1.3 meV ($3K_B T/2$). However, the additional broadening also occurs due to the point defects induced by either non-stoichiometry or lattice/thermal mismatch between the deposited materials and substrates. In our case, the PL line width at 10 K is around 44 meV which depicts that the additional broadening of the peak has been occurred due to the point defects. This indicates that the growth conditions and selection of substrate play an important role in the growth of high quality materials since they can create point defects in oxide semiconductors which are similar to carrier doping. The observed broad band edge emission indicates the high concentration of point defects which is further substantiated by the dominant green emission. Thus, the broadening of the peak is attributed to the enhancement of the free carrier concentration induced by the point defects in the nanowires as substantiated by the blue shift of $A_1(LO)$ phonon mode.

2. One dimensional Mo doped n-type ZnO nanowires on p-type Si

The size, shape and density of ZnO NWs were characterized by using field emission scanning electron microscopy (FESEM, Carl Zeiss -Sigma). The chemical composition of the obtained NWs was identified by Energy-dispersive x-ray spectroscopy (EDS). The optical characteristics of the NWs were investigated using photoluminescence (PL) and absorption measurements. The PL measurements were performed at room temperature with the 325 nm line of a He-Cd laser.

For electrical measurements, the space between the ZnO NWs is filled with an insulating layer of poly vinyl alcohol (PVA) by spin coating followed by baking the substrate at 120 °C for 40 min under Ar ambient. A 200 nm thick gold film was deposited on the top of ZnO as cathode by thermal evaporation with a shadow mask and a layer of gold film was deposited on the back side of the p⁺-Si substrate to form Ohmic contact. Finally an n-ZnO NWs/p⁺-Si heterostructure was obtained. The current–voltage (I-V) characteristic of the device was measured by a source meter (Keithley 2400, Keithley Instruments, Inc., OH, USA).

The general morphology of ZnO nanowires was obtained using field emission scanning electron microscopy. As shown in Fig. 8, ZnO nanowires were vertically well aligned with uniform length, diameter and distribution density. The average diameters of the undoped ZnO and ZnO: 2 wt% Mo NWs are 58.6 nm and 82.4 nm respectively. It was observed that the diameter increases with doping when Mo ion replaces Zn in the substitutional sites. Fig. 9 shows the size distributions of ZnO NWs for undoped and doped samples. Their average length for 1 hour growth and density on p⁺-Si substrate were found to be 1.5 μm and $3.74 \times 10^9 \text{ cm}^{-2}$. Further, about two-third of the Si substrate surface is devoid of NWs. The hexagon shaped morphology of the NWs could be clearly observed as shown in FESEM images (see inset).

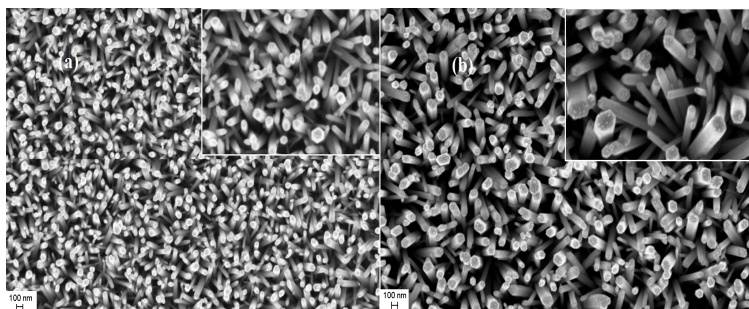


Fig. 8. FESEM image of the (a) Undoped ZnO (b) ZnO:Mo 2 wt% grown on p⁺-Si substrate

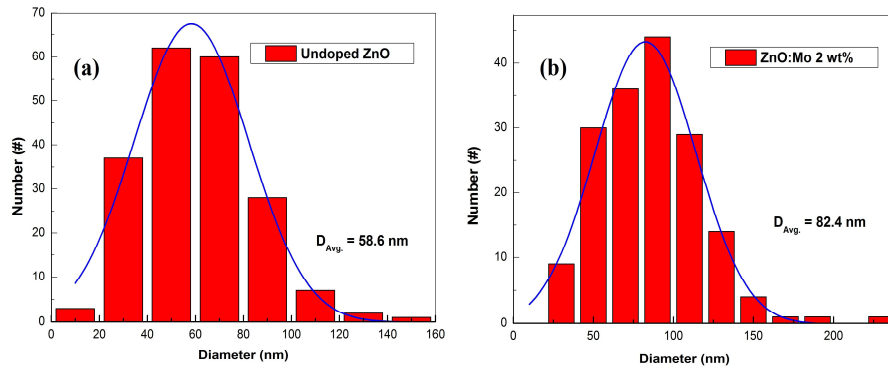


Fig. 9. Size distribution of (a) Undoped (b) Doped with 2 Wt% Mo ZnO NWs

EDS of ZnO:Mo 2 Wt% nanowires grown on p^+ -Si was performed, and the resulting spectrographic data is shown in Fig 10. The Mo concentration (in weight%) in the nanowires was found to be 0.68 depending on the amount of Mo precursor used. EDS determines the composition of the synthesized ZnO nanostructures, and the results confirm the doping in ZnO NWs. Quantitative EDS analysis showed that the atom percent ratio of Zn to O was about 1:1 with the presence of Mo in ZnO. The presence of the Si peak in the EDS pattern can be assigned to the Si substrate. Further, no indication of oxide impurities in our final product was observed.

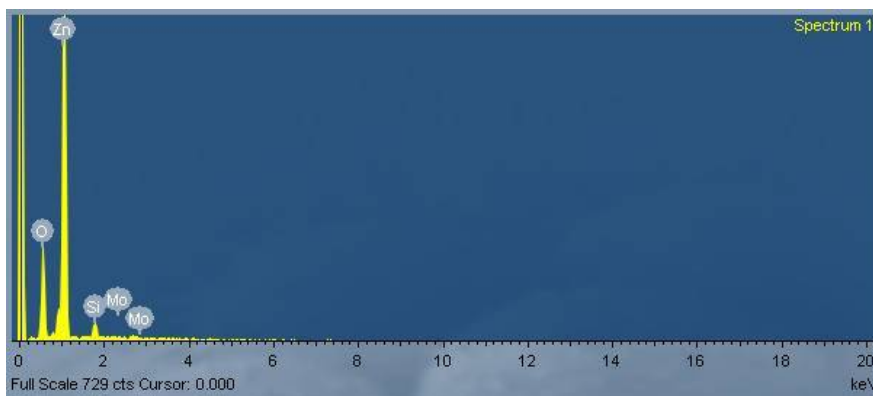


Fig. 10 EDS spectrum of Mo-doped ZnO nanowires

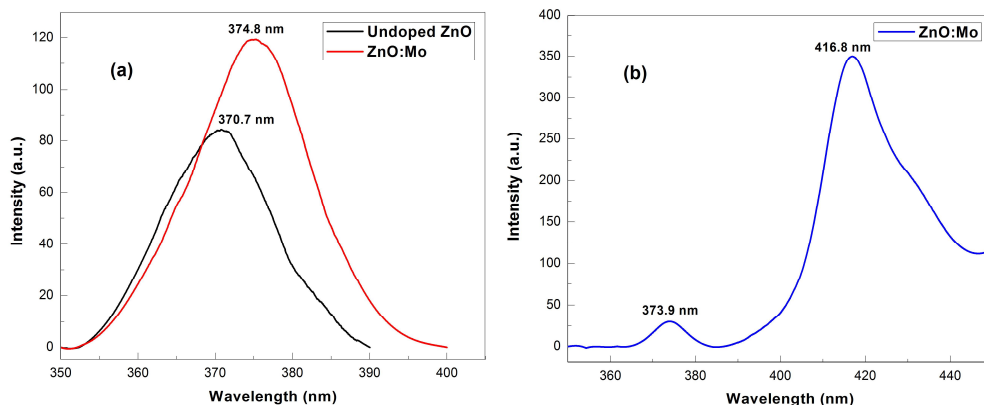


Fig. 11. Room temperature (a) near band edge emissions of undoped ZnO and ZnO:Mo (b) PL spectrum of Zn:Mo NWs ($\lambda_{ex} = 325$ nm)

The PL measurements were performed to evaluate the optical quality of the obtained ZnO NWs. Fig.11 shows typical room temperature photoluminescence (PL) spectra of ZnO NWs with an excitation wavelength of 325 nm at room temperature. It could be seen that the PL spectrum of the undoped ZnO NWs exhibits a dominant UV emission at 370.7 nm (3.34 eV) while Mo doped NWs show strong UV emission at 374.8 nm (3.31 eV). The UV emission can be ascribed to the near band edge emission of the wide band gap of ZnO. It was observed that the doping ZnO with MoO₃ decreases the optical band gap of the resulting material. Figure 11 (b) shows PL spectrum of Mo doped ZnO NWs which include the intense band to band emission corresponding to MoO₃ at 416.8 nm (2.97 eV) along with the band edge emission at around 373.9 nm (3.31 eV).

Fig. 12 shows the I-V characteristics of the *n*-ZnO NWs/p+-Si substrate heterostructure of ZnO without and with Mo doping. The I-V relationship for a heterojunction is given by:

$$I = I_s \left[\exp\left(\frac{qV}{k_B T}\right) - 1 \right]$$

where I is the current; I_s the saturation current; V , the applied voltage across the heterojunction from p-side to n-side; k_B , the Boltzmann constant; and T is the absolute temperature. The typical rectifying behavior of device could clearly be observed. The forward current increases more rapidly for doped device than that of the undoped one. There was no emission in the visible region because the diode currents were of the order of tenths of μA for large material resistance ($\sim 10^6 \Omega$).

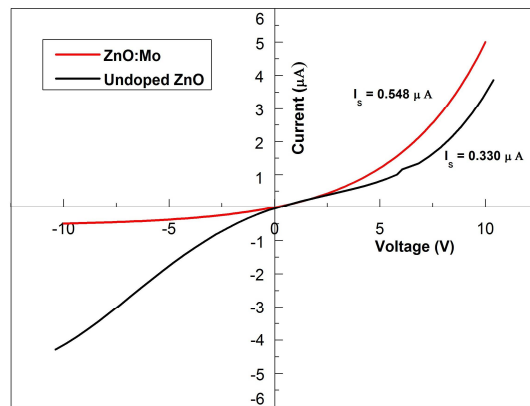


Fig. 12. I-V characteristics of the n-ZnO nanowires/p⁺-Si substrate heterostructure of ZnO without and with Mo doping

The low threshold for undoped device under reverse bias could be ascribed to the band alignment of the p-Si/n-ZnO heterojunction at the interface. Further, the series resistance (R_s) for the undoped and doped samples were found to be 38.9 M Ω and 11.8 M Ω respectively. The R_s can be obtained by calculating the slope in an $I/(dI/dV)$ versus I graphs in the high voltage region ($V > E_g/q$, where E_g is energy band gap) of the I - V characteristic curves.

3. Fabrication of n-ZnO/p-GaN on heterojunction Light Emitting Diode

We grew p-GaN epitaxial graphene layer on commercially available c-plane Al₂O₃ substrates. Van der Pauw measurements were performed at 300 K to confirm the free hole carrier concentration. Following this, the ZnO seed layer was prepared by using either simple chemical route or by RF sputtering. In simple chemical method, a 10 mM seed layer solution of zinc acetate dehydrate and 2-propanol was first prepared and then spin coated on p-GaN/Al₂O₃ substrates at 2000 rpm for 30 s. The substrates were then annealed at 100°C for 1 min after each spin coating to enhance adhesion. A uniform seed layer was obtained after five layers of spin coating.

1D Nanowire arrays were fabricated by radio frequency (RF) magnetron sputtering on p-GaN, following an insulating polystyrene/spin of glass film was deposited by spin coating to fill the space between the nanowires homogeneously in order to insulate the uncovered p-GaN areas and to overcome multiple scattering losses of photons which can improve the extraction efficiency of device structure. Then, indium tin oxide (100nm) and Ni/Au (30/30nm) are deposited on n-ZnO and p-GaN as n- and p-electrodes, respectively, to form LED structure. The current voltage characteristic of the fabricated LED structure is shown in Figure 13, which ensure the formation of p-n junction between n-ZnO and p-GaN. The LED structure exhibits a strong rectification behavior with turn ON voltage of 2.9V, which offers the possibility of light emission. However, the light emission was very poor and detected by EL measurements with weak intensity. We suspect that the presence of non-passivated surface defects in the nanowalls might alter the electron injection and therefore recombination mechanism could be strongly suppressed. However, we employ a novel approach by passivating the surface

defects by depositing PMMA polymer to enhance the recombination rate of the electron-hole pair at the heterojunction and this research is extensively going on in our laboratory.

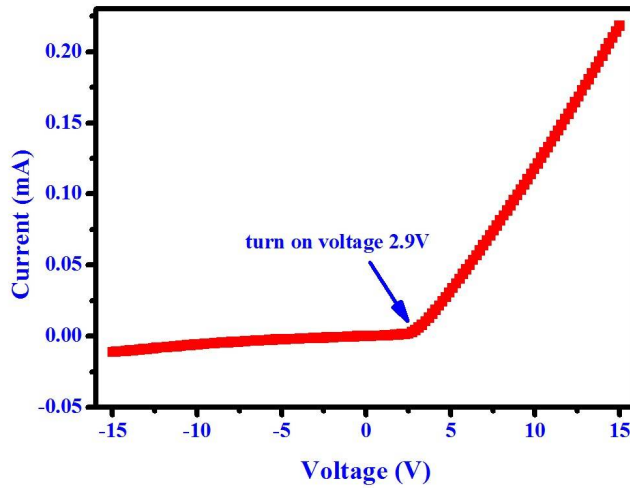


Fig.13: Room temperature I-V characteristics of the LED structure.

Summary

In summary, vertically aligned ZnO nanowires have been grown successfully on silicon (111) and p-type GaN epitaxial layers by rf-sputtering under optimized growth parameters. The diameter, length and density distributions of the nanowires under different growth durations indicate that the growth of the nanowires governed by the migration length of adatoms which strongly influenced by pressure and temperature. The structural study of the nanowires illustrates the highly crystalline nature and hexagonal wurtzite structure of the nanowires with preferential orientation along the c-axis. The characteristics of E_2^{high} phonon mode corroborates with the XRD results of high crystalline quality with strain free nature of ZnO nanowires. A blue shift of $A_1(\text{LO})$ phonon mode along with broad band edge PL emission confirm the enhancement of the free carrier concentration in the nanowires due to the point defects. The pre-dominant green emission at 2.28 eV is attributed to the electron transitions between shallow donor (V_{O}) and shallow acceptor (V_{Zn}) energy levels. The I-V curves of the resulting n-ZnO NWs /p⁺-Si heterostructure exhibit p-n junction diode characteristics. Further, n-ZnO/p-GaN hybrid LED device structure shows strong rectification behavior confirming p-n junction with low turn on voltage (2.9 V). However, the emission intensity and peak wavelength from CL need to be improved. In future, the diode characteristics will be improved to realize visible emission from the hybrid LED.

References:

1. D. Appell, *Nature* 419, 553 (2002).
2. L. Samuelson, *Materials Today* 6, 22 (2003).
3. X. Duan, Y. Huang, Y. Cui, J. Wang and C. M. Lieber, *Nature* 409, 66 (2001).
4. Y. Cui, Q. Wei, H. Park, and C. M. Lieber, *Science* 293, 1289 (2001).
5. K. S. Shankar and A. K. Raychaudhuri, *Mater. Sci. and Engg. C* 25, 738 (2005).
6. Z. L. Wang, *Adv. Mater.* 12, 1295 (2000).
7. G. C. Yi, C. R. Wang and W. I. Park, *Semi. Sci. Technol.* 20, S22 (2005).
8. Wang, Z. L. *ACS Nano*, 2, 1987 (2008).
9. W.I. Park and G. C. Yi *Adv. Mater.* 16, 87 (2004).
10. P.H. Yeh, Z. Li and Z. L. Wang, *Adv. Mater.* 21, 4975 (2009).
11. M. Law, L.E. Greene, J. C. Johnson, R. Saykally and P. D. Yang *Nat. Mater.* 4, 455 (2005).
12. Y. Zhang, C. Wu, Y. Zheng and T. Guo, *J. Semicond.* 33, 023001 (2012).
13. W.T. Chiou, W. Y. Wu and J. M. Ting, *Diam. Relat. Mater.* 12, 1841 (2003).
14. D. J. Lee, J. Y. Park, Y. S. Yun, Y. S. Hong, J. H. Moon, B. T. Lee and S. S. Kim, *J. Cryst. Growth*, 276, 458 (2005).
15. J. H. Tian, J. Hu, S. S. Li, F. Zhang, J. Liu, J. Shi, X. Li, Z. Q. Tian and Y. Chen, *Nanotechnology*, 22, 245601 (2011).
16. W. B. Wu, G. D. Hu, S. G. Cui, Y. Zhou and H. T. Wu, *Cryst. Growth Des.* 8, 4014 (2008).
17. Y. G. Wei, W. Z. Wu, R. Guo, D. J. Yuan, S. M. Das and Z. L. Wang, *Nano Lett.* 10, 3414 (2010).
18. J. J. Dong, X. W. Zhang, Z. G. Yin, S. G. Zhang, H. R. Tan, J. X. Wang, Y. Gao, F. T. Si, H. L. Gao, *ACS Appl. Mater. Interfaces* 3, 4388 (2011).
19. Y. J. Lee, T. L. Sounart, J. Liu, E. D. Spoeke, B. B. McKenzie, J. W. P. Hsu, J. A. Voigt, *Cryst. Growth Des.* 8, 2036 (2008).
20. X. Xiu and W. Zhao, *Chin. Phys. B* 21, 066802 (2012).
21. U. Ozgur, Y. Alivov, C. Liu, A. Teke, M. A. Reshchikov, S. Dogan, V. Avrutin, S. J. Cho and H. Morkoc, *J. Appl. Phys.* 98, 041301 (2005).
22. D. C. Look, *Mat. Sci. Eng. B. Adv.* 80, 383 (2001).
23. K. U. Rempel, A. A. Migdisov, A. E. Williams-Jones, *Geochimica et Cosmochimica Acta* 70, 687 (2006).
24. A. Chithambararaj and A. C. Bose, Beilstein, *J. Nanotechnol.* 2, 585 (2011).
25. S.M. Sze, *Physics of Semiconductor Devices*, Wiley, New York, (1981).
26. S.H. Dahal, D.L. Baptisa, K.B.K. Teo, R.G Lacerda, D.A. Jefferson and W.I. Milne, *Nanotechnology*, 17, 4811-4818, (2006).
27. P. Sundara Venkatesh, V. Ramakrishnan and K. Jeganathan, *CrystEngComm.*, 2012, DOI:10.1039/C2CE25220A
28. O. Lupan, V.M. Guérin, I.M. Tiginyanu, V.V. Ursaki, L. Chow, H. Heinrich and T. Pauporté, *J. Photoch. Photobio. A*, 2010, 211, 65 - 73.
29. K. Jeganathan, R. K. Debnath, R. Meijers, T. Stoica, R. Calarco, D. Grützmacher and H. Lüth, *J. Appl. Phys.*, 2009, 105, 123707.

Contribution to the Society

LEDs are an emerging technology in today's electronic display and lighting applications. The use of LEDs in lighting technology is described as Solid State Lighting, which is a new emerging concept in light technology as LED lamps are intense, energy efficient, environment friendly and no toxic chemicals involved in this process. The development of Nanowire based LEDs will be great breakthrough for domestic display and lighting applications. We have achieved NWs based LEDs in intense white light like emission. Further, our current activity is focused onto enhance the characteristics of the emission with low turn on voltage suitable for lighting applications.

List of Publications

1. P. Sundara Venkatesh, V. Ramakrishnan, and **K. Jeganathan** (2013): Investigations on the growth of manifold morphologies and optical properties of ZnO nanostructures by radio frequency magnetron sputtering, *AIP Advances*, 3, 082133.
2. P. Sundara Venkatesh, V. Ramakrishnan, and **K. Jeganathan** (2013): Investigations on the growth and optical properties of one dimensional ZnO nanostructures grown by radio frequency magnetron sputter deposition, *Mater. Res. Bull.*, 48, 3811 - 3816.
3. P. Sundara Venkatesh, and **K. Jeganathan** (2013): Investigations on the growth and characterization of vertically aligned zinc oxide nanowires by radio frequency magnetron sputtering, *J. Solid State Chem.*, 200, 84 - 89.
4. P. Biswas and **K. Jeganathan** (2015): Hydrothermal synthesis of one dimensional Mo-doped n-type ZnO nanowires on p-type Si substrate, *Materials Focus* (American Scientific Publishers), 4,366.
5. P. Sundara Venkatesh, V. Ramakrishnan, and **K. Jeganathan** (2016): Raman silent modes in vertically aligned undoped ZnO nanorods, *Physica B: Condensed Matter* 481, 204-208.

Investigations on the growth of manifold morphologies and optical properties of ZnO nanostructures grown by radio frequency magnetron sputtering

P. Sundara Venkatesh, V. Ramakrishnan, and K. Jeganathan

Citation: *AIP Advances* **3**, 082133 (2013); doi: 10.1063/1.4820386

View online: <http://dx.doi.org/10.1063/1.4820386>

View Table of Contents: <http://aipadvances.aip.org/resource/1/AAIDBI/v3/i8>

Published by the AIP Publishing LLC.

Additional information on AIP Advances

Journal Homepage: <http://aipadvances.aip.org>

Journal Information: <http://aipadvances.aip.org/about/journal>

Top downloads: http://aipadvances.aip.org/features/most_downloaded

Information for Authors: <http://aipadvances.aip.org/authors>

ADVERTISEMENT



www.goodfellowusa.com

Goodfellow

metals • ceramics • polymers • composites

70,000 products

450 different materials

small quantities *fast*

Investigations on the growth of manifold morphologies and optical properties of ZnO nanostructures grown by radio frequency magnetron sputtering

P. Sundara Venkatesh,¹ V. Ramakrishnan,² and K. Jeganathan^{1,a}

¹Centre for Nanoscience and Nanotechnology, School of Physics, Bharathidasan University, Tiruchirappalli-620 024, Tamilnadu, India.

²Department of Laser Studies, School of Physics, Madurai Kamaraj University, Madurai-625 021, Tamilnadu, India.

(Received 16 June 2013; accepted 21 August 2013; published online 29 August 2013)

The growth of ZnO nanostructures under various combinations of argon and oxygen pressures by radio frequency magnetron sputtering has been reported. The anisotropic transformation of nanostructures from the vertical standing nanorods to self branched lateral nanowires has been observed due to the change in the migration length of the adatoms owing to the deposition pressure and temperature. A dominant (002) reflection having narrow full width at half maximum of the vertical standing nanorods depicts the preferential orientation along c-axis of wurtzite ZnO with high crystalline nature. It is further substantiated by a sharp E_2^{high} phonon mode of ZnO nanorods at 437.2 cm^{-1} . A broad green emission at 2.28 eV pertaining to oxygen vacancies that quenches with increasing the oxygen pressure due to the compensation of oxygen vacancies while zinc vacancy mediated emission at 3.01 eV is enhanced. © 2013 Author(s). All article content, except where otherwise noted, is licensed under a Creative Commons Attribution 3.0 Unported License. [<http://dx.doi.org/10.1063/1.4820386>]

I. INTRODUCTION

Zinc oxide (ZnO) is one of the most fascinatingly studied metal oxide semiconductors due to its unique physical and chemical properties. ZnO has attracted the research community to consider it as a most promising material for the fabrication of various optoelectronic devices due to its wide band gap of 3.37 eV with large exciton binding energy (60 meV).¹⁻³ Manifold ZnO nanostructures such as nanowires,⁴ nanoribbons,⁵ nanoflowers,⁶ nanosheets,⁷ nanofibres⁸ and nanobelts⁹ have been fabricated by various deposition techniques with different growth approaches such as vapor liquid solid (VLS) and vapor solid (VS) transformation in which the former approach utilizes the external catalyst to manipulate the anisotropic growth of nanostructures. In VLS approach, the catalyst remain on the apex of the nanostructures and likely to incorporate as a foreign atoms into the growing lattice. This catalytic droplet is an undesirable external impurity for the fabrication of devices and the incorporated foreign atoms into the host material also reduce the efficiency of the devices.^{10,11} Hence, an alternative approach is essential for the fabrication of nanostructures without any external catalyst which is possible by VS approach. Therefore, the VS approach has received a great attention for the fabrication of high quality nanostructures.

Among the various dimensional ZnO nanostructures, the fabrication of one dimensional (1D) ZnO nanostructures have received a tremendous attention due to its increased surface area and fundamental building blocks for future nanoscale devices. It is well known that the evolution of 1D nanostructures depends on the growth parameters. Recently, it is observed that the surface

^aAuthor to whom correspondence should be addressed. Postal address: Dr. K. Jeganathan, Associate Professor, Centre for Nanoscience and Nanotechnology, School of Physics, Bharathidasan University, Tiruchirappalli-620 024, Tamilnadu, India. Phone: +91-431-2407 057. Fax: +91-431-2497 045, 2407 020. E-mail: kjeganathan@yahoo.com

morphologies of the nanostructures are also affected by the variations in the miscut angle of substrates.¹² Various deposition techniques have employed for the fabrication of different morphological nanostructures by tuning the growth parameters, but the radio frequency (rf) magnetron sputtering is one of the least investigated techniques for the growth of nanostructures where as it is widely employed for the deposition of thin films. Further, it is one of the controlled deposition techniques in terms of scale-up and mass production¹³ which makes it an effective economic approach for the industrial applications. Hence, many research groups have paid their attention on the growth of 1D nanostructures using the rf-magnetron sputtering due to its excellent properties of materials since the growth was carried out under vacuum condition.^{14–18}

In recent years, ZnO nanowires were grown on the interlayer (Cu/Ti) coated substrates and reported that the surface morphologies of the nanostructures depends on the interlayer.^{19–21} Further, it was observed that the crystalline nature of the nanowires was enhanced from polycrystalline to single crystalline by the introduction of oxygen into the chamber, but there are no noticeable changes in the surface morphology of the nanowires.¹⁹ In addition, it is reported that the evolution of nanostructures such as nanowires and nanobelts depends on the deposition rate of the materials.²² It is obvious that the deposition rate depends on many growth parameters such as deposition pressure, substrate temperature, rf-power and target–substrate distance. Moreover, it is inversely proportional to the deposition pressure due to the increased number of collisions between the sputtered molecules/atoms and gas molecules. The deposition pressure is expected to affect the growth of the nanostructures through the variations in the migration length of the adatoms. Further, there are no reports on the evolution of ZnO nanostructures with respect to deposition pressure and substrate temperature by rf-magnetron sputtering. Therefore, it is motivated to investigate the evolution of ZnO nanostructures according to the growth parameters such as deposition pressure and substrate temperature.

The present work exemplifies the fabrication of manifold 1D nanostructure by means of manipulating the migration length of the adatoms by varying the growth parameters such as substrate temperature and rf-power with the combinations of argon and oxygen pressures using rf-magnetron sputtering. The anisotropic transformation of nanostructures from the vertical standing nanorods to self branched lateral nanowires has been observed and its growth mechanism based on the atomistic transport is briefly discussed. The optical transitions in manifold morphologies have been investigated by the low temperature photoluminescence (LTPL) studies and further the various energy levels of emission are analyzed and correlated with the point defects.

II. EXPERIMENTAL SECTION

ZnO nanostructures were grown on n-type silicon (111) substrates with a vicinal off-angle of $\sim \pm 0.5^\circ$ under various combinations of argon and oxygen pressures by the rf-magnetron sputtering. The details of the growth conditions are described elsewhere.²³ The deposition of ZnO nanostructures was carried out under various substrate temperatures of 350, 450 and 550 °C and pressures of 0.01, 0.05 and 0.1 mbar respectively. The target-substrate distance (~ 50 mm) and rf-power (60 W) were kept as constant. The deposition rate and thickness of the deposited ZnO on the substrates were monitored by *in-situ* quartz crystal oscillator located near to the substrate holder during the deposition processes. The sputtering rate of the materials at the substrate temperature of 550 °C was reduced from 2.1 (at 0.01 mbar) to 0.3 Å/sec (at 0.1 mbar) with the increase of deposition pressure owing to the large number of collisions.

The surface morphology of the samples was examined using a field emission scanning electron microscope (FESEM, Carl Zeiss - Sigma) with a maximum resolution of 1.2 nm. The crystalline nature and phase orientation of the ZnO nanostructures were analyzed by a Rigaku X-ray diffractometer with CuK_α radiation of wavelength $\lambda = 1.5406$ Å. Room temperature micro-Raman spectra of ZnO nanostructures were recorded in the back scattering geometry using a LabRam HR800 Raman spectrometer. The wavelength of 632.8 nm He–Ne laser was used as an excitation source and the laser beam was focused through a microscope (100X) with a spot size of ~ 1 μm . LTPL measurements were performed using a HORIBA JOBIN YVON monochromator (0.55 m) with the samples placed inside a closed cycle helium cryostat and 325 nm He–Cd laser was used as an

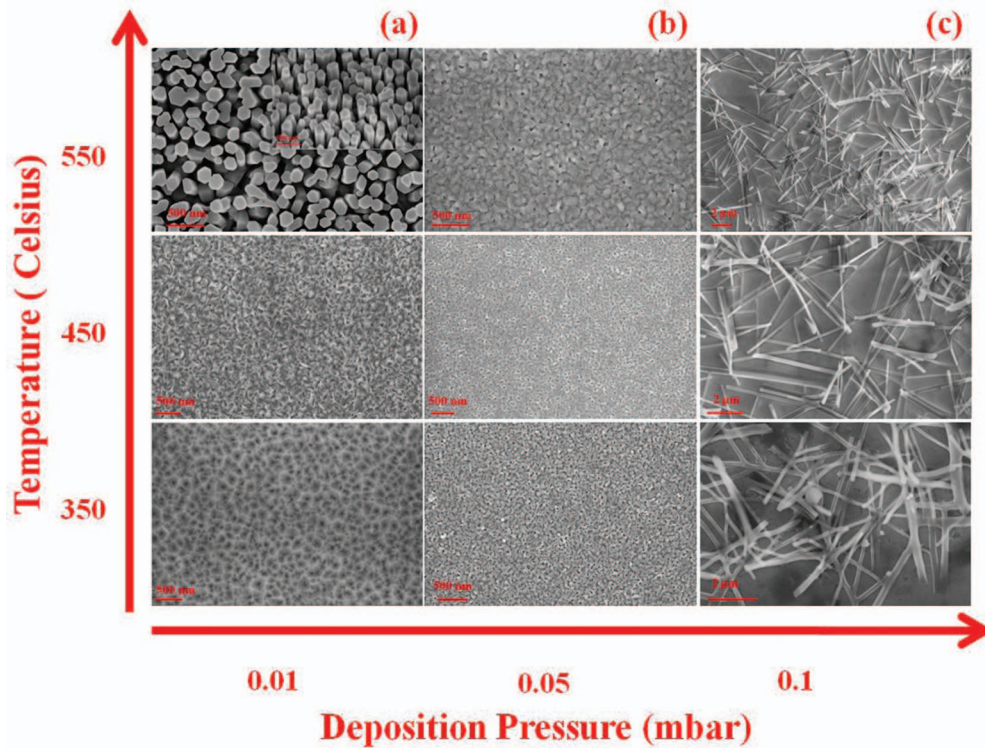


FIG. 1. FESEM images of the ZnO nanostructures grown under various substrate temperatures (350, 450 and 550 °C) and deposition pressures (0.01, 0.05 and 0.1 mbar). The inset of Fig. 1(a) shows 45° tilted view of the vertically aligned ZnO nanorods.

excitation light source. The luminescence signal from the sample was collected by a charge coupled device through an appropriate optical arrangement.

III. RESULTS AND DISCUSSION

Fig. 1 shows the FESEM images of ZnO nanostructures grown under various substrate temperatures and pressures by the rf-magnetron sputtering. The substrate temperature and pressure are varied from 350 to 550 °C and 0.01 to 0.1 mbar respectively, while the rest of the growth parameters are kept constant including the growth duration (60 min). The morphological evolution of ZnO nanostructures under various substrate temperatures and deposition pressures are analyzed.

Under pure argon pressure of 0.01 mbar, the deposition is carried out under various substrate temperatures from 350 to 550 °C. Up to the substrate temperature of 450 °C, thin film like structures are formed with rough surfaces as shown in Fig. 1(a). The thickness of the films deposited under various substrate temperatures of 350 and 450 °C are 459 and 447 nm respectively. Further increasing the substrate temperature to 550 °C, the vertical standing ZnO nanorods with perfect hexagonal cross section have been observed as shown in Fig. 1(a). The inset clearly depicts the cross sectional view of the vertically aligned ZnO nanorods on the silicon substrate. The average diameter and length of the nanorods are ~ 164 and 750 nm respectively and their density is $\sim 3 \times 10^9$ nanorods/cm². In order to understand the influence of oxygen pressure on the morphological evolution, the oxygen gas is introduced into the chamber through a needle valve while the argon pressure is kept constant at 0.01 mbar. In the (argon + oxygen) deposition pressure of 0.05 mbar, thin film like morphology with smooth surfaces is observed under various substrate temperatures from 350 to 550 °C due to the stoichiometric growth condition as shown Fig. 1(b). The thickness of the films is reduced to ~ 240 nm for the deposition pressure of 0.05 mbar at 550 °C. It is observed that the thickness of the film is decreased as compared to the film deposited under the pressure of 0.01 mbar due

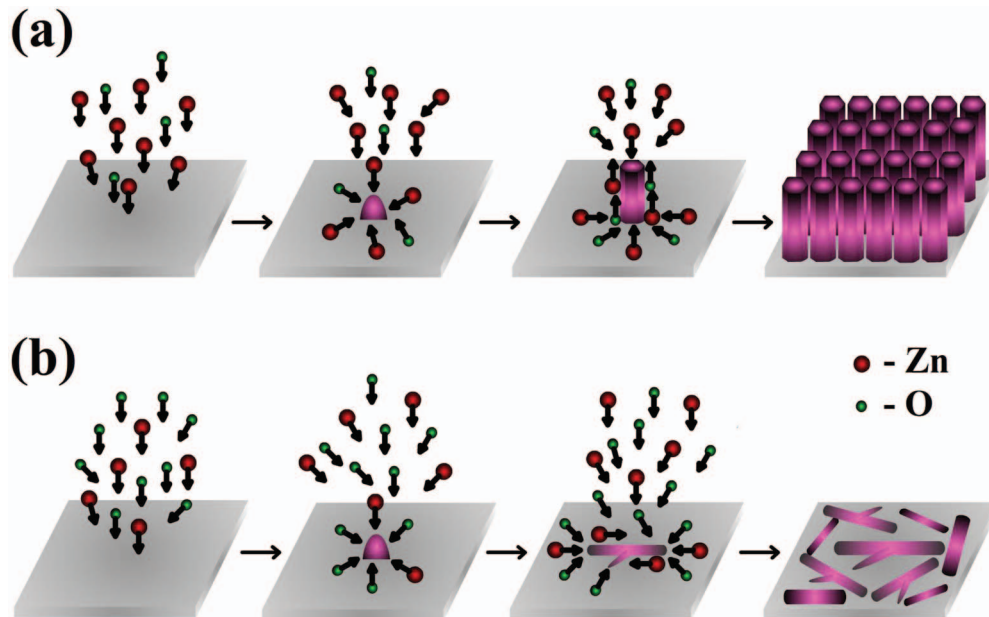


FIG. 2. Schematic representation of 1D ZnO nanostructures growth without any external catalyst.

to the increased number of collisions by increasing the deposition pressure. This evidences that the deposition rate of the materials decreases with the pressure. Further increasing the oxygen pressure to 0.1 mbar, the nanowires grew laterally along the surface of the substrates under various substrate temperatures from 350 to 550 °C as shown Fig. 1(c). The variation in the aspect ratio of the nanowires with the substrate temperature indicates that the surface mobility as well as condensation of the adatoms has strong impact on the growth rate of the nanowires with respect to the growth temperature. This clearly depicts that there is a strong correlation between the substrate temperature and aspect ratio of the nanowires. The length of the nanowires grown under the substrate temperatures of 350 and 550 °C are ~ 4.8 and $7.5 \mu\text{m}$ with the corresponding diameters of ~ 385 and 290 nm respectively. The length of the nanowires is inversely proportional to its diameter ($L \propto 1/D$) and this relation is consistent with earlier report.²⁴

It is observed that the anisotropic growth transformations have occurred from vertical standing nanorods to lateral nanowires with increase in the deposition pressure (0.01 to 0.1 mbar) for the substrate temperature of 550 °C owing to the changes in the adatom mobility which strongly depends on the deposition pressures. Hence, a detailed investigation is extended to the ZnO nanostructures grown at 550 °C under the deposition pressures of 0.01, 0.05 and 0.1 mbar to understand the growth mechanism, structural and optical properties of the nanostructures.

The schematic representation of the growth mechanism for the vertical standing nanorods and self branched lateral nanowires is shown in Fig. 2. The observed nanostructures illustrate that the deposition pressures could provoke the anisotropic manifold structures under vapor solid mechanism via the variations in migration length of the adatoms.

In the vapor deposition techniques, the adatoms can contribute the growth by the direct impingement and migration through the sidewalls of the nanostructures.²⁵ In the case of direct impingement of adatoms on a tip of the nanorods; the growth rate is reduced for the smaller diameter nanorods and vice versa due to the Gibbs–Thomson effect. But, in the case of surface migration of the adatoms through the side walls of the nanorods along with direct impingement, the growth rate is higher for the thinner nanorods and vice versa.²⁴ Further, the growth of the nanostructures will be enhanced only if the length of the nanostructures is smaller than the migration length, otherwise it will be desorbed from the surface of the nanostructures. This suggests that the migration length of adatoms vary with the deposition pressure and it is high for the low deposition pressure (0.01 mbar). Further, the number of adatoms reaching the growth fronts under low deposition pressure is also high due to

the reduced number of collisions. Hence, this elevated number of adatoms with high migration length promotes the axial growth by the process of sidewall diffusion along with the direct impingements as shown in Fig. 2(a). But, in the oxygen rich condition with 0.1 mbar of deposition pressure, the adatom mobility of zinc is drastically reduced which increases the reactivity of zinc adatoms with oxygen that facilitates the formation of localized ZnO nuclei by reducing the surface energy. The incoming radicals on the growth front are confined on the nucleated dots which decide the diameters and the resultant 1D nanostructures. At the high deposition pressure, the migration length of adatoms and the number of adatoms reaching the growth fronts are also reduced due to the increased number of collisions. This reduced number of adatoms with small migration length leads to the lateral growth of the nanostructures which is schematically shown in Fig. 2(b). Further, the secondary nucleation is initiated on the surface of the nanowires and the self branched lateral nanowires have grown due to the reduced migration length of zinc adatoms under oxygen rich deposition pressure.

The migration length of the adatoms generally depends on many factors such as pressure and nature of the gases present in the chamber. In order to substantiate this, we compare the growth of 1D ZnO nanostructures under various argon sputtering pressures with the similar conditions. The diameter of the nanostructures increases with the argon sputtering pressure due to the decrease in migration length of adatoms which is expected to enhance the lateral growth by the increased number of collisions.²⁶ Further, the vertical standing nanorods are slightly deviated from its orientation with increasing the argon pressure. In this case, the argon sputtering pressure reduces the migration length of the sputtered molecules only by the collisions because it is an inert gas, does not participate in the chemical reaction. But, in the oxygen deposition pressure, the migration length of adatoms will be reduced in two ways i) by the collisions with the sputtered molecules/atoms and ii) by the reaction with the sputtered molecules/atoms. Consequently, the number of adatoms reaching the growth fronts and its migration length are considerably reduced as compared to the deposition carried out under argon pressure of 0.1 mbar. Hence, the migration length and the number of adatoms reaching the growth front play a crucial role on the anisotropic transformation of nanostructures with respect to the deposition pressure.

Fig. 3 shows the XRD patterns of ZnO nanostructures grown on silicon (111) substrates under pure argon and various combinations of argon and oxygen pressures. The dominant (002) reflection of the nanostructures grown under the pressures of 0.01 and 0.05 mbar indicates the preferential orientation along c-axis with hexagonal wurtzite crystal structure. The (002) peak position (34.398°) of the vertical standing nanorods is slightly shifted to the lower angle side from its standard bulk counterpart (JCPDS-36-1451). It represents that the nanorods are compressively strained. The higher angle side shift of the (002) peak about 0.102° for the thin films grown under the deposition pressure of 0.05 mbar confirms the presence of the tensile strain. The observed results corroborate with the earlier reports that the deposition pressure has a strong influence on the strain.^{27,28} It is obvious that the lattice mismatch between ZnO and the silicon substrate is about 40% and it will affect the crystalline nature of the nanostructures by the introduction of strain according to its footprints. In the case of thin films grown under the deposition pressure of 0.05 mbar, it is fully spread over the substrate whereas the nanorods grown under the deposition pressure of 0.01 mbar have smaller footprints on the substrate. Hence, the nanorods have high crystalline nature as compared to the thin films due to its smaller foot prints. The narrow full width at half maximum (FWHM) of the vertical standing nanorods (0.180°) as compared to the thin films (0.214°) substantiates the high crystalline quality of the nanorods. In the deposition pressure of 0.1 mbar, the density of the self branched laterally aligned ZnO nanowires on the silicon substrate is low as shown in Fig. 1(c). Consequently, the diffraction signal is expected to be very weak and results no diffraction peaks to the detection limit of a XRD detector as shown in Fig. 3(c).

Micro-Raman spectra of ZnO nanostructures are recorded in the back scattering geometry and depicted in Fig. 4. The observed peaks at 99 and 437 cm^{-1} are attributed to the E_2 (low) and E_2 (high) phonon modes respectively. The dominant E_2 (low) phonon mode at $\sim 99.76\text{ cm}^{-1}$ with narrow FWHM (1.6 cm^{-1}) indicates the high optical properties and is attributed to the lattice vibrations of the zinc atoms. E_2 (high) phonon mode around at 437 cm^{-1} is a characteristic peak of wurtzite ZnO and attributed to the lattice vibration of oxygen atoms.²⁹ Hence, the investigation of E_2 (high) mode should yield useful information about the crystalline nature of the nanostructures.

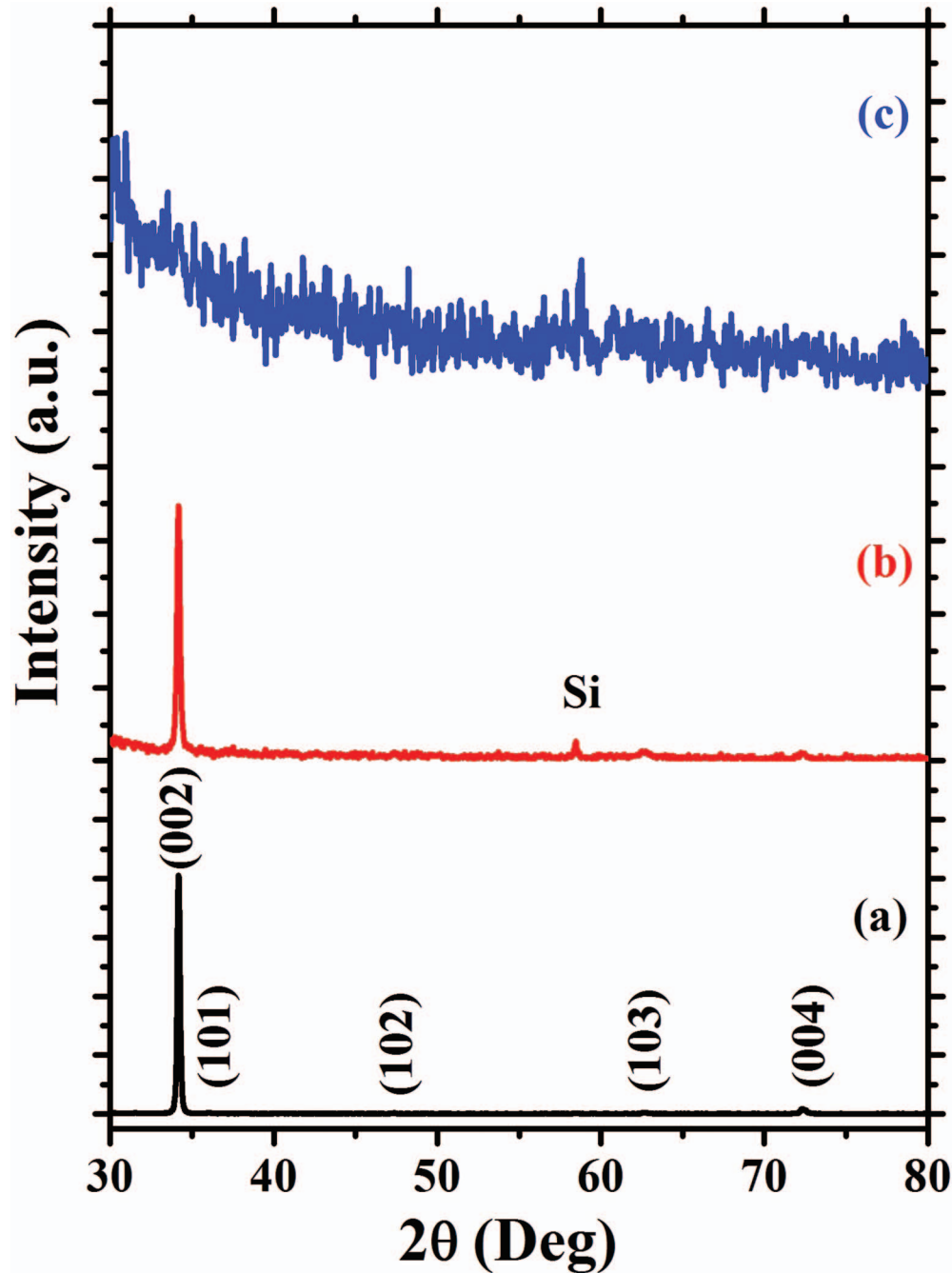


FIG. 3. XRD pattern of the ZnO nanostructures grown under various pressures (a) 0.01 mbar, (b) 0.05 mbar and (c) 0.1 mbar at 550°C

E_2 (high) phonon mode of the vertically aligned ZnO nanorods is observed at 437.2 cm^{-1} which is in good agreement with the bulk ZnO crystal.³⁰ It reveals the high crystalline nature of the nanorods with hexagonal wurtzite crystal structure which is further confirmed by the narrow FWHM of E_2 (high) phonon mode ($\sim 8\text{ cm}^{-1}$). However, it experiences a small compressive strain since it is blue shifted about 0.2 cm^{-1} from its standard value (437 cm^{-1}) and consistent with the XRD results. E_2 (high) peak positions of the thin films and nanowires grown under the deposition pressures of 0.05 and 0.1 mbar at 550°C are 434.57 and 436.3 cm^{-1} respectively. It represents

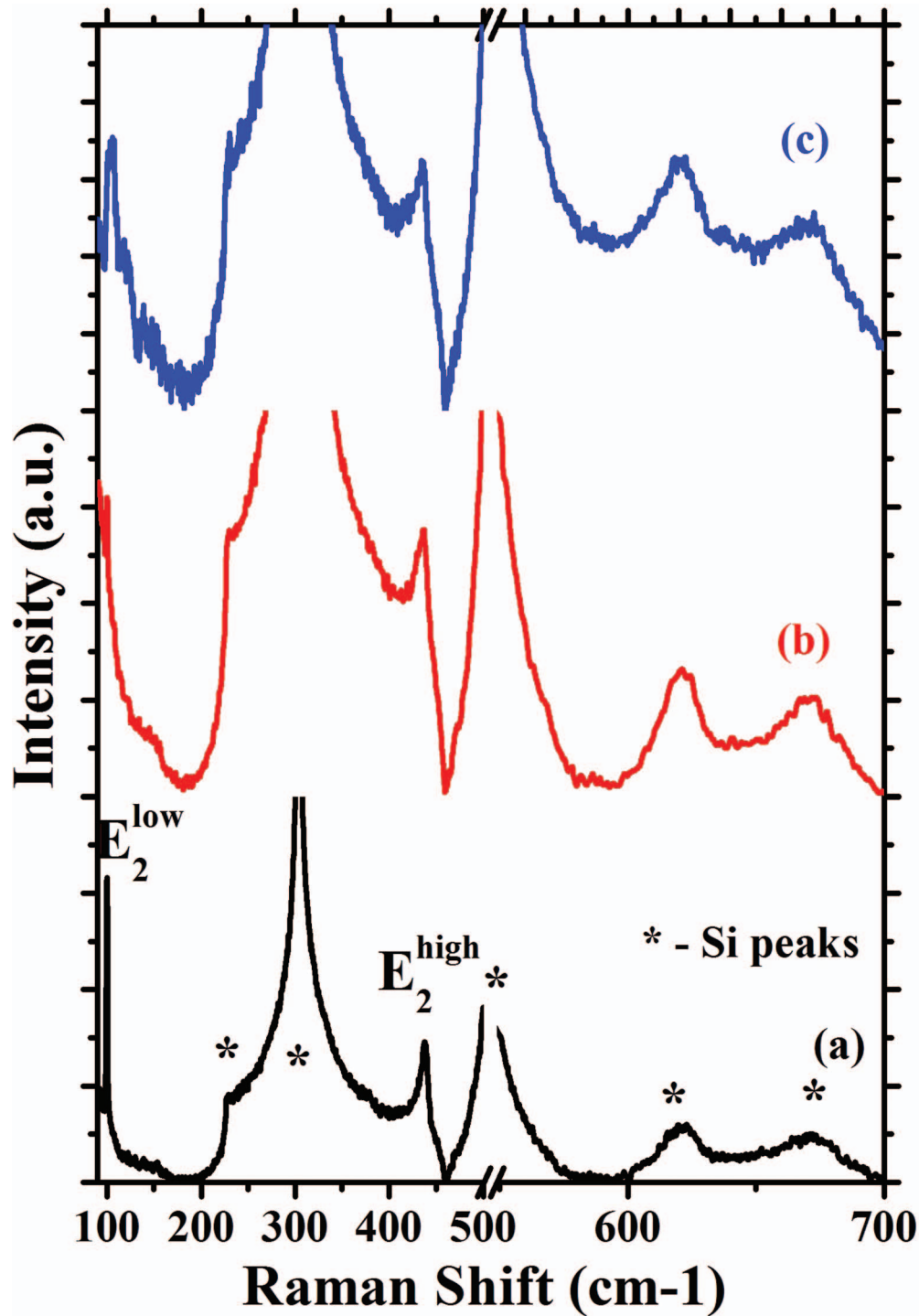


FIG. 4. Micro-Raman spectra of the ZnO nanostructures recorded in the back scattering geometry using He-Ne laser (632.8 nm) as an excitation source. (a) 0.01 mbar, (b) 0.05 mbar and (c) 0.1 mbar

that E_2 (high) phonon mode of the thin films and nanowires grown under various combinations of argon and oxygen pressures shifts towards the red side from its standard value. This red shift of the E_2 (high) phonon mode reveals the presence of tensile strain in the nanostructures and indicates the poor crystalline nature which is further substantiated by the broad FWHM as ~ 12.3 and $\sim 11.5 \text{ cm}^{-1}$ for the thin films and nanowires respectively. The E_2 (high) peak position and FWHM of

TABLE I. E_2^{high} peak position and FWHM of ZnO nanostructures grown under various pressures (0.01, 0.05 and 0.1 mbar) at 550 °C by the rf-magnetron sputtering.

Pressure (mbar)	Peak position (cm^{-1})	FWHM (cm^{-1})
0.01 (Pure Ar)	437.2	~8.0
0.05 (Ar + O ₂)	434.6	~12.3
0.1 (Ar + O ₂)	436.3	~11.5

the ZnO nanowires grown under the deposition pressure of 0.1 mbar depict better crystalline nature as compared to the thin films due to the smaller footprints of lateral nanowires on the substrate. It well corroborates with the XRD results. It is obvious that the quality of the nanostructures depends on the foot prints of ZnO on the silicon substrates due to the large lattice mismatch between them. The variation of E_2 (high) peak position and FWHM of the nanostructures grown under pure argon and various combinations of argon & oxygen pressures are shown in Table I. The additional Raman peaks at $\sim 228, 301, 520, 620$ and 670 cm^{-1} are associated to the silicon substrate.³¹

LTPL measurements of undoped ZnO nanostructures are carried out over the temperature range of 10–300 K as shown in Fig. 5. LTPL spectra of undoped ZnO nanostructures show a UV emission located at $\sim 3.36 \text{ eV}$ which is assigned to the transition of neutral donor bound exciton (D^0X) emission.³² D^0X peak shifts monotonically towards the low energy side as the temperature increased from 10–300 K. This red shift of the UV emission over this temperature range is due to the thermal expansion of the lattice and electron-phonon interactions. Further, the intensity of D^0X emission quenches with increasing the temperature as a result of the refreezing of phonons and stimulation of non-radiative recombination processes. It was reported that the longitudinal optical (LO) phonon modes are separated by 71–73 meV.³³ Hence, the observed peaks at ~ 3.283 and 3.193 eV are assigned to 1LO and 2LO phonon replicas of D^0X emission respectively.³² Further, the peaks at $\sim 3.310, 3.237$ and 3.157 eV correspond to the donor acceptor pair (DAP), 1LO and 2LO phonon replicas of DAP respectively.³⁴ The above observed peaks are similar for the nanostructures grown under various deposition pressures such as 0.01, 0.05 and 0.1 mbar. However, we have observed that there are changes in the visible emissions of the nanostructures according to the argon & oxygen deposition pressures. Generally, in the undoped ZnO, the visible emissions are attributed to the consequence of intrinsic point defects such as oxygen vacancy (V_O), zinc vacancy (V_{Zn}), oxygen interstitials (O_i), zinc interstitials (Zn_i), antisites of oxygen (O_{Zn}) and antisites of zinc (Zn_O) which are depending on the growth conditions. In the intrinsic point defects, V_O, Zn_i and Zn_O are the donor type defects and V_{Zn}, O_i and O_{Zn} are the acceptor type defects. Further, the formation energies of intrinsic point defects are different from one another and also depend on the growth parameters.

Various defect mediated visible emissions are observed at 3.01, 2.86, 2.66, 2.28, 1.81 and 1.60 eV for the samples grown under various deposition pressures such as 0.01, 0.05 and 0.1 mbar. The peaks at 3.01 and 2.28 eV are quite similar for all the samples, but the intensity differs with respect to the deposition pressures. It is recognized that V_{Zn} will act as an acceptor and creates an acceptor level above the valence band. Further, it was accounted that the energy difference between the conduction band minimum and the zinc vacancy level (V_{Zn}) is about 3.06 eV.³⁵ This illustrates that the acceptor level is well above the valence band about 0.3 eV. We believe that the observed peak around at 3.01 eV is attributed to the electron transitions from the conduction band minimum to the V_{Zn} level and this transition provides a clear evidence for the presence of zinc vacancies in the nanostructures. Furthermore, the oxygen vacancies create an energy level around at 0.3–0.5 eV below the conduction band minimum and act as a donor level. A broad peak around at 2.28 eV corresponds to the green emission and indicates the presence of oxygen vacancies. This green luminescence is attributed to the electron transitions from the shallow donor level (V_O) to a shallow acceptor level (V_{Zn}).^{23,36,37} Further, the intensity quenching of green luminescence with increasing the oxygen deposition pressure from 0.01 to 0.1 mbar evidences the compensation of oxygen vacancies in the nanostructures. The intensity ratio of D^0X/VE and D^0X/GE is plotted in Fig. 6 as a function of deposition pressure. The intensity of zinc vacancy mediated emission observed

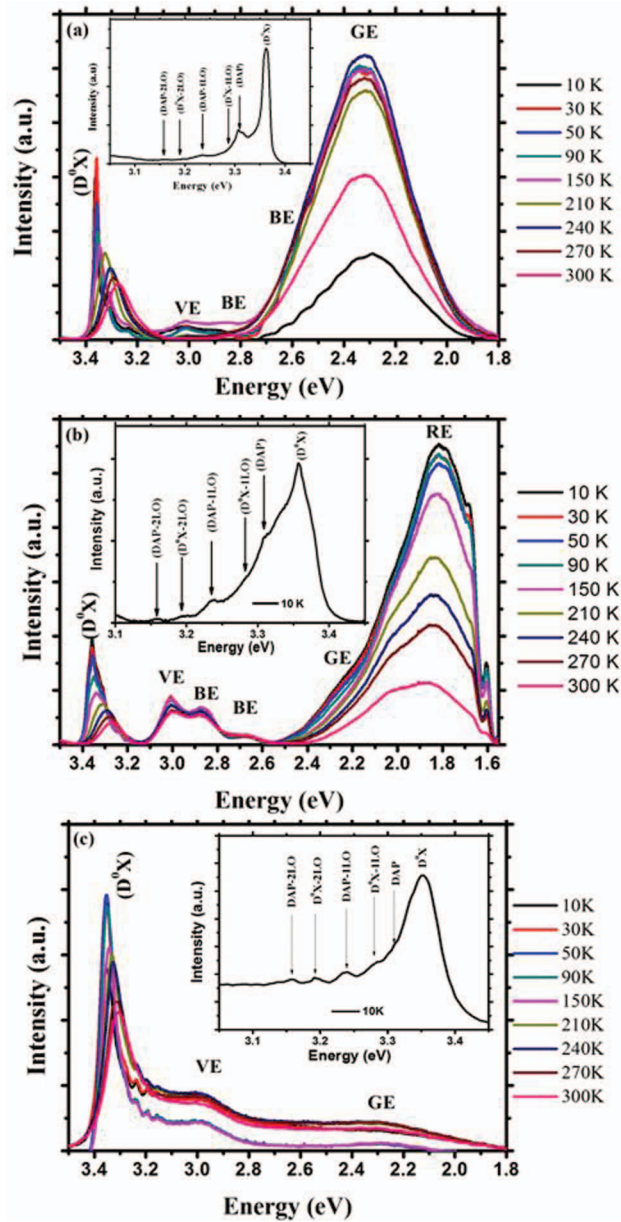


FIG. 5. Low temperature photoluminescence spectra of ZnO nanostructures grown under various pressures (a) 0.01 mbar, (b) 0.05 mbar, (c) 0.1 mbar at 550 °C and the inset depicts the corresponding enlarged view of photoluminescence spectrum at 10 K.

at 3.01 eV increases as shown in Fig. 6 which indicates the increase of zinc vacancies with the oxygen deposition pressure.³⁸

The blue emission at 2.86 and 2.67 eV are also observed for the vertical standing nanorods and thin films grown under the deposition pressures of 0.01 and 0.05 mbar respectively. Zn_i produces the shallow and deep level donors at 0.5 and 1.3 eV below the conduction band minimum. In the observed emission spectra, the peak at 2.86 eV is assigned to the transition of electrons from the shallow donor level formed by Zn_i to the valence band maximum.³⁹ Further, the additional blue emission at 2.67 eV corresponds to the transition of electrons from the conduction band to the singly ionized zinc vacancy (V_{Zn}^-).⁴⁰

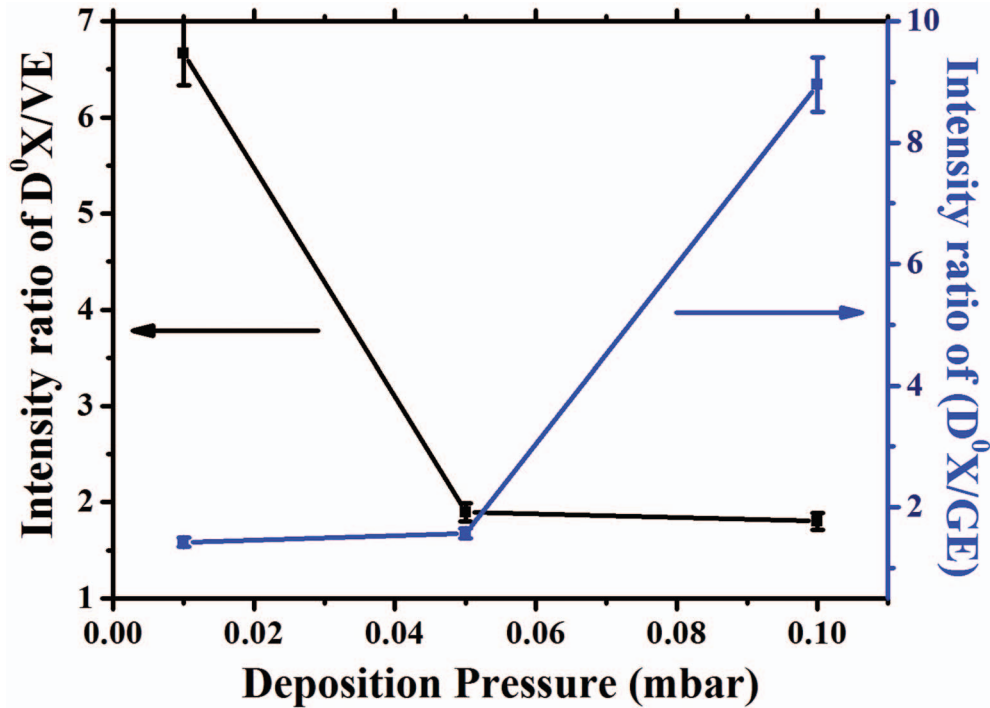


FIG. 6. Intensity variations of D⁰X/VE and D⁰X/GE as a function of deposition pressure.

Despite blue and green emissions, the red and near infrared emissions are also observed at 1.81 and 1.60 eV respectively in the thin films grown under the deposition pressure of 0.05 mbar. The intense red emission at ~ 1.81 eV can be attributed to the oxygen interstitials as corroborates with the earlier report.⁴¹ Further, this red emission is not observed in the vertically and self branched lateral ZnO nanowires grown under the pressures of 0.01 and 0.1 mbar respectively. The similar behavior is also observed in ZnO thin films deposited under O₂/Ar+O₂ ratio of 0.3³⁸ which is not observed for pure argon and higher oxygen ratio of O₂/Ar+O₂ = 1 as due to the formation of point defects not only depends on the growth temperatures, but also depends on the deposition pressures.³⁸ The additional infrared emission located at 1.60 eV, twice of D⁰X, can be attributed to the second order grating diffraction of a monochromator.⁴²

IV. CONCLUSION

ZnO nanostructures have been successfully grown on silicon (111) substrates by the rf-magnetron sputtering without any external catalyst. The anisotropic transformation of vertical to lateral nanowires takes place due to the change in the migration length of adatoms with respect to the deposition pressure. The structural and optical characterizations reveal the high crystalline nature of the vertically aligned ZnO nanorods that extremely depends on the footprints of the nanostructures on the substrates. The violet and green emissions at 3.01 and 2.28 eV confirm the presence of zinc and oxygen vacancies in the nanostructures and the oxygen vacancy mediated emission quenches with increasing the oxygen deposition pressure whereas the zinc vacancy mediated emission intensity is slightly increased.

ACKNOWLEDGMENTS

KJ acknowledges Department of Science and Technology (DST), Govt. of India for the infrastructural facility under the schemes of Fund for Improvement of Science and Technology Infrastructure in Universities and Higher Educational Institutes (FIST) and Nanomission (Contract

No. SR/NM/NS-77/2008). KJ also acknowledges University Grants Commission (UGC) Govt. of India, for the partial financial assistance under the contract no. 41-963/2012(SR). PSV acknowledges Council of Scientific and Industrial Research (CSIR), Govt. of India for the award of a senior research fellowship (SRF). PSV also would like to thank Mr. V. Purushothaman and R. Parameshwari for their technical assistance and fruitful discussions.

- ¹ J. Song, X. Wang, E. Riedo, and Z. L. Wang, *J. Phys. Chem. B* **109**, 9869 (2005).
- ² P. C. Chang, Z. Fan, D. Wang, W. Y. Tseng, W. A. Chiou, J. Hong, and J. G. Lu, *Chem. Mater.* **16**, 5133 (2004).
- ³ P. Sundara Venkatesh, V. Ramakrishnan, and K. Jeganathan, *CrystEngComm.* **14**, 3907 (2012).
- ⁴ R. Guo, J. Nishimura, M. Matsumoto, M. Higashihata, D. Nakamura, and T. Okada, *Appl. Phys. B* **94**, 33 (2009).
- ⁵ L. Wang, K. Chen, and L. Dong, *J. Phys. Chem. C* **114**, 17358 (2010).
- ⁶ L. Han, D. Wang, J. Cui, L. Chen, T. Jiang, and Y. Lin, *J. Mater. Chem.* **22**, 12915 (2012).
- ⁷ A. Umar and Y. B. Hahn, *Nanotechnology* **17**, 2174 (2006).
- ⁸ Z. Zhu, L. Zhang, J. Y. Howe, Y. Liao, J. T. Speidel, S. Smith, and H. Fong, *Chem. Commun.* 2568 (2009).
- ⁹ B. Q. Cao, Z. M. Liu, H. Y. Xu, H. B. Gong, D. Nakamura, K. Sakai, M. Higashihata, and T. Okada, *CrystEngComm.* **13**, 4282 (2011).
- ¹⁰ Z. Zhong, H. Gong, Y. Ma, Y. Fan, and Z. Jiang, *Nanoscale Res. Lett.* **6**, 322 (2011).
- ¹¹ E. R. Hemesath, D. K. Schreiber, E. B. Gulsoy, C. F. Kisielowski, A. K. Petford-Long, P. W. Voorhees, and L. J. Lauhon, *Nano Lett.* **12**, 167 (2012).
- ¹² J. E. Allen, E. R. Hemesath, D. E. Perea, J. L. Lensch-Falk, Z. Y. Li, F. Yin, M. H. Gass, P. Wang, A. L. Bleloch, R. E. Palmer, and L. J. Lauhon, *Nat. Nanotechnol.* **3**, 168 (2008).
- ¹³ J. H. Park, H. K. Park, J. Jeong, W. Kim, B. K. Min, and Y. R. Do, *J. Electrochem. Soc.* **158**, K131 (2011).
- ¹⁴ Y. T. Lin, C. Y. Chen, C. P. Hsiung, K. W. Cheng, and J. Y. Gan, *Appl. Phys. Lett.* **89**, 063123 (2006).
- ¹⁵ H. Jung, R. Kuljic, M. A. Strosio, and M. Dutta, *Appl. Phys. Lett.* **96**, 153106 (2010).
- ¹⁶ Q. L. Liua, Y. Bandob, and J. Q. Hub, *J. Cryst. Growth* **306**, 288 (2007).
- ¹⁷ R. Tararam, E. Joanni, R. Savu, P. R. Bueno, E. Longo, and J. A. Varela, *ACS Appl. Mater. Interfaces* **3**, 500 (2011).
- ¹⁸ V. G. Dubrovskii, I. P. Soshnikov, N. V. Sibirev, G. E. Cirilin, and V. M. Ustinov, *J. Cryst. Growth* **289**, 31 (2006).
- ¹⁹ W. T. Chiou, W. Y. Wu, and J. M. Ting, *Diamond Relat. Mater.* **12**, 1841 (2003).
- ²⁰ M. T. Chen and J. M. Ting, *Thin Solid Films* **494**, 250 (2006).
- ²¹ T. L. Chou, W. Y. Wu, and J. M. Ting, *Thin Solid Films* **518**, 1553 (2009).
- ²² S. Choopun, N. Hongsith, E. Wongrat, T. Kamwanna, S. Singkarat, P. Mangkorntong, and N. Mangkorntong, *J. Am. Ceram. Soc.* **91**, 174 (2008).
- ²³ P. Sundara Venkatesh, V. Purushothaman, S. Esakki Muthu, S. Arumugam, V. Ramakrishnan, K. Jeganathan, and K. Ramamurthi, *CrystEngComm.* **14**, 4713 (2012).
- ²⁴ D. S. Kim, U. Gösele, and M. Zacharias, *J. Cryst. Growth* **311**, 3216 (2009).
- ²⁵ E. I. Givargizov, *Highly Anisotropic Crystals*, Reidel, Dordrecht, 1987.
- ²⁶ P. Sundara Venkatesh, V. Ramakrishnan, and K. Jeganathan, *Mater. Res. Bull.* **48**, 3811–3816 (2013).
- ²⁷ D. W. Hoffman and J. A. Thornton, *J. Vac. Sci. Technol.* **17**, 380 (1980).
- ²⁸ J. A. Thornton and D. W. Hoffman, *Thin Solid Films* **171**, 5 (1989).
- ²⁹ J. Serrano, F. J. Manjón, A. H. Romero, F. Widulle, R. Lauck, and M. Cardona, *Phys. Rev. Lett.* **90**, 055510 (2003).
- ³⁰ T. C. Damen, S. P. S. Porto, and B. Tell, *Phys. Rev.* **142**, 570 (1966).
- ³¹ P. Sundara Venkatesh and K. Jeganathan, *J. Solid State Chem.* **200**, 84 (2013).
- ³² K. Sakai, K. Noguchi, A. Fukuyama, T. Ikari, and T. Okada, *Jpn. J. Appl. Phys.* **48**, 085001 (2009).
- ³³ Ü. Özgür, Ya. I. Alivov, C. Liu, A. Teke, M. A. Reshchikov, S. Doğan, V. Avrutin, S. J. Cho, and H. A. Morkoç, *J. Appl. Phys.* **98**, 041301 (2005).
- ³⁴ B. P. Zhang, N. T. Binh, Y. Segawa, K. Wakatsuki, and N. Usami, *Appl. Phys. Lett.* **83**, 1635 (2003).
- ³⁵ Z. Fang, Y. Wang, D. Xu, Y. Tan, and X. Liu, *Opt. Mater.* **26**, 239 (2004).
- ³⁶ E. Gür, S. Tüzemen, K. Meral, and Y. Onganer, *Appl. Phys. A: Mater. Sci. Process.* **94**, 549 (2009).
- ³⁷ C. L. Hsu, S. J. Chang, Y.-R. Lin, S. Y. Tsai, and I. C. Chen, *Chem. Commun.* 3571 (2005).
- ³⁸ S. Jeong and C. Lee, *J. Anal. Sci. Tech.* **2**, 59 (2011).
- ³⁹ L. L. Zhang, C. X. Guo, J. G. Chen, and J. T. Hu, *Chin. Phys.* **14**, 586 (2005).
- ⁴⁰ S. Bayan and D. Mohanta, *J. Appl. Phys.* **110**, 054316 (2011).
- ⁴¹ M. Koyano, P. Quocbao, L. T. Thanhbinh, L. Hongha, N. Ngoclong, and S. Katayama, *Phys. Status Solidi (a)* **193**, 125 (2002).
- ⁴² M. Wang, E. J. Kim, E. W. Shin, J. S. Chung, S. H. Hahn, and C. Park, *J. Phys. Chem. C* **12**, 1920 (2008).



Investigations on the growth and optical properties of one dimensional ZnO nanostructures grown by radio frequency magnetron sputter deposition



P. Sundara Venkatesh^a, V. Ramakrishnan^b, K. Jeganathan^{a,*}

^a Centre for Nanoscience and Nanotechnology, School of Physics, Bharathidasan University, Tiruchirappalli 620 024, Tamilnadu, India

^b Department of Laser Studies, School of Physics, Madurai Kamaraj University, Madurai 625 021, Tamilnadu, India

ARTICLE INFO

Article history:

Received 28 January 2013

Received in revised form 3 May 2013

Accepted 27 May 2013

Available online 5 June 2013

Keywords:

A. Nanostructures

A. Semiconductors

B. Sputtering

C. Raman spectroscopy

D. Luminescence

ABSTRACT

We report the fabrication of one dimensional ZnO nanostructures under various argon sputtering pressures by radio frequency magnetron sputter deposition technique. The transition of the nanostructures from vertical to inclined is monotonously increased with the argon sputtering pressure owing to the decrease in migration length of the adatoms by the increased number of collisions. The blue shift, intensity quenching and peak broadening of $A_1(\text{LO})$ phonon mode in the Raman spectra indicates the increase of free carrier concentration with the argon sputtering pressure due to the enhancement of point defects such as zinc and oxygen vacancies. The dominant neutral donor to bound exciton emission with narrow full width at half maximum implies the high optical quality of the nanostructures irrespective of argon sputtering pressure. The characteristic of visible emission at 3.01 and 2.28 eV provides a strong evidence for the existence of zinc and oxygen vacancies in ZnO nanostructures.

© 2013 Elsevier Ltd. All rights reserved.

1. Introduction

Various deposition techniques [1–7] have been employed for the fabrication of one dimensional (1D) zinc oxide (ZnO) nanostructures. Among the various physical vapor deposition techniques, the magnetron sputter deposition has received a great attention due to its high throughput and high quality of deposition at low cost. It is widely used, because of the large area deposition of thin films/nanostructures under various sputtering conditions such as substrate temperature, sputtering pressure and sputtering power.

ZnO is a well known compound semiconductor with a wide band gap of 3.37 eV and a large exciton binding energy (60 meV) at room temperature which attracted considerable attention as a promising material for the fabrication of optoelectronic devices such as light emitting diodes and laser diodes with high operating temperature. The main advantage of ZnO in the field of optoelectronic applications is its large exciton binding energy as compared to other materials such as GaN and ZnSe [8]. This value is approximately equal to 2.4 times the room temperature thermal energy. Hence, it is a very suitable material for the fabrication of optoelectronic devices with high optical efficiency. Nevertheless,

the understanding of exciton recombination and point defects in 1D ZnO nanostructures are very important for the applications perspective.

Low temperature photoluminescence (LTPL) studies are essential to analyze the point defects, because the room temperature photoluminescence (PL) spectra may exhibit dominant ultraviolet (UV) and no defect mediated emissions in the visible region even in presence of considerable point defects in the nanostructures [9]. The point defects will affect the electrical and optical properties of the materials which will reduce the efficiency of the devices. Hence, many research groups have paid more attention on the analysis of point defects and correlate them with the visible emissions to divulge the origin of transitions [10]. Therefore, a careful analysis of point defects and their correlation with the emissions are very essential.

In the sputter deposition technique, the composition of argon and oxygen plays a major role in the quality and morphology of the nanostructures. It was observed that the crystalline nature of the nanowires was enhanced from polycrystalline to single crystalline by the introduction of oxygen into the chamber, but there is no noticeable change in the surface morphology of the nanowires [6]. Furthermore, the argon sputtering pressure plays an important role in the microstructure formation of the thin films and the high crystallinity of the films with larger grains are ascribed to the decrease in the collisions under low argon sputtering pressure [11].

* Corresponding author. Fax: +91 431 2497 045/2407 020.

E-mail addresses: kjeganathan@yahoo.com, jagan@physics.bdu.ac.in (K. Jeganathan).

In the present work, the argon sputtering pressure dependent surface morphology, structural and optical properties of 1D ZnO nanostructures grown by radio frequency magnetron sputter deposition technique on n-type silicon (1 1 1) substrates have been investigated in detail. The quasi alignment of nanostructures found to transit from vertical to lateral having inclined self-assembled like structure with the argon sputtering pressure. The activation energy, carrier concentration and the nature of strain found to strongly depend on the sputtering pressure. Further, the green emission at 2.28 eV is identified to be the transition between the oxygen vacancy (V_O) and zinc vacancy (V_{Zn}) levels.

2. Experimental

Self assembled 1D ZnO nanostructures were grown on n-type silicon (1 1 1) substrates under various argon sputtering pressures by the rf magnetron sputter deposition technique. Pure ZnO powder (99.999%, Alfa Aesar) was used as a source material to prepare a 2 in. target which was used as resource for the fabrication of 1D nanostructures. The silicon substrates were cleaned by the standard RCA cleaning procedures in order to remove the native oxide layers from the surface of the substrates. Initially, the chamber was evacuated to the base pressure of 5×10^{-6} mbar and then the undoped ZnO target was presputtered for 10 min under pure argon atmosphere of ~ 0.01 mbar with the intension of removing the surface impurities of the target. The details of the growth conditions can be found elsewhere [12]. The deposition was carried out under various pure argon sputtering pressures (0.01, 0.035 and 0.1 mbar) for 60 min with the rf power of 60 W and the substrate temperature is kept at 650 °C.

The surface morphologies of undoped 1D ZnO nanostructures were examined by a field emission scanning electron microscope (FESEM, Carl Zeiss – Sigma) with the maximum resolution of 1.2 nm. The crystalline nature and phase orientation of the nanostructures were analyzed by a Rigaku X-ray diffractometer with Cu K_α radiation of wavelength $\lambda = 1.5406$ Å. Room temperature micro Raman spectra of 1D ZnO nanostructures were recorded in the back scattering geometry using a LabRam HR800 Raman spectrometer. The wavelength of 632.8 nm He–Ne laser was used as an excitation source and the laser beam was focused through a microscope (100 \times) with a spot size of ~ 1 μ m. The temperature dependent PL spectra were recorded using a HORIBA JOBIN YVON monochromator (0.55 m) over the temperature range of 10–300 K with a 325 nm He–Cd laser as an excitation source. The luminescence signal from the nanostructures was collected by a charge coupled device through an appropriate optical arrangement.

3. Results and discussion

Fig. 1(a)–(c) represents the FESEM images of 1D ZnO nanostructures grown under various argon sputtering pressures of 0.01, 0.035 and 0.1 mbar by the rf magnetron sputter deposition technique. The average diameter of the nanostructures increases with the increasing argon sputtering pressure where the average length of the nanostructures decreases. The average diameter of the nanostructures grown under the argon sputtering pressures of 0.01, 0.035 and 0.1 mbar are ~ 124 , 137 and 154 nm respectively and its corresponding lengths are ~ 960 , 810 and 640 nm. Further, the growth direction of the nanostructures also clearly shifts from vertical to inclined with the argon sputtering pressure. At high argon sputtering pressure, the structure completely inclined and partly self assembles to form a flower like pattern as described in Fig. 1(c).

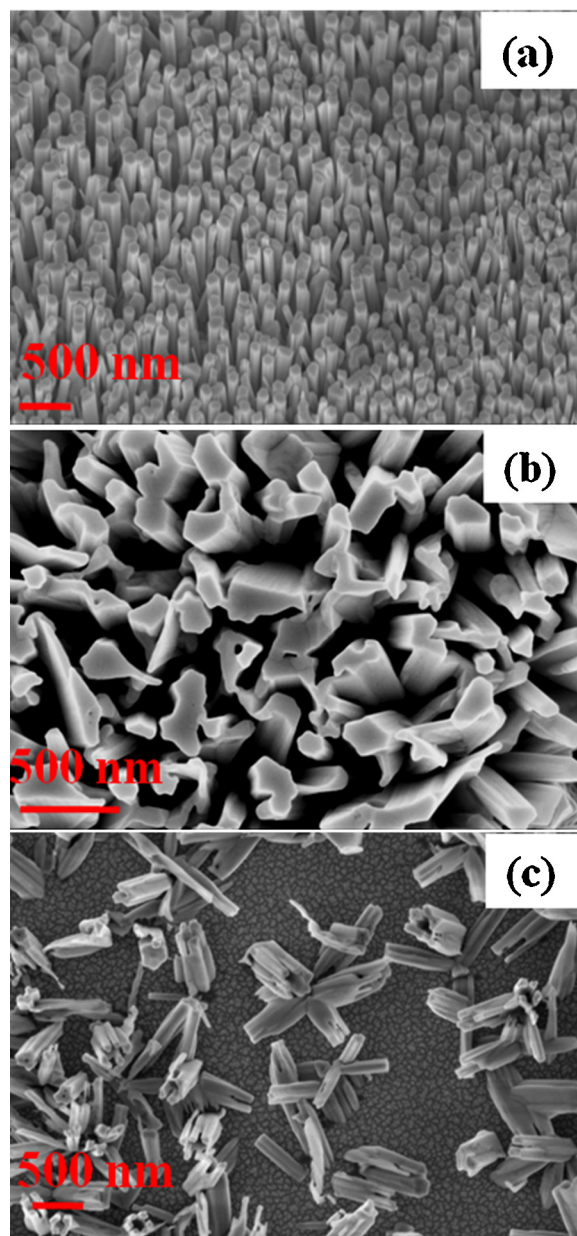


Fig. 1. FESEM images of ZnO nanostructures grown by the rf magnetron sputter deposition technique under various argon pressures (a) 0.01 mbar, (b) 0.035 mbar and (c) 0.1 mbar.

In general, the reagent species motivate the growth of the nanostructures both in axial and radial directions [13]. Hence, the growth morphology and physical axis of the 1D nanostructures are expected to be strongly depend on the growth conditions such as pressure and substrate temperature. The vertically aligned nanostructures at low argon sputtering pressure of 0.01 and 0.035 mbar can be linked to the large mean free path of the adatoms which posses high migration length and promote the axial growth of the nanostructures by the process of side wall surface diffusion along the direct impingement. But, in the case of small mean free path, the adatoms will have small migration length and the adatoms may likely be absorbed on the side walls of the nanostructures and promote the radial growth as seen in Fig. 1(c) [14,15]. It represents that the migration length of the adatoms is inversely proportional to the pressure. Further, the mean free path decreases with the increase of sputtering pressure owing to the high density of collisions. Hence, the surface

migration of the adatoms enhances the vertical growth of the nanostructures if the length of the nanostructures is smaller than the migration length, otherwise it will be desorbed from the surface or accumulates on the surface to promote the radial growth of the nanostructures. Consequently, the increase of diameter and decrease of length of the nanostructures with the sputtering pressure is in line of our expectation due to its smaller mean free path. Further, the above discussion reiterates that the migration length of adatoms directs the axial as well as radial growth of nanostructures depending upon the sputtering pressure.

Fig. 2(a) depicts the XRD pattern of 1D ZnO nanostructures grown under various argon sputtering pressures. All the observed peaks are indexed according to the standard bulk ZnO. In addition to this, a weak and broad peak around at 43.07° corresponds to the SiO_2 which well agrees with the standard result (JCPDS No. 89-6335). It provides an evidence for the presence of SiO_2 layer on the top surface of the silicon substrate, which may be formed due to the oxidation of the silicon substrate during the early stage of

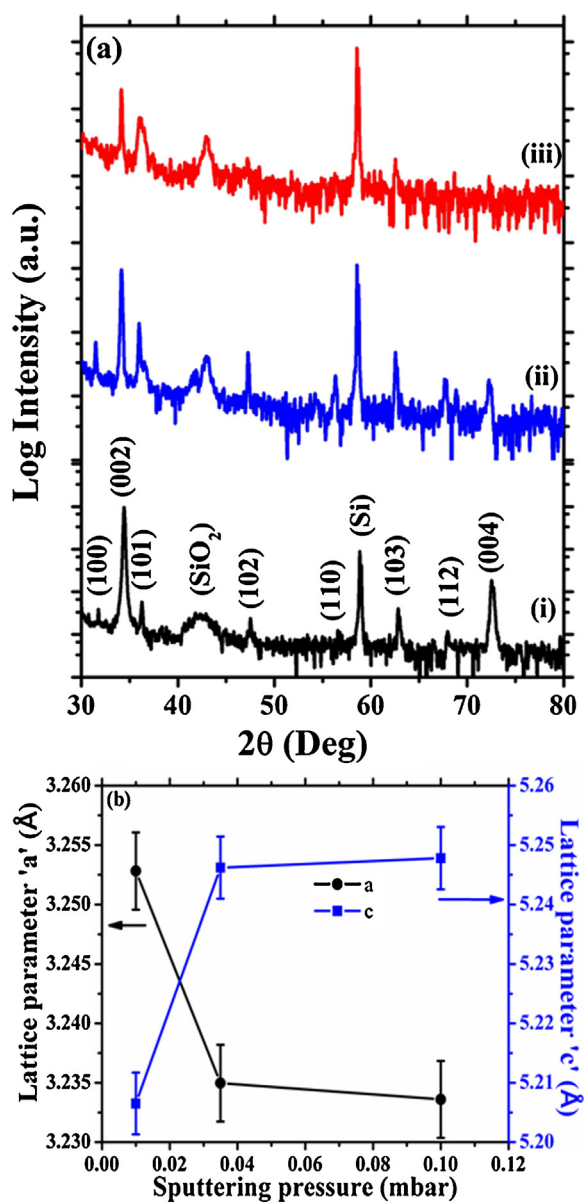


Fig. 2. (a) Typical X-ray diffraction pattern of 1D ZnO nanostructures grown under various argon pressures (i) 0.01 mbar, (ii) 0.035 mbar and (iii) 0.1 mbar and (b) Variation of lattice parameters 'a' and 'c' as a function of argon sputtering pressure.

the growth from the sputtered reactive species of oxygen. Further, the peak around at 59.15° corresponds to (2 2 2) reflection of silicon substrate. The dominant (0 0 2) peak indicates a preferential orientation of the nanostructures along the *c*-axis which is perpendicular to the substrate surface with wurtzite structure of ZnO. The intensity of the (0 0 2) and (0 0 4) peaks decreases and the (1 0 1) peak intensity increases with increasing the argon sputtering pressure, which indicates that the orientation of the nanostructures slightly off-oriented from its *c*-direction. This corroborates with the surface morphological changes as shown in Fig. 1(a)–(c). The position of the (0 0 2) peak is observed at 34.412° for the nanostructures grown under the argon pressure of 0.01 mbar which is near to the standard bulk ZnO (JCPDS No. 79-2205) and however the nanostructures are slightly compressed. When the argon sputtering pressure is increased to 0.1 mbar, the (0 0 2) peak shifts towards the lower angles as compared to the standard bulk ZnO as well as the vertical standing nanostructures grown under the argon sputtering pressure of 0.01 mbar, indicative of compressive strain. Further, the full width at half maximum (FWHM) (0.1478° , 0.1612° and 0.1663°) increases with the argon sputtering pressure (0.01, 0.035 and 0.1 mbar) and also confirms the deterioration of crystalline quality of nanostructures. The variation of in-plane and out-plane lattice parameters 'a' and 'c' with the argon sputtering pressure is shown in Fig. 2(b) and provides a conclusive evidence for the presence of compressive strain in the nanostructures and increases with the pressure.

Fig. 3(a) shows the micro-Raman spectra of 1D ZnO nanostructures grown under various argon sputtering pressures of 0.01, 0.035 and 0.1 mbar. The spectra have similar patterns irrespective of sputtering pressure. The dominant peak at 99.3 cm^{-1} corresponds to the E_2^{low} phonon mode of ZnO, which is attributed to the lattice vibrations of zinc atoms. The narrow FWHM of E_2^{low} phonon mode (1.8 cm^{-1}) indicates the high optical quality of the nanostructures and the intensity of the E_2^{low} phonon mode decreases with the increasing argon sputtering pressure due to the degradation of optical quality of the nanostructures. The observed peak at around 437 cm^{-1} is attributed to the lattice vibrations of the oxygen atoms and assigned as E_2^{high} phonon mode [16]. It is very sensitive to the strain and presence of E_2^{high} phonon mode confirms the wurtzite crystal structure of ZnO. The peak positions of the E_2^{high} phonon mode are 437.8 , 438.3 and 438.4 cm^{-1} for the nanostructures grown under various argon sputtering pressures of 0.01, 0.035 and 0.1 mbar respectively. The linear blue shift of the E_2^{high} phonon mode from its standard bulk value (437 cm^{-1}) indicates the presence of compressive strain [17]. The crystalline nature of the nanostructures decreases with the increase of argon sputtering pressure as evidenced by the widening of E_2^{high} phonon mode as shown in Fig. 3(b). The observed crystalline behaviour corroborates with the XRD results. Further, the FWHMs of E_2^{high} phonon mode are ~ 6.7 , 9.9 and 11 cm^{-1} for the nanostructures grown under the argon sputtering pressures of 0.01, 0.035 and 0.1 mbar respectively. The appearance of a peak at 276 cm^{-1} could be attributed to the relaxation of the Raman selection rules by the breakdown of the translation symmetry of the crystal lattice. It is assigned as $B_1(\text{low})$ which is silent mode in the Raman spectrum of ZnO. The additionally observed peak at 380 cm^{-1} corresponds to $A_1(\text{TO})$ phonon mode and it is forbidden in the back scattering geometry of measurements. However, the observation of this quasi phonon mode may be attributed to a small deviation from the back scattering geometry due to break in wave vector.

Earlier report shows that both the $B_1(\text{low})$ and $B_1(\text{high})$ modes exhibit similar intensities and the width of $B_1(\text{low})$ mode is smaller than the width of $B_1(\text{high})$ [18]. But, in our case, the intensity of the observed peak near at 583 cm^{-1} is small as compared to the

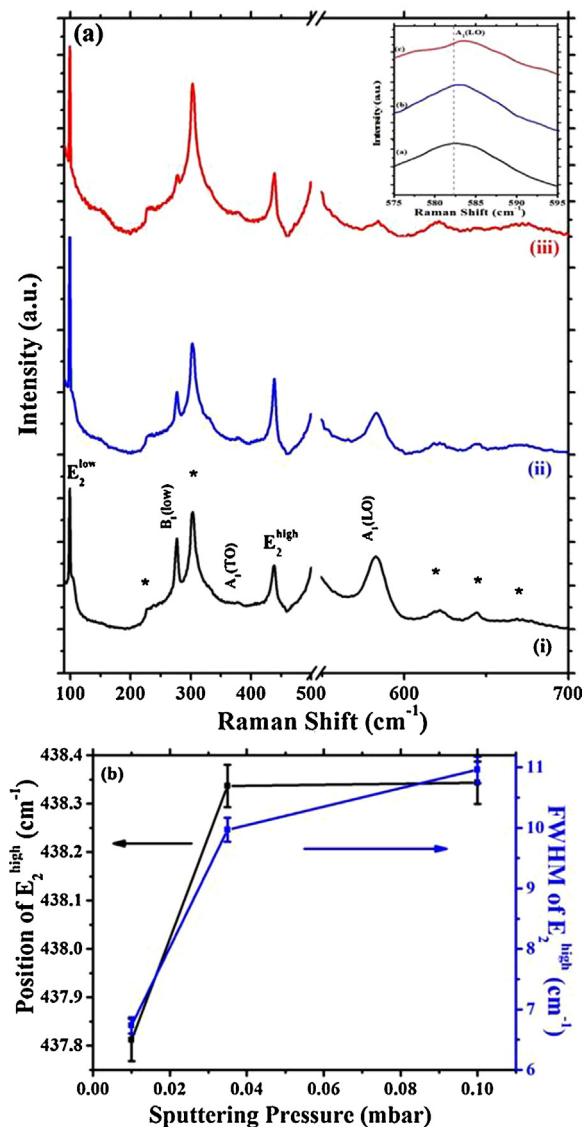


Fig. 3. (a) Micro-Raman spectra of 1D ZnO nanostructures recorded in the back scattering geometry (i) 0.01 mbar, (ii) 0.035 mbar, (iii) 0.1 mbar and the inset shows the blue shift of A₁(LO) phonon mode. (b) Variation of peak position and FWHM of E₂(high) phonon mode as a function of sputtering pressure.

B₁(low). Hence, it could not be assigned as B₁(high). Therefore, it can be attributed to either E₁(LO) or A₁(LO) phonon mode. According to the selection rule of back scattering geometry, the polar phonon mode E₁(LO) is forbidden [19]. Further, the appearance of E₁(LO) is attributed to the deficiency of oxygen [20]. The oxygen deficiency is expected to increase with the increase of argon sputtering pressure as described in PL. If the observed phonon mode is corresponding to the E₁(LO), then the intensity of this phonon mode should have increased with the increase of argon sputtering pressure. But, it is decreasing with the increasing argon pressure. Hence, it could not be attributed to the E₁(LO) phonon mode. Thus, the observed peak is assigned to be A₁(LO) and it is generally observed at the wave number of 574 cm⁻¹. In our case, it is blue shifted (583 cm⁻¹) from its original position (574 cm⁻¹) owing to the increase in the free carrier concentration and depicted in the inset of Fig. 3(a). A strong correlation has already been established between the position of A₁(LO) mode and free carrier concentrations [21]. Furthermore, the A₁(LO) phonon mode experiences a shift in higher wave numbers, broadening of peak and decrease in intensity with increasing free carrier concentration

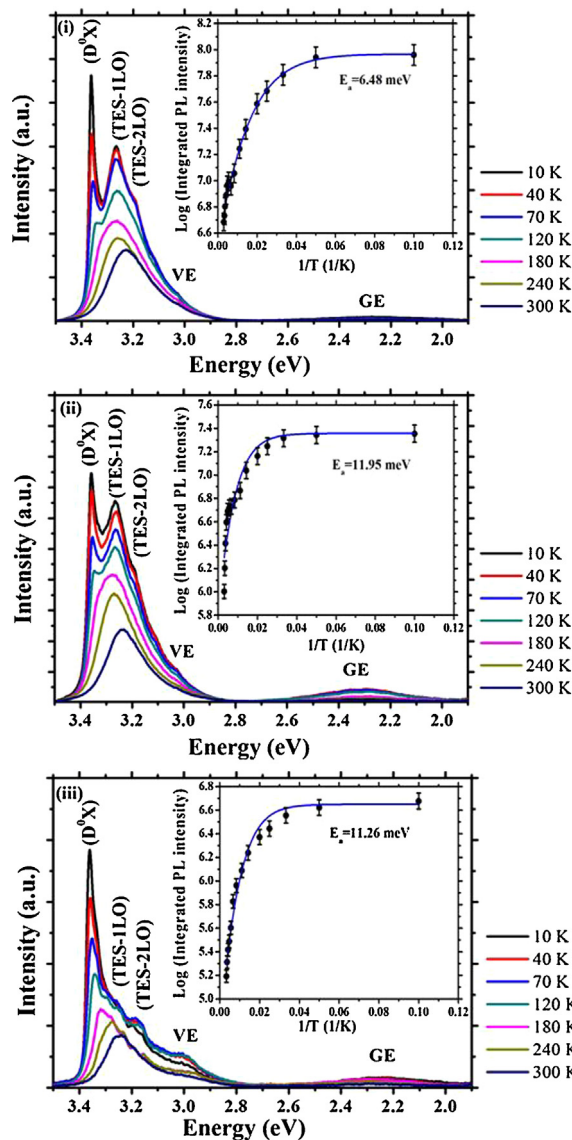


Fig. 4. Temperature dependent PL spectra of ZnO nanostructures grown under various argon sputtering pressures of (i) 0.01 mbar, (ii) 0.035 mbar, (iii) 0.1 mbar and the inset shows the corresponding integrated PL intensity variation of D⁰X emission vs. the inverse of temperature.

due to the strong coupling of phonons with plasmons [4,22,23]. The FWHM of A₁(LO) phonon mode for the nanostructures grown under the argon sputtering pressures of 0.01, 0.035 and 0.1 mbar are ~13.3, 13.6 and 15.4 cm⁻¹ respectively.

Fig. 4 shows the LTPL spectra of 1D ZnO nanostructures grown under various argon sputtering pressures. At 10 K, PL spectra exhibit similar peaks at 3.363, 3.258 and 3.183 eV irrespective of argon sputtering pressure. The dominant emission peak at ~3.363 eV is denoted as D⁰X and it is attributed to the neutral donor to bound excitons [24]. Further, the intensity of D⁰X emission quenches with increasing the measurement temperature as a result of the refreezing of phonons and stimulation of non-radiative recombination processes. The longitudinal optical (LO) phonon energy of bulk ZnO is reported to be ~72 meV [25]. The observed emission peaks at 3.258, and 3.183 eV are associated to the first and second LO phonon replicas of two electron satellite (TES) lines. It is in good agreement with the earlier reports [10,24]. It is well known that zinc vacancies (V_{Zn}) will act as an acceptor and create an acceptor level above the valence band. It was reported that the energy difference between the conduction band minimum

and the zinc vacancy level (V_{Zn}) is about 3.06 eV [26]. This shows that the acceptor level is well above the valence band about 0.3 eV. We believe that the observed violet emission (VE) around at 3.01 eV is attributed to the electron transitions from the conduction band minimum to V_{Zn} level and this transition provides a clear evidence for the presence of zinc vacancies in the nanostructures. Further, a broad and weak peak around 2.28 eV corresponds to green emission (GE) of the visible spectrum and this green luminescence is attributed to the electron transition from the shallow donor level (V_o) to a shallow acceptor level (V_{Zn}) [12,27]. This transition indicates the presence of oxygen and zinc vacancies in the nanostructures which are all the common point defects observed in ZnO owing to its small formation energy [28]. The observed green emission quenches with the increasing temperature due to the phonon scattering process and the similar behaviours are observed in all 1D ZnO nanostructures grown under various argon sputtering pressures. Further, the intensity of the violet and green emissions consistently increases with the argon sputtering pressure and indicates that the zinc and oxygen vacancies increase with the pressure. The above discussion evidences that the quality of the nanostructures deteriorates with the argon sputtering pressure which well corroborates with the XRD and Raman results. The high emission intensity ratio (I_{UV}/I_{DL}) of the nanostructures grown under the argon sputtering pressure of 0.01 mbar confirms the high crystalline and optical qualities which deteriorate with the argon sputtering pressure (not shown).

D^0X peak energy decreases with increasing the ambient temperature due to the electron phonon interactions and the expansion of the lattice (not shown). The experimental variation of band gap is fitted by an empirical Varshni formula [29].

$$E(T) = E(0) - \left(\frac{\alpha T^2}{T + \beta} \right) \quad (1)$$

where $E(T)$ and $E(0)$ are the band gap at an absolute temperature T and 0 K respectively. α and β are the Varshni thermal coefficients. The above coefficients are extracted from the best fitted results of neutral donor to bound exciton emission using Eq. (1). The obtained values of $E(0)$ for the 1D nanostructures grown under various argon sputtering pressures of 0.01, 0.035 and 0.1 mbar are 3.3651, 3.3612 and 3.3628 eV respectively. The fitting parameters (α and β) significantly varies with the argon sputtering pressure and can be related to the dilation of the ZnO lattice. The obtained values are in good agreement with the reported values [30].

The inset of Fig. 4 shows the corresponding integrated PL intensity variation of D^0X emission as a function of inverse of temperature for the 1D ZnO nanostructures grown under various argon sputtering pressures. The PL intensity decreases with the increasing temperature due to the thermal quenching and described by the following equation [31].

$$I(T) = \frac{I(0)}{(1 + A * \exp(-E_a/KT))} \quad (2)$$

where $I(T)$ is the PL intensity at temperature T (K), $I(0)$ is the PL intensity at 0 K, A is a proportionality constant, E_a is the activation energy of the thermal quenching process, K is a Boltzmann constant and T is a thermodynamic temperature. The activation energies of the 1D ZnO nanostructures grown under various argon sputtering pressures of 0.01, 0.035 and 0.1 mbar are 6.48, 11.95 and 11.26 meV respectively. The activation energy of ZnO nanostructure increases with the argon sputtering pressure. In general, the increase of activation energy is expected to quench the luminescence signal [32] as due to the deterioration of the optical quality of the ZnO nanostructures with the argon sputtering pressure. This quenching of dominant bound exciton emission is in good agreement with the reported values of the 1D ZnO

nanostructures [33–36]. At 10 K, the D^0X line widths of the 1D nanostructures grown under various argon sputtering pressures of 0.01, 0.035 and 0.1 mbar are 0.0226, 0.0265 and 0.0301 eV respectively. It linearly increases with the argon sputtering pressure and provides a conclusive evidence for the deterioration of the optical quality of nanostructures which is consistency with the activation energy. Further, the line width of the peak increases gradually up to ~ 150 K and then it increases almost exponentially to the ambient temperature in all 1D nanostructures grown under various argon sputtering pressures (not shown).

4. Conclusion

Quasi-aligned 1D ZnO nanostructures have been successfully grown on silicon (1 1 1) substrates by the rf magnetron sputter deposition technique under various argon pressures. The transition of structural morphology of the 1D ZnO nanostructures with the sputtering pressure is driven by the change in migration length of the adatoms which promotes the radial growth due to the increased number of collisions between the sputtered and argon gas molecules. The structural studies suggest that the increase in argon pressure introduces the compressive strain in the nanostructures which also depends on the foot prints of the nanostructures on the substrate. A blue shift of $A_1(LO)$ phonon mode ascertains the enhancement of the free carrier concentration in nanostructures with the sputtering pressure. The predominant D^0X emission with narrow FWHM is a sign of good optical quality of the ZnO nanostructures and quenches with the increasing argon pressure as well as measurement temperature. The observed violet and green emissions at 3.01 and 2.28 eV confirm the existence of zinc and oxygen vacancies in the nanostructures.

Acknowledgements

KJ acknowledges Department of Science and Technology (DST), Govt. of India for the infrastructural facility under the schemes of Fund for Improvement of Science and Technology Infrastructure in Universities and Higher Educational Institutes (FIST) and Nano-mission (Contract No. SR/NM/NS-77/2008). KJ also acknowledges University Grants Commission (UGC) Govt. of India, for the partial financial assistance under the contract no. 41-963/2012(SR). PSV acknowledges UGC, Govt. of India for the award of a UGC – meritorious fellowship. The authors would like to thank Miss P. Sangeetha for experimental assistance with Raman spectroscopy. PSV also would like to thank Dr. M. K. Jayaraj and Dr. P. M. Aneesh, Department of Physics, Cochin University of science and technology, Cochin, Kerala for their valuable discussions.

References

- [1] Y.W. Heo, L.C. Tien, D.P. Norton, B.S. Kang, F. Ren, B.P. Gila, S.J. Pearton, *Appl. Phys. Lett.* 85 (2004) 2002–2004.
- [2] S. Choopun, H. Tabata, T. Kawai, *J. Cryst. Growth* 274 (2005) 167–172.
- [3] Z.W. Pan, Z.R. Dai, Z.L. Wang, *Science* 291 (2001) 1947–1949.
- [4] A.-J. Cheng, Y. Tzeng, H. Xu, S. Alur, Y. Wang, M. Park, T.-h. Wu, C. Shannon, D.-J. Kim, D. Wang, *J. Appl. Phys.* 105 (2009) 073104.
- [5] S.W. Kim, S. Fujita, S. Fujita, *Appl. Phys. Lett.* 86 (2005) 153119.
- [6] W.T. Chiou, W.Y. Wu, J.M. Ting, *Diamond Relat. Mater.* 12 (2003) 1841–1844.
- [7] Y.J. Xing, Z.H. Xi, Z.Q. Xue, X.D. Zhang, J.H. Song, R.M. Wang, J. Xu, Y. Song, S.L. Zhang, D.P. Yu, *Appl. Phys. Lett.* 83 (2003) 1689–1691.
- [8] Manoj Kumar, R.M. Mehra, A. Wakahara, M. Ishida, A. Yoshida, *J. Appl. Phys.* 93 (2003) 3837.
- [9] K.H. Tam, C.K. Cheung, Y.H. Leung, A.B. Djurišić, C.C. Ling, C.D. Beling, S. Fung, W.M. Kwok, W.K. Chan, D.L. Phillips, L. Ding, W.K. Ge, *J. Phys. Chem. B* 110 (2006) 20865–20871.
- [10] Ü. Özgür, Ya I. Alivov, C. Liu, A. Teke, M.A. Reshchikov, S. Doğan, V. Avrutin, S.J. Cho, H.A. Morkoç, *J. Appl. Phys.* 98 (2005) 041301.
- [11] K.Y. Chan, B.S. Teo, *IET Sci. Meas. Technol.* 1 (2007) 87–90.

- [12] P. Sundara Venkatesh, V. Purushothaman, S. Esakki Muthu, S. Arumugam, V. Ramakrishnan, K. Jeganathan, K. Ramamurthi, *CrystEngComm* 14 (2012) 4713–4718.
- [13] Y. Yan, L. Zhou, Z. Han, Y. Zhang, *J. Phys. Chem. C* 114 (2010) 3932–3936.
- [14] Y.G. Yan, Y. Zhang, H.B. Zeng, J.X. Zhang, X.L. Cao, L.D. Zhang, *Nanotechnology* 18 (2007) 175601.
- [15] Y.G. Yan, L.X. Zhou, *Appl. Phys. A: Mater. Sci. Process.* 92 (2008) 401–405.
- [16] K.A. Alim, V.A. Fonoberov, M. Shamsa, A.A. Balandin, *J. Appl. Phys.* 97 (2005) 124313.
- [17] F. Decremps, J.P. Porres, A.M. Saitta, J.C. Chervin, A. Polian, *Phys. Rev. B* 65 (2002) 092101.
- [18] F.J. Manjón, B. Marí, J. Serrano, A.H. Romero, *J. Appl. Phys.* 97 (2005) 053516.
- [19] F. Wang, H. He, Z. Ye, L. Zhu, H. Tang, Y. Zhang, *J. Phys. D: Appl. Phys.* 38 (2005) 2919–2922.
- [20] J.J. Wu, S.C. Liu, *J. Phys. Chem. B* 106 (2002) 9546–9551.
- [21] M. Kuball, *Surf. Interface Anal.* 31 (2001) 987–999.
- [22] K. Jeganathan, R.K. Debnath, R. Meijers, T. Stoica, R. Calarco, D. Grützmacher, H. Lüth, *J. Appl. Phys.* 105 (2009) 123707.
- [23] G.S. Sun, X.F. Liu, H.L. Wu, G.G. Yan, L. Dong, L. Zheng, W.S. Zhao, L. Wang, Y.P. Zeng, X.G. Li, Z.G. Wang, *Chin. Phys. B* 20 (2011) 033301.
- [24] K. Sakai, K. Noguchi, A. Fukuyama, T. Ikari, T. Okada, *Jpn. J. Appl. Phys.* 48 (2009) 085001.
- [25] T. Makino, Y. Segawa, M. Kawasaki, *J. Appl. Phys.* 97 (2005) 106111.
- [26] Z. Fang, Y. Wang, D. Xu, Y. Tan, X. Liu, *Opt. Mater.* 26 (2004) 239.
- [27] E. Gür, S. Tüzemen, K. Meral, Y. Onganer, *Appl. Phys. A: Mater. Sci. Process.* 94 (2009) 549–554.
- [28] Z.Q. Chen, M. Maekawa, A. Kawasuso, S. Sakai, H. Naramoto, *J. Appl. Phys.* 99 (2006) 093507.
- [29] Y.P. Varshni, *Physica* 34 (1967) 149–154.
- [30] D. Sentosa, B. Liu, L.M. Wong, Y.V. Lim, T.I. Wong, Y.L. Foo, H.D. Sun, S.J. Wang, *J. Cryst. Growth* 319 (2011) 8–12.
- [31] R.S. Ajimsha, R. Manoj, P.M. Aneesh, M.K. Jayaraj, *Curr. Appl. Phys.* 10 (2010) 693–697.
- [32] X. Gu, K. Huo, G. Qian, J. Fu, P.K. Chu, *Appl. Phys. Lett.* 93 (2008) 203117.
- [33] B.K. Meyer, H. Alves, D.M. Hofmann, W. Kriegseis, D. Forster, F. Bertram, J. Christen, A. Hoffmann, M. Strabburg, M. Dworzak, U. Haboek, A.V. Rodina, *Phys. Status Solidi (b)* 241 (2004) 231–260.
- [34] H. Najafav, S. Ohshio, S. Iida, H. Saitoh, Y. Fukada, *Jpn. J. Appl. Phys.* 42 (2003) 3490–3495.
- [35] Z.N. Urgessa, O.S. Oluwafemi, J.K. Dangbegnon, J.R. Botha, *Physica B* 407 (2012) 1546–1549.
- [36] K.J. Hong, T.S. Jeong, C.J. Youn, *J. Ceram. Process. Res.* 13 (2012) 149–153.



ELSEVIER

Contents lists available at [SciVerse ScienceDirect](http://www.sciencedirect.com)

Journal of Solid State Chemistry

journal homepage: www.elsevier.com/locate/jssc

Investigations on the growth and characterization of vertically aligned zinc oxide nanowires by radio frequency magnetron sputtering

P. Sundara Venkatesh, K. Jeganathan*

Centre for Nanoscience and Nanotechnology, School of Physics, Bharathidasan University, Tiruchirappalli 620024, Tamil Nadu, India

ARTICLE INFO

Article history:

Received 9 October 2012

Received in revised form

28 December 2012

Accepted 19 January 2013

Available online 29 January 2013

Keywords:

ZnO nanowires

Sputtering

Raman

Carrier concentration

Photoluminescence

Point defects

ABSTRACT

Undoped vertically aligned ZnO nanowires have been grown on silicon (111) substrates by the rf magnetron sputtering technique without metal catalyst. The diameter, length and density distributions of the nanowires have been analyzed with respect to the different growth durations. The tapering of the nanowires is observed for the growth duration of 120 min owing to the insufficient adatoms on the growth front. In the X-ray diffraction pattern, the dominant (002) peak with narrow full width at half maximum (FWHM) of ZnO nanowires indicates the *c*-axis orientation and high crystalline nature with hexagonal wurtzite crystal structure. The narrow FWHM of E_2^{low} and E_2^{high} phonon modes (1.4 and 9.1 cm^{-1}) provide an additional evidence for the high crystalline and optical properties of the nanowires. The low temperature photoluminescence spectra are dominated by the green emission at ~ 2.28 eV induced by the electron transitions between shallow donor and acceptor energy levels.

© 2013 Elsevier Inc. All rights reserved.

1. Introduction

Among the various forms of one dimensional (1D) nanostructures, the nanowires and nanorods have received a great deal of interest due to its unique physical and chemical properties with increased surface area and building blocks for functional nanodevices. For practical applications, the vertically aligned nanowires or nanorods have received a significant attention due to the effective relaxation of stress at the lateral surface, which makes it possible to grow defects free nanowires or nanorods on highly mismatched substrates that is impossible for two dimensional films. Among the various semiconducting nanowires, zinc oxide (ZnO) is a suitable material for various potential applications such as light emitting diodes [1,2], solar cells [3], varistors [4], laser diodes [5], spintronics [6] and sensors [7] due to its wide band gap of 3.37 eV with large exciton binding energy (60 meV) at room temperature, which is much higher than the III–V and II–VI semiconductors [8,9].

The vapor liquid solid (VLS) technique, described by Wagner and Ellis in 1964, is emerged as one of the widely employed growth mechanisms to fabricate the nanowires [10]. In this growth technique, one of the noble metals such as gold or nickel is used as catalyst in the form of thin films or nanoparticles to initiate the growth of nanowires. The diameter and density of the nanowires depend on the thickness of the catalyst layer on the substrate and the method of heat treatment [11]. Despite the advantage of controlled density,

diameter and the enhancement of growth rate along the confined crystallographic direction, there are some apparent drawbacks in this growth technique. It requires a very high temperature to form an alloy droplet for initiating the growth. After the growth, the tip of the nanowires contains the catalytic droplet which is an undesirable external impurity for the device fabrication. Hence, an alternative approach is essential for the growth of nanowires without any external catalyst which is possible by the vapor solid (VS) growth mechanism. Nanowires fabricated by VS approach relies on the direct crystallization from the vapors govern by the direct impingement and diffusion of adatoms on the side walls of nanowires. In the VS growth mechanism, the initial nucleation is induced by the defects such as screw dislocation and it does not contain any droplet at the tip of the nanowires [12], consequently, it is very suitable for the growth of the nanowires in the applications perspective.

In the present work, we have grown vertically aligned ZnO nanowires without any external catalyst under different growth durations by radio frequency (rf) magnetron sputtering technique on n-type silicon (111) substrates. The nanowires grown for 120 min were extensively investigated in order to understand the structural and optical properties of the nanowires for the applications of optoelectronic device fabrication. The photoluminescence spectrum exhibits an intense and broad green emission at low temperature owing to the vacancy mediated transitions.

2. Material and methods

Vertically aligned undoped ZnO nanowires were grown on n-type silicon (111) substrates under different growth durations

* Corresponding author. Fax: +91 431 2497 045, 2407 020.

E-mail addresses: srnmcpphysics@gmail.com (P.S. Venkatesh), kjeganathan@yahoo.com, jagan@physics.bdu.ac.in (K. Jeganathan).

by the rf magnetron sputtering technique. A pure 2 in. ZnO target was used as a source material for the growth of nanowires and it was prepared by a simple solid state reaction technique. In order to remove the native oxide layer from the surface of the silicon substrate, the standard RCA cleaning procedure was followed prior to loading the substrate into the chamber. Initially, the chamber was evacuated to the base pressure of 5×10^{-6} mbar and the oxide target was pre-sputtered about 10 min under pure argon (Ar) atmosphere in order to remove the impurities present on the surface of the target. The growth of nanowires was carried out under the partial pressure of 0.01 mbar in pure Ar atmosphere with the fixed rf power of 60 W. The details of the growth conditions can be found elsewhere [13]. The deposition rate ($\sim 3.6 \text{ \AA}/\text{sec}$) of the sputtered materials was monitored by the in-situ digital thickness monitor (Model DTM-101).

The surface morphology and composition of the nanowires were examined by a field emission scanning electron microscope (FESEM, Carl Zeiss-Sigma) equipped with the energy dispersive X-ray spectrometer (EDX, Oxford instruments-INCAx). The phase orientation of the nanowires was investigated by a Rigaku X-ray diffractometer with $\text{CuK}\alpha$ radiation ($\lambda = 1.5406 \text{ \AA}$). The vibrational phonon studies of the nanowires were performed by a Lab Ram HR800 micro-Raman spectrometer with an excitation wavelength of 632.8 nm. The temperature dependent photoluminescence (PL) measurements were recorded using a HORIBA JOBIN YVON monochromator (0.55 m) over the temperature range of 10–330 K by the closed cycle helium cryostat. He–Cd laser (325 nm) with a power of 30 mW was used as an excitation source and the dispersed luminescence signal from the sample was collected by a charge coupled device through an appropriate optical arrangement.

3. Results and discussion

The FESEM images shown in Fig. 1 depict the top and 45° tilted views of ZnO nanowires grown under different growth durations of 15, 30, 60 and 120 min respectively. The FESEM images clearly show that the nanowires are vertically aligned on the substrates having hexagonal cross section. Further, the density, length and diameter distributions of the ZnO nanowires exhibit a strong dependence of growth duration. Fig. 2 represents the variations of average diameter, density and length of the nanowires for different growth durations. The average diameter of the nanowires increases gradually up to the growth duration of 60 min, after that the diameter leads to decrease by the increase of the growth duration to 120 min which is attributed to the tapering of the nanowires. The reason for tapering is clearly described below. Furthermore, the average length of the nanowires found to increase linearly from 150 to 1394 nm with the increase of the growth duration from 15 to 120 min.

The density of the nanowires increases up to 30 min growth duration ($0.57 \times 10^{10} \text{ cm}^{-2}$) as due to the formation of new nuclei on the substrate. Nevertheless, the density decreases to $0.36 \times 10^{10} \text{ cm}^{-2}$ with the increase of the growth duration to 60 min and this trend can be attributed to the coalescence of closely spaced nanowires at the boundaries due to the lateral growth [14]. Further increasing the growth duration to 120 min, the perfect hexagonal cross section of the vertical standing nanowires grown for 60 min is transformed into the needle like structure. This transformation is attributed to the insufficient adatoms on the growth front. In contrast, the density of nanowires found to monotonously increase ($1.44 \times 10^{10} \text{ cm}^{-2}$) with the increase of growth duration to 120 min. This unusual behavior can be explained by the multiple tapering on the edges of nanowires which obviously result the high density nanowires in extended growth duration of 120 min.

Further, it is reported that the polarity of the nanostructures do not vary by thinning of NWs with the result of extended growth duration [15]. Hence, it is expected that there will be no change in the polarity as well as surface chemistry of the nanowires grown under the growth durations of 60 and 120 min, as long as the growth direction remains along *c*-axis of ZnO. Furthermore, the structural and optical properties of the well oriented and vertically aligned nanowires are very important for the fabrication of efficient optoelectronic devices [16,17]. Consequently, a detailed investigation has been extended to the nanowires grown under pure Ar atmosphere for 120 min at 550 °C.

A tilt view (45°) of the vertically aligned ZnO nanowires grown on n-type silicon (111) substrate using the rf magnetron sputtering technique is shown in Fig. 3(a). One can easily observe that the nanowires have tapered tips and are well aligned vertically with an average diameter of 80 nm and length of about $\sim 1.4 \mu\text{m}$. Generally, the growth of the nanowires is promoted by the direct impingement of adatoms on the tip of the nanowires in addition to the migration of adatoms through the side walls of the nanowires [18,19]. In the case of adatoms migration through the side walls of the nanowires, the growth is enhanced only if the migration length of the adatoms is greater than the length of the nanowires, otherwise it will be desorbed from the surface of the nanowires and hence direct impingement of adatoms are only responsible for the subsequent growth of nanowires. Therefore, the migration lengths of the adatoms is an important parameter and depends on the many growth parameters such as substrate temperature, sputtering pressure, target–substrate distance and further the position of nanowires on the substrate surface. If the energy of the adatoms is small, consequently the migration length becomes small. Hence, it could not reach the growth front of the nanowires. Therefore, the number of adatoms on the tip of the nanowires will be reduced which may induce the tapering in the nanowires. In our case, the tip of the nanowires is not tapered up to the growth duration of 60 min and its length is about 625 nm. Further increasing the growth duration to 120 min, the length of the nanowires is approximately doubled ($\sim 1394 \text{ nm}$). On the other hand, the ZnO nanowires have tapered tips as shown in Fig. 3(a). It could be ascribed that the migration length of the adatoms is expected to be $\sim 1 \mu\text{m}$ as the tapering occur at above this length for the given growth conditions. Due to the smaller migration length of adatoms, the tapering is observed in the nanowires grown for 120 min. EDX spectrum of the vertically aligned ZnO nanowires is recorded using the electron beam of 10 kV accelerating voltage as shown in Fig. 3(b). The vertically aligned ZnO nanowires consist of purely zinc and oxygen. The presence of silicon in the EDX spectrum is associated to the substrate, which is attributed to the interaction of electron with the silicon substrate through the air gap between the vertical standing nanowires. With the detection limit of EDX, there are no impurities found in the array of nanowires.

Fig. 4 depicts the X-ray diffraction pattern of undoped ZnO nanowires grown on silicon (111) substrate for 120 min by the rf magnetron sputtering technique. The dominant and weak peaks at 34.43° and 72.63° correspond to (002) and (004) reflections of ZnO respectively, which confirm the hexagonal wurtzite structure of the nanowires with the preferential orientation along *c*-axis. The narrow full width at half maximum (FWHM, 618 arcsec) of the dominant (002) peak reveals the high crystalline nature of the nanowires. The observed peak at 28.55° corresponds to the (111) reflection of silicon (JCPDS-78-2500) which is attributed from the substrate. Further, the additional peaks at 44.54° and 64.56° correspond to the silicon dioxide (JCPDS-89-3606). The appearance of the silicon dioxide peak confirms the existence of silicon dioxide layer on the surface of the substrate, which may be formed during the earlier stage of growth at elevated temperature by the process of oxidation

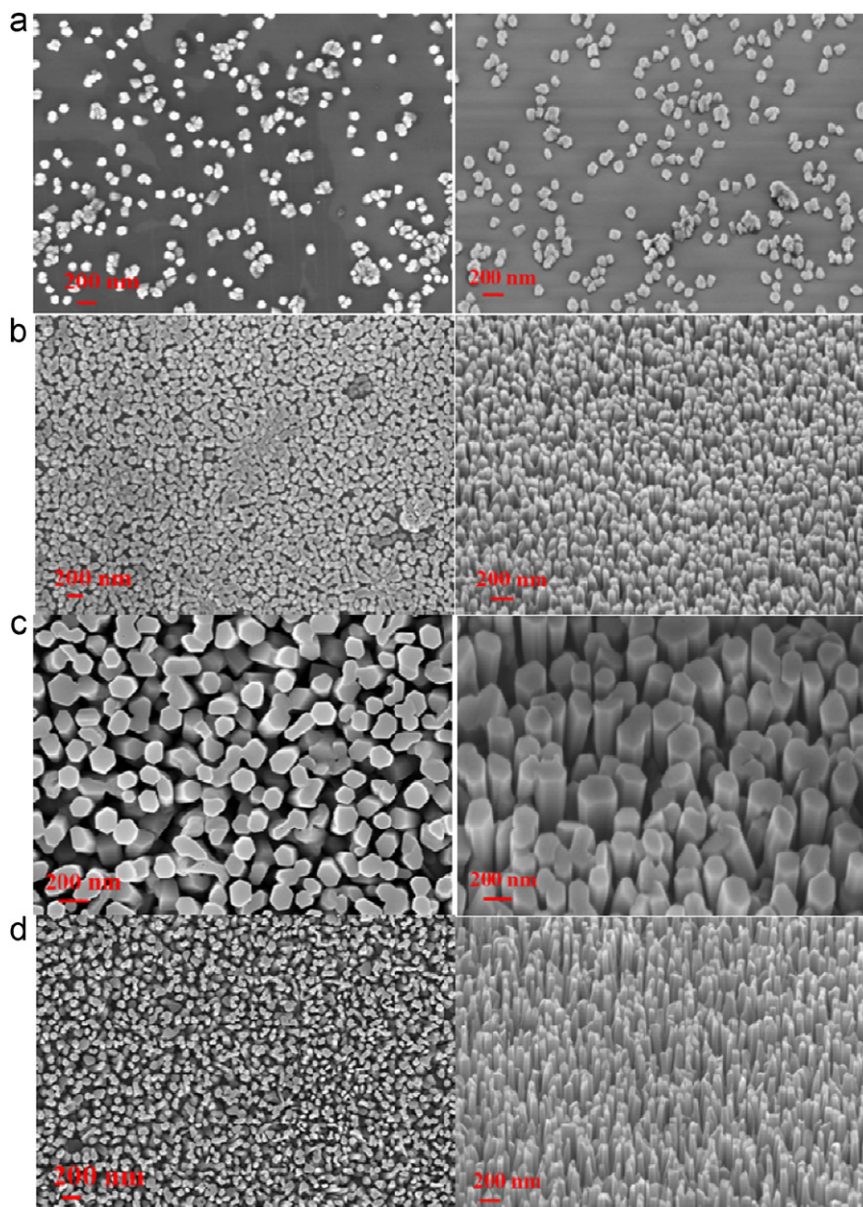


Fig. 1. FESEM top and 45° tilted views of ZnO nanowires grown at different growth durations. (a) 15 min, (b) 30 min, (c) 60 min and (d) 120 min.

from the reactive oxygen radicals. In addition to this, a very small peak at 62.87° belongs to the (103) reflection of ZnO. The observation of this weak peak indicates the quasi-alignment of nanowires. The calculated in-plane and out-plane lattice parameters ($a=3.251 \text{ \AA}$ and $c=5.204 \text{ \AA}$) are in good agreement with the standard bulk values which demonstrates that the nanowires are completely relaxed with high crystalline quality despite large mismatch between ZnO and silicon substrate.

Fig. 5(a) shows a typical micro-Raman spectrum of the vertically aligned ZnO nanowires grown on the silicon substrate. The sharp and dominant peaks at 99.4 and 437.1 cm^{-1} correspond to the non-polar E_2 phonon modes. The dominant peak at 99.4 cm^{-1} is attributed to the lattice vibrations of zinc atoms and assigned as E_2^{low} phonon mode. The peak at 437.1 cm^{-1} corresponds to E_2^{high} phonon mode and attributed to the lattice vibrations of oxygen atoms, which is very sensitive to crystalline nature and defects of the nanostructures. The appearance of E_2^{high} phonon mode confirms the wurtzite structure of the ZnO nanowires. The peak positions of the E_2 phonon modes are in good agreement with the standard bulk values of ZnO [20]. The narrow FWHM (1.4 and 9.1 cm^{-1}) of the

non-polar phonon modes (E_2^{low} and E_2^{high}) substantiates the high optical and crystalline qualities of the nanowires which corroborates with the XRD results. The peak at 276 cm^{-1} is assigned as $B_1(\text{low})$ and the appearance of this peak evidences the breakdown of translational symmetry in the nanostructures [21]. The observed peak at 582 cm^{-1} could not be attributed to the $E_1(\text{LO})$ phonon mode, because it is one of the forbidden modes of vibration in the back scattering geometry. Hence, it may be attributed to either $B_1(\text{high})$ or $A_1(\text{LO})$. It is well known that $B_1(\text{low})$ and $B_1(\text{high})$ modes are silent. However, the earlier reports show that the silent modes are observable in the case of nanostructures due to the breakdown of the translational symmetry. These modes should be comparable in intensities and the line width of $B_1(\text{low})$ mode must be very small as compared to $B_1(\text{high})$ mode [22]. But, in our case, the intensities of the silent mode are not comparable. Consequently, the peak at 582 cm^{-1} could not be attributed to $B_1(\text{high})$ mode. Therefore, the observed peak is assigned to be $A_1(\text{LO})$ and it is generally observed at the wave number of 574 cm^{-1} . It is blue shifted from its original position owing to the increase of free carrier concentration. A strong correlation have already been established between position of the

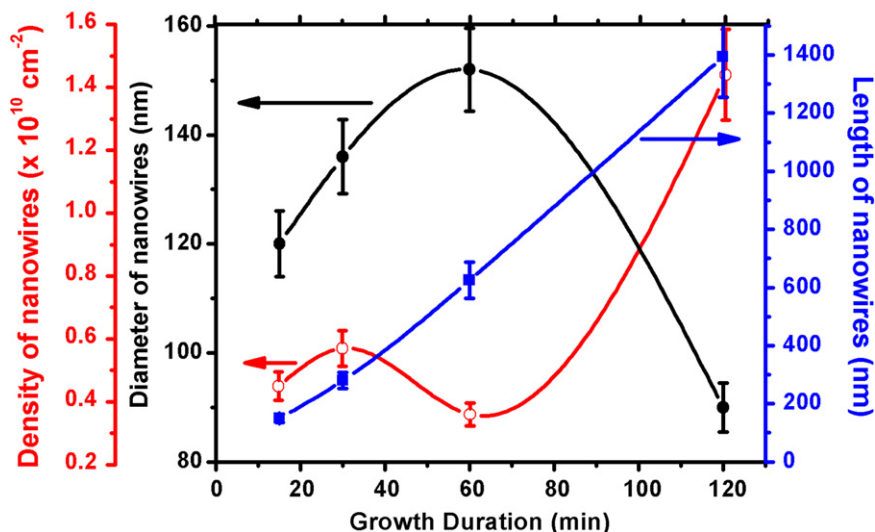


Fig. 2. Diameter, length and density distributions of ZnO nanowires as a function of different growth durations.

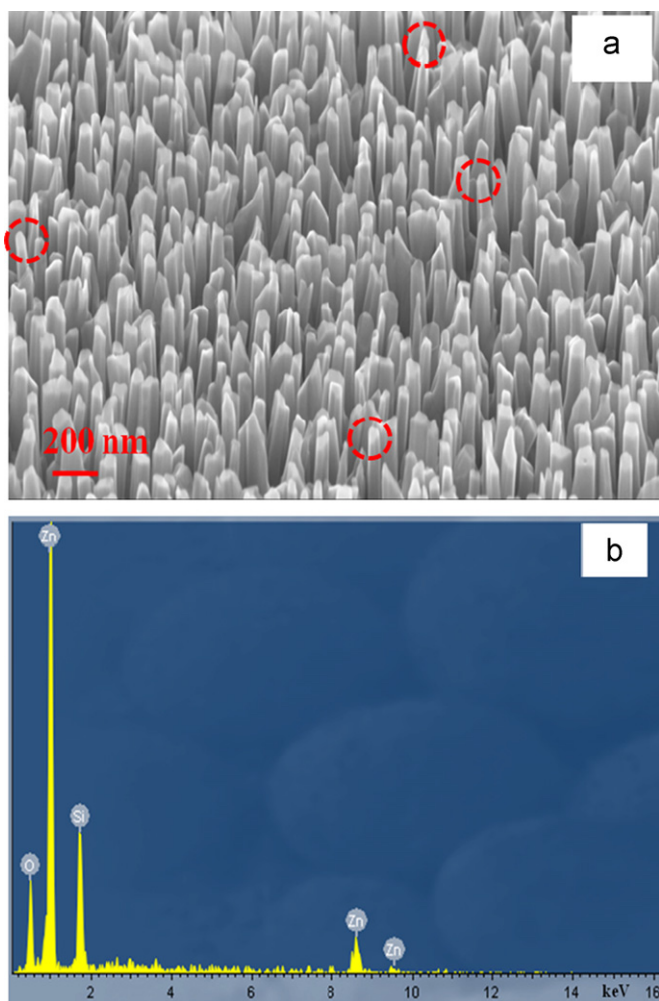


Fig. 3. (a) 45° tilted view of the vertically aligned ZnO nanowires grown on the silicon (111) substrate for the growth duration of 120 min. (b) EDX spectrum of the array of ZnO nanowires.

$A_1(\text{LO})$ mode and free carrier concentrations [23]. The $A_1(\text{LO})$ phonon mode shifts to the higher wave numbers with broadening of peak owing to the coupling between phonons and plasmons

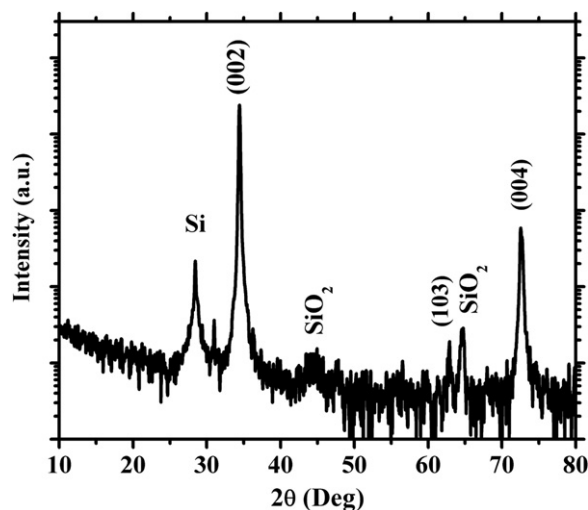


Fig. 4. XRD pattern of vertically aligned ZnO nanowires (The silicon and silicon dioxide peaks arise from the substrate).

[24–26], can be associated to the increase of free carrier concentration in ZnO nanowires. The peaks at 233, 302, 520, 620 and 670 cm^{-1} are attributed from the silicon substrate. The micro-Raman spectrum of the bare silicon substrate is shown in Fig. 5(b) for the comparison and the enlarged view shown in the inset of Fig. 5(b) clearly depicts the weak peaks.

Fig. 6(a) shows the temperature dependent PL spectra of the undoped ZnO nanowires measured in the temperature range of 10–330 K. The observed emission peak at 3.343 eV is typical donor to bound exciton (D^0X) emission [27]. By increasing the temperature from the low temperature (10 K) to room temperature, D^0X peak shifts monotonically towards the low energy side. A 166 meV red shift of the band edge emission over this temperature range is caused by the thermal expansion of the lattice and electron–phonon interactions. The intensity of the peak decreases with increasing the temperature as a result of the refreezing of phonons and stimulation of non-radiative recombination processes. It is reported that the longitudinal optical (LO) phonon energy of bulk ZnO is ~ 72 meV [28]. The observed emission peaks at 3.26 and 3.18 eV are associated to the first and second LO phonon replicas of two electron satellite lines [29]. The dominant and broad emission at 2.28 eV is associated to

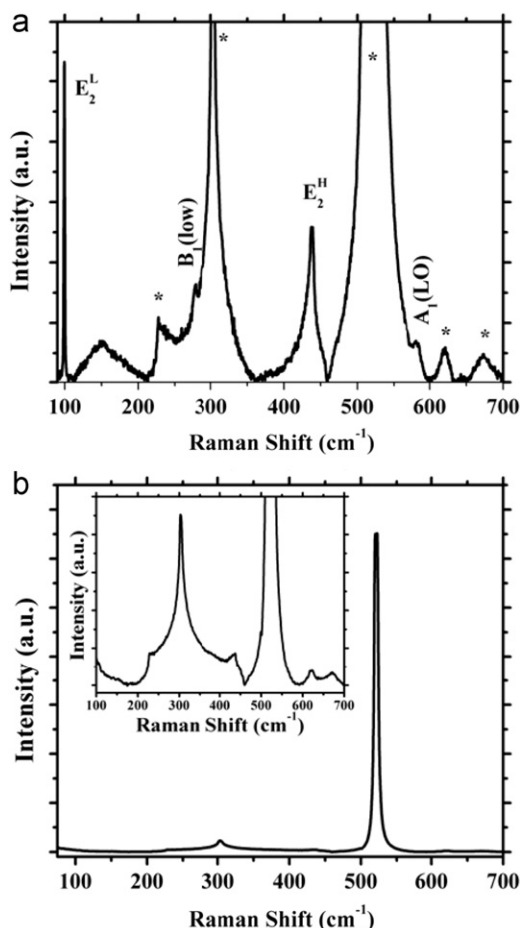


Fig. 5. (a) Micro-Raman spectrum of vertically aligned ZnO nanowires recorded in back scattering geometry with an excitation wavelength of 632.8 nm. (b) Micro-Raman spectrum of the bare silicon substrate. The inset shows the enlarged view of the Raman spectrum of silicon.

the singly ionized oxygen vacancies and this green luminescence is attributed to the electron transition from the shallow donor level (V_o) to a shallow acceptor level (V_{Zn}) [13,30]. As the ZnO nanowires were grown under pure Ar atmosphere, the oxygen vacancy is expected and further the growth temperature of 550 °C is more responsible for reducing the oxygen radicals available for the crystallization at the growth front. The green emission intensity drastically increases and overshoots the D⁰X emission as the decrease of temperature. Fig. 6(b) shows the variation of D⁰X peak energy of the ZnO nanowires as a function of temperature. Varshni's empirical equation can be fitted with the experimental data to find the temperature dependence of D⁰X peak and can be written as [31].

$$E(T) = E(0) - \left(\frac{\alpha T^2}{T + \beta} \right)$$

where $E(T)$ and $E(0)$ are the band gap at an absolute temperature T and 0 K respectively. α and β are the Varshni thermal coefficients. From the fitted curve, the Varshni parameters $E(0)$, α and β were found to be 3.3434 eV, 1.01×10^{-3} eV/K and 1006 K respectively. The obtained values are comparable to the earlier reported values [32]. The PL line width of D⁰X emission increases with the temperature as shown in Fig. 6(b). Earlier reports show that there is a strong correlation between the broadening of band edge emission and carrier concentration [33–35]. At 10 K, if the broadening of band edge emission is solely attributed by the thermal

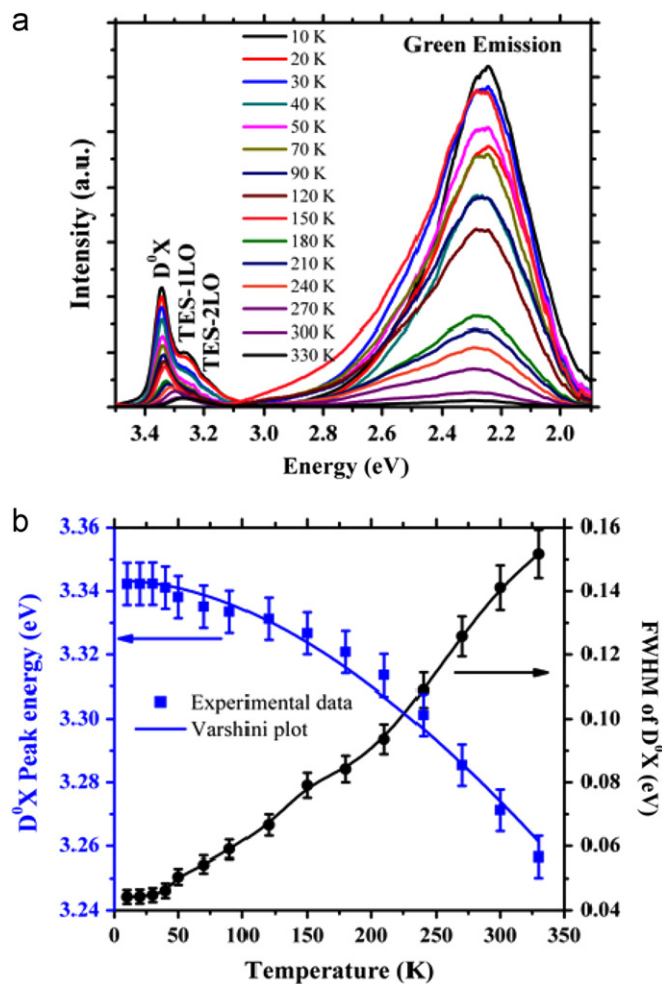


Fig. 6. (a) Temperature dependent PL spectra of ZnO nanowires grown on silicon (111) substrate. (b) Variations of D⁰X peak energy (eV) and FWHM (eV) as a function of temperature (K).

broadening, then its value should be ~ 1.3 meV ($3 k_B T/2$). However, the additional broadening also occurs due to the point defects induced by either non-stoichiometry or lattice/thermal mismatch between the deposited materials and substrates. In our case, the PL line width at 10 K is around 44 meV which depicts that the additional broadening of the peak has been occurred due to the point defects. This indicates that the growth conditions and selection of substrate play an important role in the growth of high quality materials since they can create point defects in oxide semiconductors which are similar to carrier doping. The observed broad band edge emission indicates the high concentration of point defects which is further substantiated by the dominant green emission. Thus, the broadening of the band edge emission is attributed to the enhancement of the free carrier concentration induced by the point defects in the nanowires [35] as substantiated by the blue shift of A₁(LO) phonon mode.

4. Conclusion

Vertically aligned ZnO nanowires have been grown successfully on silicon (111) substrate under pure Ar atmosphere of 0.01 mbar at 550 °C by the rf magnetron sputtering technique. The diameter, length and density distributions of the nanowires under different growth durations indicate that the growth of the nanowires governed by the migration length of adatoms which

strongly influenced by pressure and temperature. The structural study of the nanowires illustrates the highly crystalline nature and hexagonal wurtzite structure of the nanowires with preferential orientation along the *c*-axis. The characteristics of E_2^{high} phonon mode corroborates with the XRD results of high crystalline quality with strain free nature of ZnO nanowires. A blue shift of $A_1(\text{LO})$ phonon mode along with the broad band edge PL emission confirms the enhancement of the free carrier concentration in the nanowires due to the point defects. The pre-dominant green emission at 2.28 eV is attributed to the electron transitions between shallow donor (V_o) and shallow acceptor (V_{Zn}) energy levels.

Acknowledgments

One of the authors KJ acknowledges Department of Science and Technology (DST)-Nanomission under the contract no SR/NM/NS-77/2008 for the development of infrastructural facility. KJ also thanks DST, Govt. of India for the partial financial support under the scheme of Fund for Improvement of Science and Technology Infrastructure in Universities and Higher Educational Institutes (FIST). KJ also thanks University Grants Commission (UGC) for the partial financial assistance under the contract no 41-963/2012(SR). One of the authors (PSV) acknowledges UGC, Govt. of India for the award of a UGC—meritorious fellowship. The authors would like to thank Dr. V. Ramakrishnan and Miss. P. Sangeetha for the fruitful discussions on Raman scattering.

References

- [1] A. Nadarajah, R.C. Word, J. Meiss, R. Könenkamp, *Nano Lett.* 8 (2008) 534–537.
- [2] X.W. Sun, J.Z. Huang, J.X. Wang, Z. Xu, *Nano Lett.* 8 (2008) 1219–1223.
- [3] A.J. Cheng, Y. Tzeng, Y. Zhou, M. Park, T. h. Wu, C. Shannon, D. Wang, W. Lee, *Appl. Phys. Lett.* 92 (2008) 092113.
- [4] C.S. Chen, C.T. Kuo, T.B. Wu, I.N. Lin, *Jpn. J. Appl. Phys.* 36 (1997) 1169–1175.
- [5] T. Shimomura, D. Kim, M. Nakayama, *J. Lumin.* 112 (2005) 191–195.
- [6] C. Ronning, P.X. Gao, Y. Ding, Z.L. Wang, D. Schwen, *Appl. Phys. Lett.* 84 (2004) 783–785.
- [7] J.E. Nause, *III–Vs Rev.* 12 (1999) 28.
- [8] R.F. Service, *Science* 276 (1997) 895.
- [9] T. Makino, C.H. Chia, N.T. Tuan, Y. Segawa, M. Kawasaki, A. Ohtomo, K. Tamura, H. Koinuma, *Appl. Phys. Lett.* 77 (2000) 1632–1634.
- [10] R.S. Wagner, W.C. Ellis, *Appl. Phys. Lett.* 4 (1964) 89–90.
- [11] V.G. Dubrovskii, G.E. Cirilin, V.M. Ustinov, *Semiconductors* 43 (2009) 1539–1584.
- [12] N. Wang, Y. Cai, R.Q. Zhang, *Mater. Sci. Eng. R* 60 (2008) 1–51.
- [13] P.Sundara Venkatesh, V. Purushothaman, S.Esakki Muthu, S. Arumugam, V. Ramakrishnan, K. Jeganathan, K. Ramamurthi, *Cryst. Eng. Commun.* 14 (2012) 4713–4718.
- [14] R. Calarco, R.J. Meijers, R.K. Debnath, T. Stoica, E. Sutter, H. Lüth, *Nano Lett.* 7 (2007) 2248–2251.
- [15] D. Tham, C.-Y. Nam, J.E. Fischer, *Adv. Funct. Mater.* 16 (2006) 1197–1202.
- [16] R. Könenkamp, R.C. Word, C. Schlegel, *Appl. Phys. Lett.* 85 (2004) 6004–6006.
- [17] O. Lupan, T. Pauporté, B. Viana, *J. Phys. Chem. C* 114 (2010) 14781–14785.
- [18] E.I. Givargizov, *Highly Anisotropic Crystals*, Reidel, Dordrecht, 1987.
- [19] D.S. Kim, U. Gösele, M. Zacharias, *J. Cryst. Growth* 311 (2009) 3216–3219.
- [20] T.C. Damen, S.P.S. Porto, B. Tell, *Phys. Rev.* 142 (1966) 570–574.
- [21] M. Tzolov, N. Tzenov, D. Dimova-Malinovska, M. Kalitzova, C. Pizzuto, G. Vitali, G. Zollo, I. Ivanov, *Thin Solid Films* 396 (2001) 274–279.
- [22] F.J. Manjón, B. Marí, J. Serrano, A.H. Romero, *J. Appl. Phys.* 97 (2005) 053516.
- [23] M. Kuball, *Surf. Interface Anal.* 31 (2001) 987–999.
- [24] A.J. Cheng, Y. Tzeng, H. Xu, S. Alur, Y. Wang, M. Park, T. h. Wu, C. Shannon, D.J. Kim, D. Wang, *J. Appl. Phys.* 105 (2009) 073104.
- [25] K. Jeganathan, R.K. Debnath, R. Meijers, T. Stoica, R. Calarco, D. Grützmacher, H. Lüth, *J. Appl. Phys.* 105 (2009) 123707.
- [26] P. Sundara Venkatesh, V. Ramakrishnan, K. Jeganathan, *Cryst. Eng. Commun.* 14 (2012) 3907–3914.
- [27] H.M. Cheng, H.C. Hsu, Y.K. Tseng, L.J. Lin, W.F. Hsieh, *J. Phys. Chem. B* 109 (2005) 8749–8754.
- [28] T. Makino, Y. Segawa, M. Kawasaki, *J. Appl. Phys.* 97 (2005) 106111.
- [29] Ü. Özgür, Y.I. Alivov, C. Liu, A. Teke, M.A. Reshchikov, S. Doğan, V. Avrutin, S.J. Cho, H. Morkoç, *J. Appl. Phys.* 98 (2005) 041301.
- [30] E. Gür, S. Tüzemen, K. Meral, Y. Onganer, *Appl. Phys. A: Mater. Sci. Process.* 94 (2009) 549–554.
- [31] Y.P. Varshni, *Physica* 34 (1967) 149–154.
- [32] H.J. Ko, Y.F. Chen, Z. Zhu, T. Yao, I. Kobayashi, H. Uchiki, *Appl. Phys. Lett.* 76 (2000) 1905–1907.
- [33] T.N. Morgan, *Phys. Rev.* 139 (1965) A343–A348.
- [34] E. Iliopoulos, D. Doppalapudi, H.M. Ng, T.D. Moustakas, *Appl. Phys. Lett.* 73 (1998) 375–377.
- [35] V.V. Ursaki, I.M. Tiginyanu, V.V. Zalamai, E.V. Rusu, G.A. Emelchenko, V.M. Masalov, E.N. Samarov, *Phys. Rev. B* 70 (2004) 115204.

Hydrothermal Synthesis of One Dimensional Mo Doped *n*-Type ZnO Nanowires on *p*-Type Si Substrate

P. Biswas^{1,*} and K. Jagenathan²

¹School of Physics, Shri Mata Vaishno Devi University, Katra 182320, J&K, India

²Centre for Nanoscience and Nanotechnology, Bharathidasan University, Tiruchirappalli 620024, TN, India

ABSTRACT

The low temperature hydrothermal synthesis of undoped and doped *n*-type ZnO nanowires on *p*⁺ silicon substrate with seed layer was studied. The products were characterized by field emission scanning electron microscopy (FESEM) integrated with energy-dispersive X-ray spectroscopy (EDS) facility, photoluminescence spectroscopy (PL) and electrical source measurement techniques. The FESEM and EDS studies revealed vertical aligned ZnO nanowires with hexagonal morphology having equimolar concentration of Zn and O with Mo Dopant. The band edge emission of Mo doped ZnO exhibited red-shift as compared to undoped ZnO NWs. The *I*-*V* curves of resulting *n*-ZnO NWs/*p*⁺-Si heterostructure exhibit *p*-*n* junction diode characteristics. The present study may be projected as useful in developing enhanced electrical characteristics by optimizing the density and quality of ZnO NWs.

KEYWORDS: Hydrothermal, Nanowires, Seed Layer, Heterostructure.

1. INTRODUCTION

In the next two decades, the nanowire/nanorod based quasi one-dimensional materials will expect to have spectacular developments in nonmaterial research.¹ Particularly functional oxide nanowires have been emerged as significant building blocks for future electronic and photonic devices,¹⁻³ and for biomedical applications.⁴ Exhaustive research has been carried out on the potential applications of nanowires as interconnects and functional units in fabricating electronic, optoelectronic, electrochemical and electromechanical nanodevices.⁵ Compared to other low dimensional systems in which tunneling transport is required for charge carrier transfer, nanowires provide an unconfined direction for electrical conduction in device applications.⁶ In addition, there is unique density of electronic states in nanowires due to the constraint in diameters. This unique property of nanowires causes a significant difference in optical, electrical and magnetic performances compared to their bulk counterpart. Moreover, radiative recombination of charges can be improved in these physical structures, supporting the fabrication of nano-optoelectronic devices. Fine-tuning the properties of

nanowires through rational design and intelligent synthesis methods enables scientists to fabricate novel devices.⁶

Recently, ZnO nanowires have drawn the attention of the researchers due to their remarkable chemical and physical properties which make them indispensable for technological applications. They find their wide use in optoelectronics, light-emitting diodes, electromechanical devices, solar cells and sensor based applications.⁷⁻¹¹ There are a number of physical and chemical methods available for film deposition on substrates viz. thermal evaporation technique,¹² radio frequency sputtering,¹³ chemical vapour deposition¹⁴ and low temperature solution route¹⁵ (hydrothermal synthesis). Among these techniques, hydrothermal method is of particular interest as it is simple, cost-effective, low temperature and suitable for large scale production.¹⁶⁻¹⁸ Moreover, ZnO nanostructures can be tuned effectively simply by varying hydrothermal growth parameters such as concentration of seed layer solution, reaction temperature etc.¹⁹ Further, the characteristics of nanowires tend to change on doping with transition metals. For example, Mo doped ZnO thin films have been found to have good electrical conductivity.²⁰

Although a lot of work on synthesis and characterization of ZnO nanowires using various methods have been done,⁷⁻¹⁹ literature survey reveals that there is hardly any report on molybdenum (Mo) doped ZnO nanowires on *p*⁺-Si substrate through hydrothermal method.²⁰⁻²² This deficiency in literature motivated us to synthesize undoped

*Author to whom correspondence should be addressed.

Email: pankaj.biswas@smvdu.ac.in

Received: 29 June 2015

Accepted: 30 June 2015

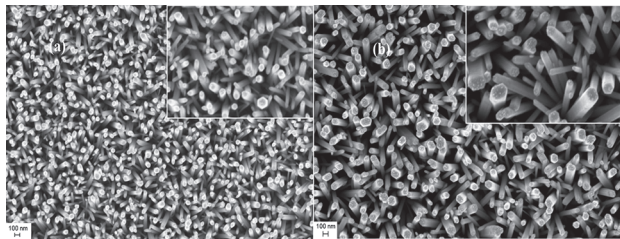


Fig. 1. FESEM image of the (a) undoped ZnO (b) ZnO:Mo 2 wt% grown on p^+ -Si substrate.

and Mo doped ZnO nanowire samples on both glass and p^+ -Si substrate using hydrothermal synthesis technique.

2. EXPERIMENTAL DETAILS

2.1. ZnO Nanowires Fabrication

Both undoped ZnO and ZnO:Mo nanowires were grown hydrothermally on p^+ -Si and glass substrates. This method is a two step process:

2.1.1. Seed Layer Preparation

The key idea to promote the growth of nanowires during synthesis was to initially prepare the seed layer. The seed layer plays an essential role in promoting nucleation and guiding oriented growth. Before it the substrates were thoroughly cleaned by sonication in acetone, isopropanol and de-ionized water for 10 min and then dried. A 10 mM seed layer solution of zinc acetate dehydrate and 2-propanol was prepared. The solution was then spin coated on *p*-type silicon [(100), boron doped, $\rho = 6 - 8 \Omega\text{-cm}$] and glass substrates at 2000 rpm for 30 s. The substrates were then annealed at 100 °C for 1 min after each spin coating to enhance adhesion. A uniform seed layer was obtained after five layers of spin coating.

2.1.2. Hydrothermal Growth of ZnO Nanowires

To grow ZnO nanowires, the substrates coated with ZnO seed layers were fixed upside down into the reaction vessel. The vessel contained zinc nitrate hexahydrate

[$\text{Zn}(\text{NO}_3)_2 \cdot 6\text{H}_2\text{O}$, 0.29748 g, 10 mM] and 0 and 2 wt% MoO_3 separately dissolved into 100 ml of de-ionized water. The reaction vessel sealed with circulating water condenser was kept at constant temperature of 90 °C for 1 hour. Finally, the samples were taken out, rinsed in de-ionized water and then dried in air and preserved for characterization.

3. CHARACTERIZATION

The size, shape and density of ZnO NWs were characterized by using field emission scanning electron microscopy (FESEM, Carl Zeiss—Sigma). The chemical composition of the obtained NWs was identified by Energy-dispersive X-ray spectroscopy (EDS) feature of FESEM. The optical characteristics of the NWs were investigated using photoluminescence (PL) and absorption measurements. The PL measurements were performed at room temperature with the 325 nm line of a He-Cd laser.

For electrical measurements, the space between the ZnO NWs is filled with an insulating layer of poly vinyl alcohol (PVA) by spin coating followed by baking the substrate at 120 °C for 40 min in a furnace. After this 1 μm thick gold film was deposited on the top of ZnO as cathode by thermal evaporation with a shadow mask and a layer of gold film was deposited on the back side of the p^+ -Si substrate to form ohmic contact. Finally an *n*-ZnO NWs/ p^+ -Si heterostructure was obtained. The current–voltage (I – V) characteristic of the device was measured by a source meter (Keithley 2400, Keithley Instruments, Inc., OH, USA).

4. RESULTS AND DISCUSSION

The general morphology of ZnO nanowires was obtained using field emission scanning electron microscopy. As shown in Figure 1, ZnO nanowires were vertically well aligned with uniform length, diameter and distribution density. The average diameters of the undoped ZnO and ZnO: 2 wt% Mo NWs are 58.6 nm and 82.4 nm respectively. It was observed that the diameter increase with

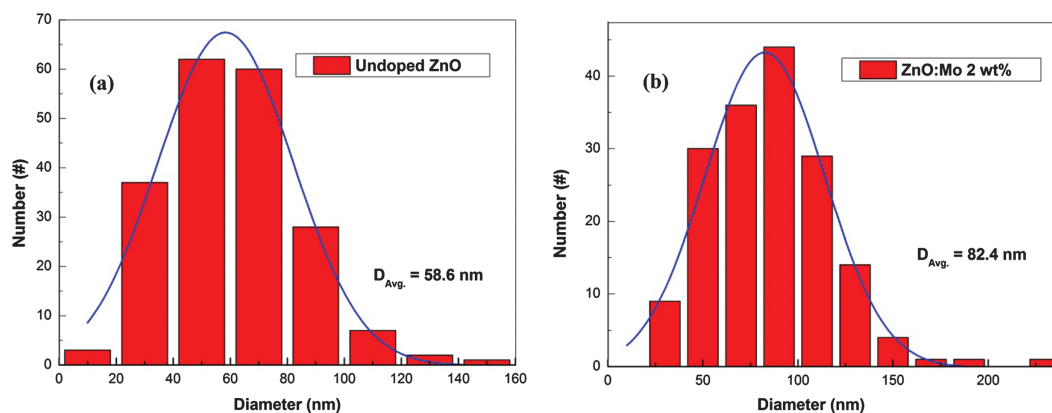


Fig. 2. Size distribution of (a) Undoped (b) Doped with 2 Wt% Mo ZnO NWs.

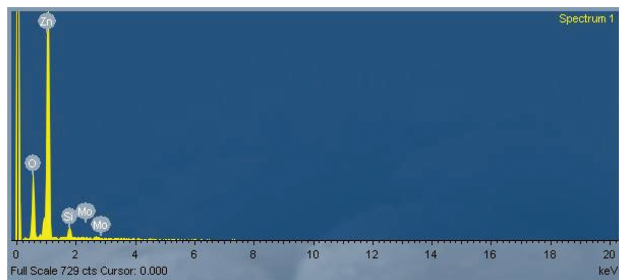


Fig. 3. EDS data of the as-grown sample of ZnO nanowires. Zn, O, Si and Mo peaks are present.

doping when Mo ion replaces Zn in the substitutional sites. Figure 2 shows the size distributions of ZnO NWs for undoped and doped samples. Their average length for 1 hour growth and density on p^+ -Si substrate were found to be $1.5 \mu\text{m}$ and $3.74 \times 10^9 \text{ cm}^{-2}$. Further, about two-third of the Si substrate surface is devoid of NWs. The hexagon shaped morphology of the NWs could be clearly observed in the top view FESEM images (see inset).

EDS of ZnO:Mo 2 Wt% nanowires grown on p^+ -Si was performed, and the resulting spectrographic data is shown in Figure 3. The Mo concentration (in weight%) in the nanowires was found to be 0.68 depending on the amount of Mo precursor used. It was expected to be higher but obtained lesser because MoO_3 dissolve sparingly in cold water.²³ EDS determines the composition of the synthesized ZnO nanostructures, and the results reveal that the NWs were composed of Zn, O, Mo, and Si. Quantitative EDS analysis showed that the atom percent ratio of Zn to O was about 1:1. The presence of the Si peak in the EDS pattern can be assigned to the Si substrate. Further, no indication of oxide impurities in our final product was observed.

The PL measurements were performed to evaluate the optical quality of the obtained ZnO NWs. Figure 4 shows typical room temperature photoluminescence (PL) spectra of ZnO NWs with an excitation wavelength of 325 nm at

room temperature. It could be seen that the PL spectrum of the undoped ZnO NWs exhibits a dominant UV emission at 370.7 nm (3.34 eV) while Mo doped NWs show strong UV emission at 374.8 nm (3.31 eV). These UV emissions were ascribed to the near band edge emission of the wide band gap of ZnO. It was observed that the doping ZnO with MoO_3 decreases the optical band gap of the resulting material. Figure 9(b) shows PL spectrum of Mo doped ZnO NWs which include the intense band to band emission corresponding to MoO_3 at 416.8 nm (2.97 eV)²³ along with the band edge emission at around 373.9 nm (3.31 eV).

Figure 5 shows the I - V characteristics of the n -ZnO NWs/ p^+ -Si substrate heterostructure of ZnO without and with Mo doping. The I - V relationship for a heterojunction is given by: Ref. [24].

$$I = I_s \left[\exp\left(\frac{qV}{k_B T}\right) - 1 \right]$$

where I is the current; I_s the saturation current; V , the applied voltage across the heterojunction from p-side to n-side; k_B , the Boltzmann constant; and T is the absolute temperature. The typical rectifying behavior of device could clearly be observed. The forward current increases more rapidly for doped device than that of the undoped one. There was no emission in the visible region because the diode currents were of the order of tenths of μA for large material resistance ($\sim 10^6 \Omega$).

The low threshold for undoped device under reverse bias could be ascribed to the band alignment of the p -Si/ n -ZnO heterojunction at the interface. Further, the series resistance (R_s) for the undoped and doped samples were found to be 38.9 M Ω and 11.8 M Ω respectively. The R_s can be obtained by calculating the slope in an $I/(dI/dV)$ versus I graphs in the high voltage region ($V > E_g/q$, where E_g is energy band gap) of the I - V characteristic curves.²⁵

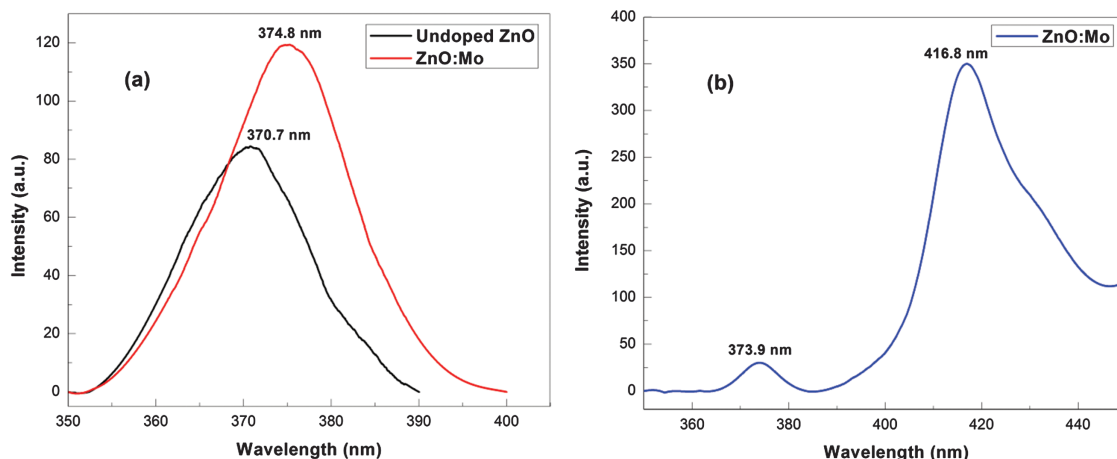


Fig. 4. Room temperature (a) near band edge emissions of undoped ZnO and ZnO:Mo (b) PL spectrum of Zn:Mo NWs ($\lambda_{\text{ex}} = 325 \text{ nm}$).

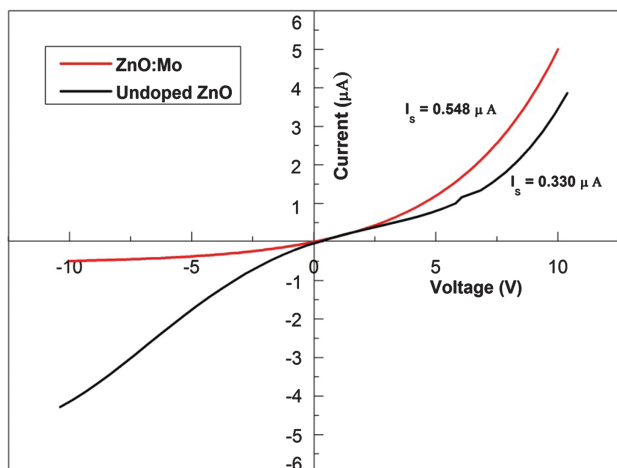


Fig. 5. I - V characteristics of the *n*-ZnO nanowires/ p^+ -Si substrate heterostructure of ZnO without and with Mo doping.

5. CONCLUSIONS

To summarize, the doped and undoped *n*-ZnO NWs/ p^+ -Si heterostructure with ZnO seed layer by low temperature hydrothermal technique have successfully been fabricated. FESEM and EDS demonstrate vertical aligned ZnO NWs with hexagonal morphology having equimolar concentration of Zn and O including Mo as dopant. The PL spectra show a decrease in optical band gap of NWs due to Mo doping into ZnO lattice. The I - V curves of the resulting *n*-ZnO NWs/ p^+ -Si heterostructure exhibit p - n junction diode characteristics. In future, the work is expected to be carried out to optimize the density and quality of ZnO NWs to enhance the characteristics to realize visible emission from the diode.

Acknowledgments: P. Biswas expresses his profound thanks to Centre for Nanoscience and Nanotechnology, Bharathidasan University, Tiruchirappalli, India for providing the research facilities to carry out this work.

References and Notes

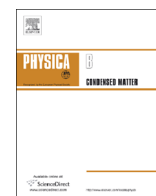
1. D. Appell, *Nature* 419, 553 (2002).
2. L. Samuelson, *Mater. Today* 6,22 (2003).
3. X. Duan, Y. Huang, Y. Cui, J. Wang, and C. M. Lieber, *Nature* 409, 66 (2001).
4. Y. Cui, Q. Wei, H. Park, and C. M. Lieber, *Science* 293, 1289 (2001).
5. K. S. Shankar and A. K. Raychaudhuri, *Mater. Sci. Engg. C* 25, 738 (2005).
6. Z. L. Wang, *Adv. Mater.* 12, 1295 (2000).
7. G. C. Yi, C. R. Wang, and W. I. Park, *Semi. Sci. Technol.* 20, S22 (2005).
8. Z. L. Wang, *ACS Nano* 2, 1987 (2008).
9. W. I. Park and G. C. Yi, *Adv. Mater.* 16, 87 (2004).
10. P. H. Yeh, Z. Li, and Z. L. Wang, *Adv. Mater.* 21, 4975 (2009).
11. M. Law, L. E. Greene, J. C. Johnson, R. Saykally, and P. D. Yang, *Nat. Mater.* 4, 455 (2005).
12. Y. Zhang, C. Wu, Y. Zheng, and T. Guo, *J. Semicond.* 33, 023001 (2012).
13. W. T. Chiou, W. Y. Wu, and J. M. Ting, *Diam. Relat. Mater.* 12, 1841 (2003).
14. D. J. Lee, J. Y. Park, Y. S. Yun, Y. S. Hong, J. H. Moon, B. T. Lee, and S. S. Kim, *J. Cryst. Growth* 276, 458 (2005).
15. J. H. Tian, J. Hu, S. S. Li, F. Zhang, J. Liu, J. Shi, X. Li, Z. Q. Tian, and Y. Chen, *Nanotechnology* 22, 245601 (2011).
16. W. B. Wu, G. D. Hu, S. G. Cui, Y. Zhou, and H. T. Wu, *Cryst. Growth Des.* 8, 4014 (2008).
17. Y. G. Wei, W. Z. Wu, R. Guo, D. J. Yuan, S. M. Das, and Z. L. Wang, *Nano Lett.* 10, 3414 (2010).
18. J. J. Dong, X. W. Zhang, Z. G. Yin, S. G. Zhang, H. R. Tan, J. X. Wang, Y. Gao, F. T. Si, and H. L. Gao, *ACS Appl. Mater. Interfaces* 3, 4388 (2011).
19. Y. J. Lee, T. L. Sounart, J. Liu, E. D. Spoeke, B. B. McKenzie, J. W. P. Hsu, and J. A. Voigt, *Cryst. Growth Des.* 8, 2036 (2008).
20. X. Xiu and W. Zhao, *Chin. Phys. B* 21, 066802 (2012).
21. U. Ozgur, Y. Alivov, C. Liu, A. Teke, M. A. Reshchikov, S. Dogan, V. Avrutin, S. J. Cho, and H. Morkoc, *J. Appl. Phys.* 98, 041301 (2005).
22. D. C. Look, *Mat. Sci. Eng. B. Adv.* 80, 383 (2001).
23. K. U. Rempel, A. A. Migdisov, and A. E. Williams-Jones, *Geochimica et Cosmochimica Acta* 70, 687 (2006).
24. A. Chithambararaj and A. C. Bose, *Beilstein, J. Nanotechnol.* 2, 585 (2011).
25. S. M. Sze, *Physics of Semiconductor Devices*, Wiley, New York (1981).



ELSEVIER

Contents lists available at ScienceDirect

Physica B

journal homepage: www.elsevier.com/locate/physb

Raman silent modes in vertically aligned undoped ZnO nanorods



P. Sundara Venkatesh^{a,b}, V. Ramakrishnan^c, K. Jeganathan^{a,*}

^a Centre for Nanoscience and Nanotechnology, School of Physics, Bharathidasan University, Tiruchirappalli 620 024, Tamilnadu, India

^b Department of Physics, Sri S. Ramasamy Naidu Memorial College, Sattur 626 203, Tamilnadu, India

^c Indian Institute of Science Education and Research, Trivandrum 695 016, Kerala, India

ARTICLE INFO

Article history:

Received 4 June 2015

Received in revised form

8 October 2015

Accepted 9 November 2015

Available online 10 November 2015

Keywords:

ZnO nanorods

Photoluminescence

Raman spectroscopy

Silent modes

ABSTRACT

We report the observation of Raman silent modes of B_1^{low} (276 cm^{-1}) and B_1^{high} (582 cm^{-1}) in vertically aligned ZnO nanorods due to the breakdown of translational symmetry. The structural studies reveal the high crystalline nature of the ZnO nanorods on the lattice mismatched silicon substrates. The dominant donor bound exciton emission and the phonon replicas signify the good quality of the nanorods which substantiate that the anomalous Raman modes could not be attributed to the intrinsic point defects. Further, our results show that the observed silent modes of wurtzite-ZnO become Raman active due to the breakdown of the wave-vector selection rule by loss of translational symmetry induced by nanorods geometry.

© 2015 Elsevier B.V. All rights reserved.

1. Introduction

Zinc oxide (ZnO) nanostructures have received a tremendous attention due to its unique properties and they are considered as fundamental building blocks for future nanoscale devices particularly in the field of optoelectronics such as light emitting and laser diodes [1–5]. Due to the large exciton binding energy of 60 meV, ZnO is one of the most promising materials for ultraviolet (UV) light emitting applications as compared to GaN since it reduces the UV lasing threshold and yields a better optical efficiency at room temperature [6]. In optoelectronic applications perspective, the optical quality of the nanostructures is a very important. In general, the optical properties of materials are mostly investigated by the temperature dependent photoluminescence measurements since it is one of the promising and powerful tools to analyze the point defects and exciton recombinations. It is found that the presence of phonon replicas in the photoluminescence spectra of nanostructures and bulk materials witness the good quality of materials [7]. In addition to this, micro-Raman spectroscopy is a versatile tool to analyze the crystalline and optical properties of materials especially nanostructures. According to the backscattering geometry of Raman selection rules, $2E_2$ and $A_1(\text{LO})$ phonon modes are only allowed phonon modes of vibration since the other modes are forbidden including the $2B_1$ symmetry phonon modes.

Recently, we have reported the growth and characterization of vertically aligned ZnO nanowires on silicon substrates by radio

frequency magnetron sputtering without metal catalyst [8]. In the Raman spectrum of grown ZnO nanowires, one of the forbidden modes (B_1^{low}) is observed in the back scattering geometry. It encourages finding a unique reason behind the observation of forbidden modes in the Raman spectrum of ZnO nanowires. Further, there is a lot of controversies occurred on the observation of anomalous Raman modes, especially B_1^{low} and B_1^{high} in the Raman spectra of ZnO. Tzolov et al. found the anomalous Raman modes at 276 cm^{-1} both in the undoped and Al doped ZnO thin films which correspond to the silent mode, B_1^{low} and it is attributed to the electric field induced Raman scattering [9]. Recently, Fe, Sb, Al, Ga and Li doped ZnO thin films grown by multistep pulsed laser deposition exhibit the anomalous Raman modes at 277, 511, 584 and 644 cm^{-1} due to the intrinsic defects and doping [10]. Further, in the case of N doped ZnO, the anomalous Raman modes at ~ 275 , 510, 582 and 643 cm^{-1} correspond to the B_1^{low} , $2B_1^{\text{low}}$, B_1^{high} and $TA + B_1^{\text{high}}$ respectively which are attributed to the local vibrational modes of N since the above vibrations are not observed on the undoped ZnO [10–12]. Hence, a detailed investigation is essential to understand the observation of anomalous Raman modes in ZnO.

In the present work, we have focussed our attention on the comparison of micro-Raman spectra of undoped ZnO nanorods and thin film grown on silicon substrates by radio frequency (rf) magnetron sputtering to understand the origin of observed anomalous Raman silent modes in ZnO nanorods.

2. Experimental section

Vertically aligned undoped ZnO nanorods and thin film were

* Corresponding author.

E-mail address: kjeganathan@yahoo.com (K. Jeganathan).

grown on silicon (111) substrates with a vicinal off-angle of $\pm 0.5^\circ$ under pure argon sputtering pressure of 6×10^{-3} mbar by rf-magnetron sputtering. The deposition parameters and processes were already described elsewhere [8,13] and that were adopted for the fabrication of ZnO thin film and nanorods. Briefly, ZnO nanorods and thin film were deposited on silicon substrates at 550 °C and 350 °C respectively. The target to substrate distance, growth duration and rf-power were kept constant as 50 mm, 60 min and 140 W respectively.

The morphology of the samples was examined using a field emission scanning electron microscope (FESEM, Carl Zeiss-Σigma) with the maximum resolution of 1.2 nm. The structural properties of the undoped ZnO nanorods and thin film were investigated by Rigaku X-ray diffractometer with Cu K_α radiation of wavelength $\lambda = 1.5406 \text{ \AA}$. The X-ray diffraction patterns were recorded using Bragg–Brentano (θ – 2θ) geometry between 30° and 80° with a step size of 0.05° for the structural identification. The exciton recombinations and point defects in the ZnO nanorods and thin film were analyzed by the temperature dependent photoluminescence measurements using a high resolution HORIBA JOBIN YVON monochromator (0.55 m) with 325 nm He–Cd laser as an excitation source. For the temperature dependent photoluminescence measurements (10–300 K), the samples were placed inside a closed cycle helium cryostat (Janis Research Company Inc., USA) and the luminescence signal from the samples was collected by a charge coupled device through appropriate optical arrangements. The resolution of photoluminescence measurement set-up is 0.025 nm and the data was collected with the step size of 0.002 nm. Room temperature micro-Raman scattering measurements of the ZnO nanorods and thin film were carried out using a LabRam HR800 Raman spectrometer in the backscattering geometry. He–Ne laser of 632.8 nm wavelength with the power of 17 mW was used as an excitation source and the laser beam was focused through an optical microscope (100x) with a spot size of $\sim 1 \mu\text{m}$. The thickness of the ZnO thin films grown under the substrate temperature of 350 °C was measured by the Filmetrics “F20” thickness measurement instrument.

3. Results and discussion

Fig. 1(a) and (b) shows the FESEM images of undoped ZnO thin film and nanorods respectively grown on silicon substrates by rf-magnetron sputtering technique. Fig. 1(a) clearly depicts the thin film like morphology with rough surfaces and its average thickness is 470 nm. Fig. 1(b) confirms the vertical alignment of ZnO nanorods with smooth surfaces and a high degree of size uniformity along the axial direction. Further, the nanorods also exhibit the hexagonal cross section along the c -axis. The average length and the diameter of the ZnO nanorods are 1.5 μm and 350 nm respectively. The inset of Fig. 1(b) shows the diameter distribution of ZnO nanorods. In the deposition of ZnO thin film and nanorods, all the growth parameters are kept identical except the substrate temperature. It is well known that the migration length of the adatoms depends on the various growth parameters such as substrate temperature and deposition pressure. In general, the growth of vertically aligned one-dimensional (1-D) nanostructures is enhanced by the adatoms in two ways either direct impingement or migration through the sidewalls of the nanostructures [14]. In the case of direct impingement of adatoms on a tip of the nanostructures, the growth rate is small for the smaller diameter nanostructures and vice versa due to the Gibbs–Thomson effect. But, in the case of surface migration of the adatoms through the sidewalls of the nanostructures along with direct impingement, the growth rate is higher for the thinner nanorods and vice versa [15]. Further, the growth of the nanostructures will

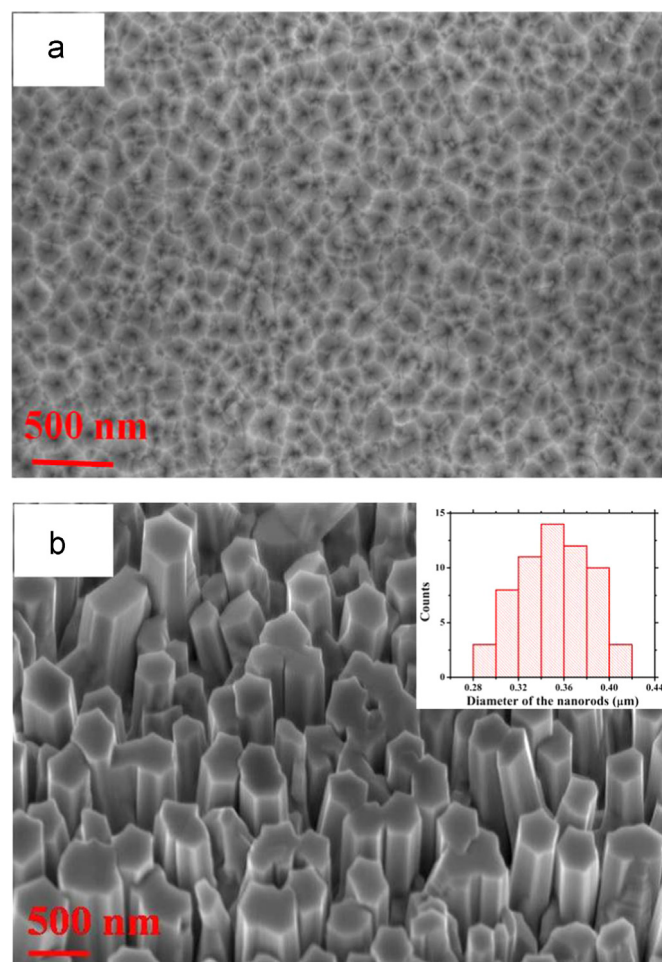


Fig. 1. FESEM images of ZnO deposited by the rf-magnetron sputtering under pure argon sputtering pressure (a) Thin film and (b) Nanorods. The inset of Fig. 1 (b) shows the diameter distribution of ZnO nanorods.

be enhanced along the axial direction only if the length of the nanostructures is smaller than the migration length, otherwise it will be desorbed from the surface of the nanostructures or enhances the lateral growth of nanostructures. Furthermore, it is found that the adatoms have high degree of migration length under elevated substrate temperatures and vice versa [16,17]. This suggests that the migration length of adatoms vary with the deposition pressure and substrate temperature. Hence, we believe that the observed vertically aligned ZnO nanorods at elevated temperature are attributed to the adatoms with higher migration length since it promotes the axial growth of the nanostructures by the process of sidewall diffusion along with the direct impingements. On the other hand, low growth temperature promotes ZnO thin film.

Fig. 2(a) depicts the X-ray diffraction (XRD) pattern of the undoped ZnO thin film and nanorods grown under pure argon sputtering pressure. All the observed peaks correspond to standard bulk counterparts of ZnO indicate the hexagonal wurtzite crystal structure. The dominant and weak peaks at $\sim 34.4^\circ$ and 72.6° correspond to the (002) and (004) reflections of wurtzite ZnO respectively. The appearance of a weak peak at 62.8° is attributed to the (103) reflection which represents the off-orientation of ZnO nanorods and thin film prefer (002) crystallographic direction. The (002) peak position of ZnO nanorods and thin film is 34.39° and 34.35° respectively which are less than the standard bulk value (34.45°) representing that the nanorods and thin film are in the state of uniform compressive stress as shown in Fig. 2

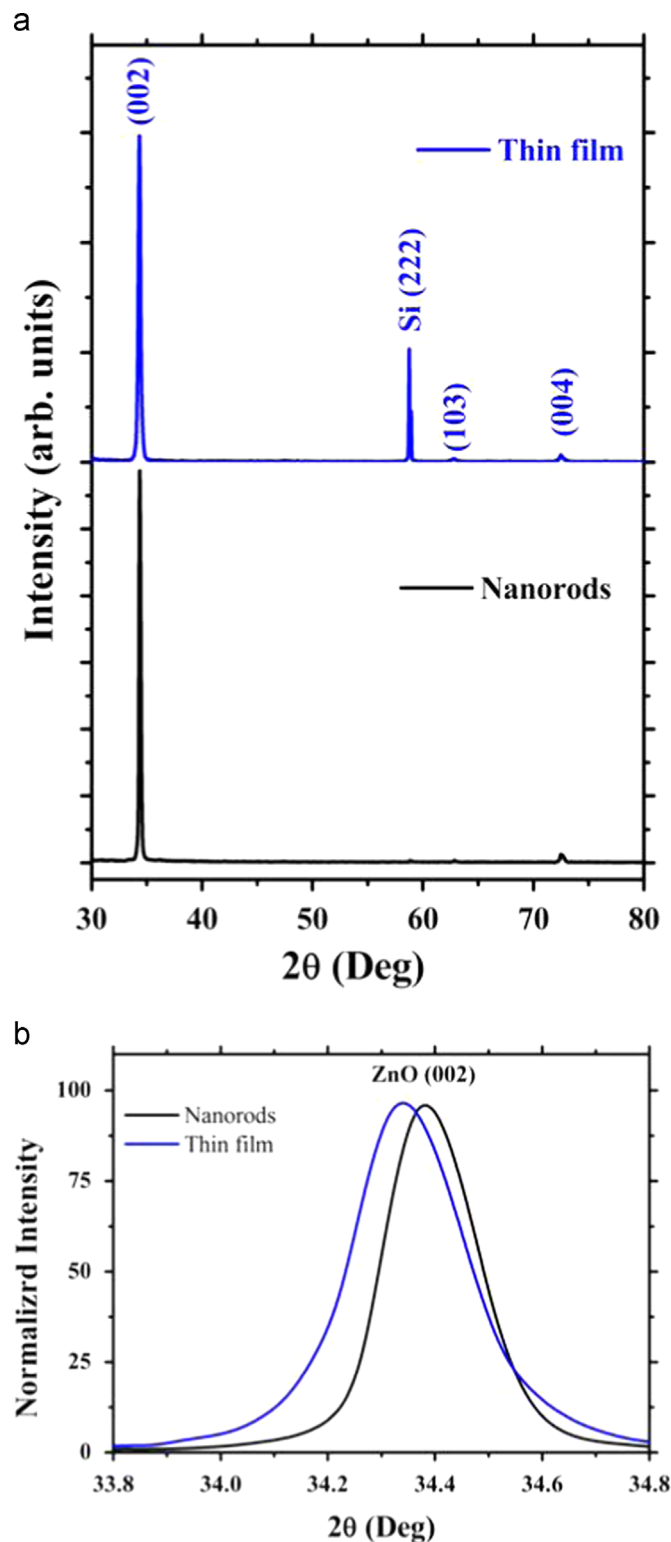


Fig. 2. (a) A typical XRD pattern of ZnO nanorods and thin film grown on the silicon (111) substrates. (b) Enlarged (002) peak position of ZnO nanorods and thin film.

(b). The thin films are extremely compressed as compared to the nanorods due to large foot prints on the lattice mismatched silicon substrate as shown in Fig. 1(a). The structural quality also reflected by the full width at half maximum (FWHM) of nanorods and thin film as ~ 558 and 723 arc-s respectively. Further, the FWHM of ZnO nanorods agree well with the bulk ZnO single crystal grown by

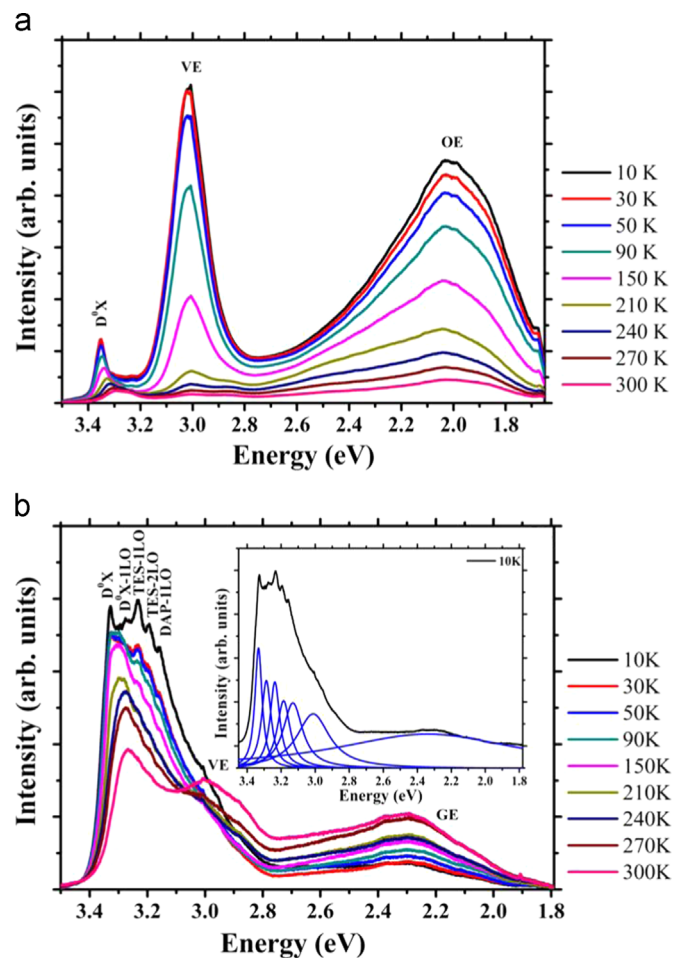


Fig. 3. Temperature dependent photoluminescence spectra of ZnO using He-Cd laser as an excitation source (a) Thin films and (b) Nanorods. The inset of Fig. 3 (b) shows the Lorentz peak fitted photoluminescence spectrum recorded at 10 K.

chemical vapor transport [18] which reflects that the crystalline nature of the nanorods is comparable to that of bulk samples. The observed results are further substantiated by the intensity ratio of $I_{(002)}/I_{(103)}$ reflections as 163 and 104 for the ZnO nanorods and thin films respectively, which also confirms the preferential orientation of nanorods with better crystalline quality.

Fig. 3 shows temperature dependent photoluminescence spectra of the ZnO thin film and nanorods grown under the substrate temperatures of 350 and 550 °C respectively. The dominant emission peak at ~ 3.35 and 3.33 eV for the thin film and nanorods respectively is attributed to the neutral donor bound exciton (D^oX) emission [19]. The intensity of D^oX emission quenches for both nanorods and thin film with increasing the temperature as a result of the refreezing of phonons. It is accounted that the longitudinal optical (LO) phonon replicas of ZnO are separated with one another by 72 meV [20]. The observation of phonon replicas in ZnO nanorods signifies the good optical quality as compared to thin film [7]. In order to depict the phonon replicas clearly, the photoluminescence spectrum recorded at 10 K is deconvoluted by Lorentz peak fitting and shown in the inset of Fig. 3(b). The peaks at ~ 3.29 , 3.25 , 3.18 and 3.13 eV correspond to the D^oX-1LO, two electron satellite (TES)-1LO, TES-2LO and donor acceptor pair (DAP)-1LO emissions respectively [19]. Further, the dominant D^oX emission as compared to defect mediated visible emissions and its phonon replicas in the ZnO nanorods also substantiate the good optical quality. The energy difference between the conduction band minimum and the zinc vacancy level (V_{Zn}) is about 3.06 eV

[21]. This clearly depicts that the acceptor level formed by V_{Zn} is well above the valence band maximum at ~ 0.3 eV. Hence, the peak at ~ 3.01 eV can be attributed to the transition of electrons from the conduction band minimum to the V_{Zn} level and this transition provides a clear evidence for the presence of zinc vacancies both in the ZnO thin film and nanorods. The intense peak at ~ 3.01 eV evidences the presence of more number of zinc vacancies in thin film samples. A broad peak around at 2.28 eV in the ZnO nanorods corresponds to oxygen vacancies and this green luminescence is attributed to the transition of electrons from the singly charged oxygen vacancy to a photo-excited hole [22,23]. This transition confirms the presence of oxygen related vacancies in the ZnO nanorods. However, the oxygen vacancy mediated emission is not observed in thin film grown under similar conditions except the substrate temperature. This suggests that the variation in the deposition temperature also affects the formation energy of the point defects. A peak at ~ 2.03 eV corresponds to the orange emission which is attributed to the oxygen interstitial related point defects in thin film [24,25]. The observed results are good agreement with our recent reports [26–28].

Micro-Raman scattering is an effective tool to analyze the material quality, phase orientation, transport properties and the interaction of phonons. Further, it is one of the non-destructive and contactless studies and subsequently it does not require any special sample preparation for the measurements. Wurtzite ZnO belongs to the space group of C_{6v}^4 which predicts that the eight sets of phonon modes are observable at wave vector $k \approx 0$ (Γ point). In the eight phonon modes of ZnO, six of them are optical phonon modes and remaining two phonon modes are acoustic. According to group theory, the optical mode at the Γ point of the Brillouin zone can be expressed by [29,30]

$$\Gamma_{opt} = 1A_1 + 2B_1 + 1E_1 + 2E_2 \quad (1)$$

$2B_1$ symmetry phonon modes are always both Raman and IR inactive. The $2E_2$ modes $\{E_2^{high}, E_2^{low}\}$ are non-polar and active in Raman scattering. E_2^{high} and E_2^{low} phonon modes are associated with the vibration of the oxygen and heavy zinc sub-lattices respectively. Both A_1 and E_1 modes are polar and hence which split into TO and LO phonons. These phonon modes are both Raman and IR active [31]. These observable phonon modes depend on the scattering geometry. In the case of backscattering geometry, the incident and scattered light has exactly parallel to its c -axis orientation of ZnO and hence E_2 and $A_1(LO)$ phonon modes are expected to emerge in the Raman scattering since the other modes are forbidden according to the Raman selection rules. Further, the E_1 phonon mode is observable only in the crossed polarization.

Fig. 4(a) shows the room temperature micro-Raman spectra of the undoped ZnO nanorods and thin film recorded in the backscattering geometry. A sharp peak at ~ 101 cm^{-1} corresponds to the E_2^{low} phonon mode of ZnO and it is attributed to the lattice vibrations of zinc atoms. The another non-polar phonon mode (E_2^{high}) at ~ 437 cm^{-1} is related to the lattice vibration of the oxygen atoms and is used to characterize the wurtzite phase of ZnO and its strain. E_2^{high} phonon modes for the ZnO nanorods and thin film are ~ 438.9 and 440.4 cm^{-1} respectively. This blue shift of the E_2^{high} phonon mode from its standard value (437 cm^{-1}) indicates the presence of compressive strain in the ZnO nanorods and thin film as shown in Fig. 4(b). FWHM of ZnO nanorods and thin film is 7.3 and 9.2 cm^{-1} , respectively. These results well corroborate with XRD studies. Further, $A_1(LO)$ phonon mode is absent for both thin films and nanorods and it is expected to be overlapped with the broad Silicon optical phonon mode at ~ 520 cm^{-1} . In contrast, it can be seen in Table 1 that all Raman active polar and non-polar modes can be observed in the backscattering geometry except forbidden silent modes for ZnO (0001)

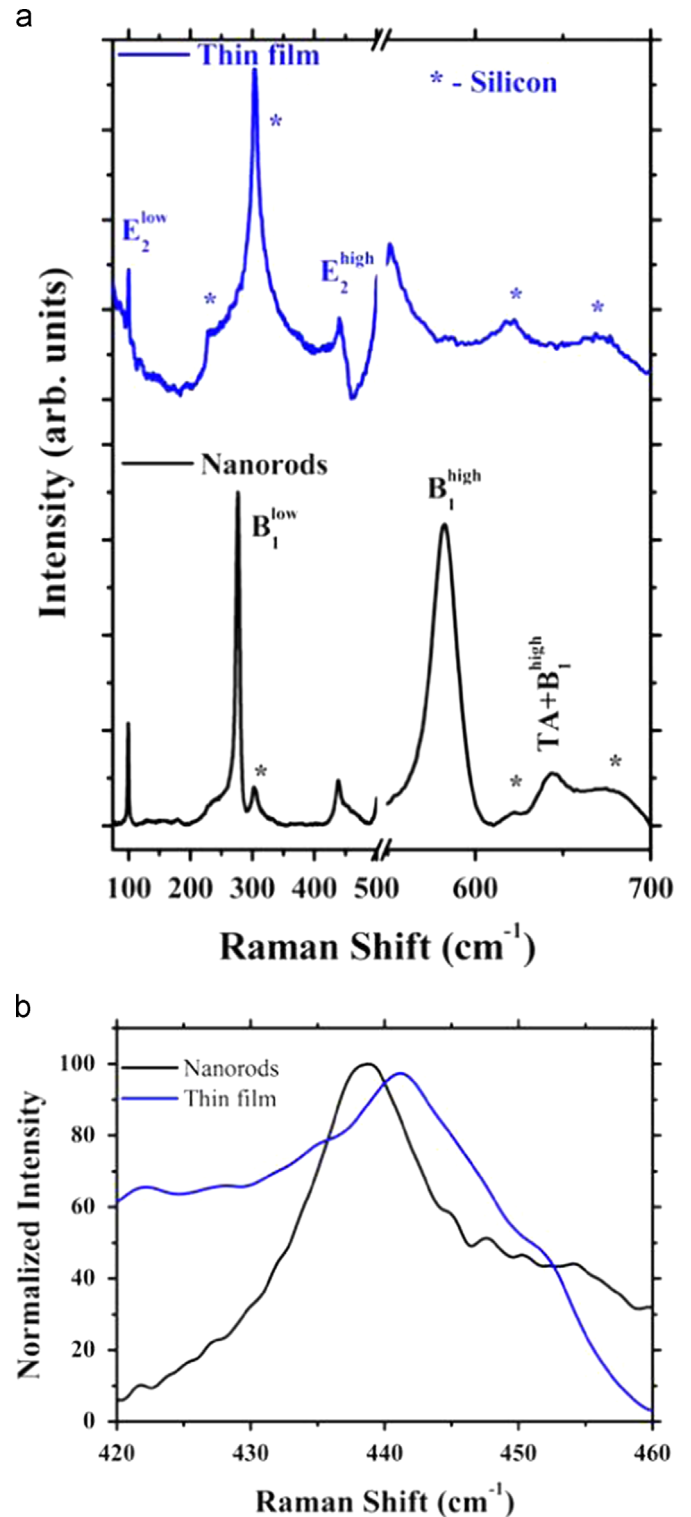


Fig. 4. (a) Micro-Raman spectra of ZnO nanorods and thin film recorded in the backscattering geometry using He–Ne laser as an excitation source. (b) Expanded E_2^{high} peak position of ZnO nanorods and thin film.

single crystalline substrate.

Table 1 shows the typical phonon frequencies and symmetries observed by Raman scattering for wurtzite ZnO nanorods and thin films. As compared to ZnO thin film, three additional peaks are observed at ~ 276 , 582 and 646 cm^{-1} for the ZnO nanorods. In general, the peak at 582 cm^{-1} is assigned to be $E_1(LO)$ mode and arises due to the oxygen deficiencies. In the backscattering

Table 1
Typical phonon frequencies and symmetries observed by Raman scattering for wurtzite ZnO nanorods and thin films.

Raman symmetry	Observed modes (cm ⁻¹)			Allowed modes in back-scattering geometry (cm ⁻¹) Z(-, -)Z ^a
	Thin film	Nanorods	Bulk ^b	
E ₂ ^{low}	102.9	100.5	101	101
2E ₂ ^{low}	-	-	208	-
B ₁ ^{low}	-	276	-	-
E ₂ ^{high} -E ₂ ^{low}	-	-	332	-
A ₁ (TO)	-	-	380	382
E ₂ ^{high}	440.4	438.9	437	437
A ₁ (LO)	-	-	574	574
B ₁ ^{high}	-	582	-	-
TA + B ₁ ^{high}	-	646	-	-

^a See Ref. [35].

^b See Ref. [34].

geometry, it is one of the forbidden modes according to the Raman selection rules. In addition, there is no noticeable change in the intensity of this peak with respect to post annealing under various ambient such as oxygen and vacuum atmospheres [13]. Therefore, the peak at 582 cm⁻¹ could not be assigned as E₁(LO) mode which is also absent in thin films. In addition, the observed peak could not be related to the A₁(LO) phonon mode since in general, the A₁(LO) phonon mode will be observed at ~574 cm⁻¹. In some exceptional cases, this phonon mode will be shifted to higher wave number side due to the higher carrier concentration and also the intensity of that peak will be quenched with the broadening of the peak. But, in the present case, the observed peak is too intense. Hence, the observed peak at 582 cm⁻¹ cannot be attributed to either A₁(LO) phonon mode or the overlapping of A₁(LO) and E₁(LO) phonon modes. Besides, the peak at 582 cm⁻¹ can not ascribed to the surface optical modes because that usually lies between the polar phonon modes of A₁(TO) and A₁(LO). These anomalous Raman modes are normally attributed to the intrinsic host-lattice defects induced by doping as well as low structural quality of the materials [10,11]. However, the present study clearly reveals that the ZnO nanorods have high crystalline and optical properties as compared to thin film. Hence, the observed anomalous Raman modes in the vertically aligned ZnO nanorods could be neither attributed to poor structural and optical qualities nor doping as corroborated by photoluminescence studies. Further, the role of point defects in the ZnO nanorods on the observation of the anomalous Raman modes can be ignored. In the recent reports, it is found that, due to the small dispersion along the Brillouin zone, the observed peaks at 276 and 582 cm⁻¹ can be attributed to the silent modes [B₁^{low} and B₁^{high}] of ZnO. Further, the B₁^{low} mode is located near to the region of low two phonon density of states (DOS) while the B₁^{high} mode is near to the region of high two phonon DOS. Hence, both B₁^{low} and B₁^{high} modes exhibit comparable intensities and the line width of B₁^{low} mode (6.41 cm⁻¹) is one third of the width of B₁^{high} (18.37 cm⁻¹). Therefore, the observed peaks at ~276, 582 and 646 cm⁻¹ are assigned as B₁^{low}, B₁^{high} and TA + B₁^{high} which agree well with the earlier report [13,32]. These anomalous Raman silent modes can be ascribed to the quasi-backscattering geometry in Raman spectra as the incident and scattered wave vector is appeared to be non-zero (k≠0) due to the breakdown of translational symmetry in ZnO nanorods. The additional Raman peaks at ~228, 301, 520, 620, 670 cm⁻¹ are associated to the silicon substrate, and that are in good agreement with the earlier reports [8,33].

4. Conclusion

Vertically aligned undoped ZnO nanorods and thin film have been successfully grown on silicon substrates under various growth temperatures. The observation of Raman silent modes in the ZnO nanorods confirms the breakdown of translational symmetry in 1-D nanostructures. The structural study of ZnO nanorods reveals the wurtzite crystal structure with high crystalline nature which is further substantiated by micro-Raman studies. The dominant donor bound exciton emission and the phonon replicas indicate that the Raman silent modes could not be ascribed to the poor structural or optical quality of the ZnO nanorods rather difference in incident and scattered wave vectors (k≠0) due to the breakdown of translational symmetry induced by nanorods geometry.

Acknowledgments

KJ thanks Department of Science and Technology (DST), Govt. of India for the financial support to develop the infrastructural facility under the scheme of FIST(2007).

References

- [1] M.J. Chen, J.R. Yang, M. Shiojiri, *Semicond. Sci. Technol.* 27 (2012) 074005.
- [2] Y.S. Choi, J.W. Kang, D.K. Hwang, S.J. Park, *IEEE Trans. Electron. Dev.* 57 (2010) 26.
- [3] C.H. Liu, J.A. Zapien, Y. Yao, X.M. Meng, C.S. Lee, S.S. Fan, Y. Lifshitz, S.T. Lee, *Adv. Mater.* 15 (2003) 838.
- [4] H. Kind, H. Yan, B. Messer, M. Law, P. Yang, *Adv. Mater.* 14 (2002) 158.
- [5] Ü. Özgür, D. Hofstetter, H. Morkoç, *P. IEEE* 98 (2010) 1255.
- [6] P. Yang, H. Yan, S. Mao, R. Russo, J. Johnson, R. Saykally, N. Morris, J. Pham, R. He, H. J. Choi, *Adv. Funct. Mater.* 12 (2002) 323.
- [7] S. Ramanathan, S. Bandyapadhyay, L.K. Hussey, M. Muñoz, *Appl. Phys. Lett.* 89 (2006) 143121.
- [8] P. Sundara Venkatesh, K. Jeganathan, *J. Solid State Chem.* 200 (2013) 84.
- [9] M. Tzolov, N. Tzenov, D. Dimova-Malinovska, M. Kalitzova, C. Pizzutto, G. Vitali, G. Zollo, I. Ivanov, *Thin Solid Films* 379 (2000) 28.
- [10] C. Bundesmann, N. Ashkenov, M. Schubert, D. Spemann, T. Butz, E.M. Kaidashev, M. Lorenz, M. Grundmann, *Appl. Phys. Lett.* 83 (2003) 1974.
- [11] A. Kaschner, U. Habocek, M. Strassburg, M. Strassburg, G. Kaczmarczyk, A. Hoffmann, C. Thomsen, A. Zeuner, H.R. Alves, D.M. Hofmann, B.K. Meyer, *Appl. Phys. Lett.* 80 (2002) 1909.
- [12] F. Reuss, C. Kirchner, Th Gruber, R. Kling, S. Maschek, W. Limmer, A. Waag, P. Ziemann, *J. Appl. Phys.* 95 (2004) 3385.
- [13] P. Sundara Venkatesh, V. Purushothaman, S. Esakki Muthu, S. Arumugam, V. Ramakrishnan, K. Jeganathan, K. Ramamurthi, *CrystEngComm* 14 (2012) 4713.
- [14] E.I. Givargizov, *Highly Anisotropic Crystals*, Reidel, Dordrecht, 1987.
- [15] D.S. Kim, U. Gösele, M. Zacharias, *J. Cryst. Growth* 311 (2009) 3216.
- [16] H.P. Schönherr, J. Fricke, Z. Niu, K.J. Friedland, R. Nötzel, K.H. Ploog, *Appl. Phys. Lett.* 72 (1998) 566.
- [17] Z. Gong, Z.D. Fang, Z.H. Miao, Z.C. Niu, S.L. Feng, *Chin. Phys. Lett.* 20 (2003) 1819.
- [18] E. Ohshima, H. Ogino, I. Niikura, K. Maeda, M. Sato, M. Ito, T. Fukuda, *J. Cryst. Growth* 260 (2004) 166.
- [19] K. Sakai, K. Noguchi, A. Fukuyama, T. Ikari, T. Okada, *Jpn. J. Appl. Phys.* 48 (2009) 085001.
- [20] Ü. Özgür, Ya. I. Alivov, C. Liu, A. Teke, M.A. Reshchikov, S. Doğan, V. Avrutin, S.J. Cho, H. Morkoç, *J. Appl. Phys.* 98 (2005) 041301.
- [21] Z. Fang, Y. Wang, D. Xu, Y. Tan, X. Liu, *Opt. Mater.* 26 (2004) 239.
- [22] K. Vanheusden, C. Seager, W. Warren, D. Tallant, J. Voigt, *Appl. Phys. Lett.* 68 (1996) 403.
- [23] H. Liu, F. Zeng, Y. Lin, G. Wang, F. Pan, *Appl. Phys. Lett.* 102 (2013) 181908.
- [24] R. Menon, V. Gupta, H.H. Tan, K. Sreenivas, C. Jagadish, *J. Appl. Phys.* 109 (2011) 064905.
- [25] D. Zhang, D. Guo, X. Pu, X. Shao, R. Liu, L. Li, X. Qian, *Mater. Lett.* 63 (2009) 2290.
- [26] P. Sundara Venkatesh, S. Balakumar, K. Jeganathan, *RSC Adv.* 4 (2014) 5030.
- [27] P. Sundara Venkatesh, K. Jeganathan, *CrystEngComm* 16 (2014) 7426.
- [28] P. Sundara Venkatesh, P. Dharmaraj, V. Purushothaman, V. Ramakrishnan, K. Jeganathan, *Sens. Actuators B-Chem.* 212 (2015) 10.
- [29] W.B. Mi, H.L. Bai, H. Liu, C.Q. Sun, *J. Appl. Phys.* 101 (2007) 023904.
- [30] H.M. Zhong, J.B. Wang, X.S. Chen, Z.F. Li, W.L. Xu, W. Lu, *J. Appl. Phys.* 99 (2006) 103905.
- [31] D.F. Paragay, M. Miki-Yoshida, J. Morales, J. Solis, L.W. Estrada, *Thin Solid Films* 373 (2000) 137.
- [32] F.J. Manjón, B. Marí, J. Serrano, A.H. Romero, *J. Appl. Phys.* 97 (2005) 053516.
- [33] F. Singh, R.G. Singh, V. Kumar, S.A. Khan, J.C. Pivin, *J. Appl. Phys.* 110 (2011) 083520.
- [34] J.M. Calleja, M. Cardona, *Phys. Rev. B* 16 (1977) 3753.
- [35] T.C. Damen, S.P.S. Porto, B. Tell, *Phys. Rev.* 142 (1966) 570.